THE UNIVERSITY OF MANITOBA

A STUDY OF PRECIPITATION AND DEFORMATION MECHANISMS IN Co-Ni-Cr-BASE SUPERALLOY CONTAINING Nb and Al

by

COMONDORE RAVINDRAN

A DISSERTATION SUBMITTED TO THE FACULTY OF GRADUATE STUDIES OF THE UNIVERSITY OF MANITOBA IN PARTIAL FULFILLMENT OF THE REQUIREMENTS OF THE DEGREE OF

DOCTOR OF PHILOSOPHY

DEPARTMENT OF MECHANICAL ENGINEERING

METALLURGY

Winnipeg, Manitoba

August, 1982

A STUDY OF PRECIPITATION AND DEFORMATION MECHANISMS IN Co-Ni-Cr-BASE SUPERALLOY CONTAINING Nb and Al

BY

COMONDORE RAVINDRAN

A thesis submitted to the Faculty of Graduate Studies of
the University of Manitoba in partial fulfillment of the requirements
of the degree of

DOCTOR OF PHILOSOPHY

ABSTRACT

The precipitation hardening behaviour of two Co-Ni-Cr-Al alloys containing Nb or Ti has been studied. On aging between 873K and 1073K, the main strengthening phase in both the alloys was observed to be a homogenous precipitation of γ' phase which has an ordered Cu_3Au type F.C.C. structure. The shape of the γ' phase changed from spherical to cubical in the initial stages of aging, and the cube edges were aligned along the <100> directions. On aging for prolonged periods at 1073K, the particles coalesced to form irregular shapes. The formation of γ' follows the Engel-Brewer theory of the structure of compounds based on electronic considerations.

Carbon, present as an impurity element, was seen to form NbC/TiC precipitate. This precipitate, when present at the grain boundary, gave rise to a precipitate free zone around the boundary. Within the grain, NbC precipitated in association with stacking faults. Discontinuous precipitation of γ' occurs by localized dissolution of grain boundary NbC/TiC precipitate at sharp grain boundaries and seems to be initiated by the process of grain boundary straightening. Occasionally acicular sigma phase was also observed at the grain boundaries. This is in contradiction of predictions by Engel-Brewer and PHACOMP Analyses, and is considered to be due to localised chemical inhomogeneity.

In the small particle size range of 7-20nm diameter deformation of the Co-Ni-Cr-Nb-Al alloy occurs by the shearing of γ' particles

by pairs of moving dislocations. Dislocations bypass large particles (over 20nm in diameter) by the Orowan looping mechanism. In the diameter range of 9-20nm a transition stage encompassing a progressive increase of looping activity is seen. The alloy in the underaged state is strengthened by the order hardening mechanism proposed by Brown and Ham. The shear modulus-corrected yield strength values for underaged specimens did not increase with temperature in the range 77 to 373K, thus eliminating coherency hardening as a contributory mechanism to strengthening in the underaged condition. In the overaged alloy, deformation occurs by the Orowan looping process, and the experimental results are in excellent agreement with the mechanisms proposed by Hirsch and Humphreys and Bacon et al. Also, there is an excellent agreement between the observed incremental CRSS and theoretical incremental CRSS predicted by the Ashby mechanism if the average incremental CRSS for edge and screw dislocations is considered.

SYMBOLS

$\bar{r}$	Average particle size
$\bar{a}$	Average cube edge of particle
$\bar{r}_o$	Average particle size at the onset of coarsening
$\bar{a}_o$	Average cube edge of particle at the onset of coarsening
D	The coefficient of diffusion of solute in the matrix
C_e	The concentration of solute in equilibrium with a particle of infinite size
δ	The interfacial free energy of the particle/matrix interface
V_m	The molar volume of precipitate
ρ_c	A numerical constant related to the distribution of particle sizes
R	The molar gas constant, 1.987 cal/mole K
ρ	The dimensionless measure of particle size, $r/\bar{r}$
$f_{(r,t)}, f_{(t)}, h_{(\rho)}$	Help functions defined in section 2.4.2
T	The line-tension of dislocation
L_f	The effective interplanar spacing between particles or the average distance between the particles in the slip plane
τ	Applied shear stress resolved in the slip direction on the slip plane
ϕ	Included angle between the arms of a dislocation at an obstacle
F	The force required to shear a particle by a dislocation
N_A	The number of particles per unit area intersecting the slip plane

B	A constant used in section 2.5
γ_s	Particle/matrix interfacial energy
f_v	The volume fraction of precipitate
R	The particle radius
γ_1	The stacking fault energy of precipitate
γ_2	The stacking fault energy of matrix
$\bar{\omega}$	Mean ribbon width of stacking fault
K	Partial dislocation separation force
α	Partial dislocation separation distance
G	The shear modulus of matrix
L''	The average distance between force centres
r_s	The average radius of a particle intersected by a slip band, $(2/3)^{1/2}r$
r_o	Inner cut-off radius
w	The elastic repulsion between the strongly paired dislocations, which is usually taken as unity
γ_{APB}	Antiphase Boundary Energy
ν	Poisson's ratio
L	The spacing between two obstacles
L_o	The mean planar spacing of obstacles; Orowan spacing, $0.81N_A^{-1/2}$
L_s	The square lattice spacing, $N_A^{-1/2}$
a_p	The lattice parameter of γ' precipitate
a_m	The lattice parameter of matrix
r'_o	Minimum dislocation loop radius
σ_o	o.2% tensile yield strength of the matrix

σ	0.2% tensile yield strength of the alloy
V_{L1_2}, N_{hkl}	Constants used in the calculcation of APB energy by a theoretical method
Z_{AB}	The number of first nearest neighbour atoms
F_A, F_B	Atomic fractions of A and B atoms
T_c	The critical ordering temperature
k	The Boltzmann Constant, 1.38×10^{-16} ergs/deg.
ϵ	The constrained lattice strain, or γ/γ' lattice misfit
$\Delta\tau$	Incremental flow stress

ACKNOWLEDGEMENTS

I wish to express my gratitude and appreciation to my thesis advisor, Dr. M. C. Chaturvedi for his guidance, encouragement and patience. As my mentor, he has molded me into a scientist and a practical metallurgist through stimulating deep interest in all aspects of Metallurgy, especially in Electron Microscopy and Alloy Development.

I also wish to express my thanks to Dr. J. R. Cahoon for his encouragement and keen interest in the completion of this work, and suggestions for the improvement of this thesis.

I thank Mr. J. Van Dorp for his technical assistance, and Mr. P. Mitra for drafting services.

I thank Mrs. Karen Nedohin for the excellent typing of this thesis.

I thank my employers, Manitoba Rolling Mills (Canada) Limited, and in particular, Mr. R. R. Robertson, President and General Manager, for his encouragement which was a major factor in enabling completion of this thesis.

I thank my wife, Shanti, for her constant encouragement, endurance and active participation, which rendered the completion of this work possible.

CONTENTS

LIST OF TABLES

LIST OF FIGURES

1. INTRODUCTION

The recent interest in energy conservation has renewed emphasis on the development of high temperature materials since many processes operate more efficiently at higher temperatures. Cobalt-base superalloys have shown promise in view of their demonstrated advantages, viz., high structural stability at elevated temperatures and excellent thermal-fatigue resistance. Also, cobalt-base superalloys can be used at temperatures a few hundred degrees higher than nickel-base superalloys.[1] Cobalt-base and nickel-base superalloys are mostly strengthened by the precipitation of γ', $Ni_3(Al,Ti,Nb)$ phase which has an ordered $L1_2$-type F.C.C. structure.

From the literature review in the next chapter, it is evident that the strengthening mechanisms of cobalt-nickel-base superalloys have not yet been fully analysed. Most of the work has been carried out on the precipitation strengthening of nickel-base superalloys.

In view of this situation, it was decided to investigate the precipitation and particle growth phenomena in Co-Ni-Cr-Al alloys with niobium or titanium additions. The dislocation-precipitate interaction and its influence on the mechanical properties were also studied.

2. LITERATURE REVIEW

2.1 GENERAL

In the last twenty-five years, considerable attention has been focussed on the metallurgy of nickel-base and cobalt-base alloys because of the high temperature applications of these materials. The commercial development of age hardening superalloys containing aluminum and/or titanium has enhanced the interest in the precipitation of intermetallic compounds as well as in the correlation of structure and properties.

Superalloy technology is greatly dependent on the understanding of precipitation of phases; type, distribution, morphology and the mechanisms of strengthening. Most of the early work was on the age hardening of nickel-base alloys[2-6]. However, considerable attention in the following years was given to the strengthening mechanisms in chromium-nickel austenitic steels[7-10]. Several authors[11-14] have reviewed the effects of titanium and aluminum additions to nickel-rich alloys. In most of the instances, the nickel-base superalloys are strengthened by the precipitation of an ordered F.C.C. γ' phase. Carbide phases also precipitate in these alloys. Essentially, the precipitation of these phases and solid solution strengthening in the F.C.C. matrix are the main causes of strengthening in superalloys. In the case of cobalt-base alloys, it is common to find only γ' and carbides. Strength in cobalt alloys is obtained principally through

a combination of solid-solution effects and carbide precipitation. Sims[1] has reviewed the subject of strengthening in cobalt base alloys.

Cobalt-nickel-base alloys are in most cases similar to the general group of nickel-base alloys in that they can be strengthened by the precipitation of γ', $Ni_3(Al,Ti,Nb)$ which has an ordered F.C.C. structure.

2.2 CHEMICAL COMPOSITION

The logical development of cobalt-nickel-base alloys can be seen from the periodic table of elements as illustrated by Sims (Figure 1)[1]. The first class consists of elements that prefer and constitute the F.C.C. austenitic matrix. These are from Group V, VI and VIII and include nickel, cobalt, iron, chromium, molybdenum, tungsten and vanadium. The second class of elements prefer and constitute the γ' precipitate Ni_3Al. These elements are from Group III, IV and V and include aluminum. Titanium, niobium and tantalum can substitute for aluminum in Ni_3Al. Magnesium, boron, carbon and zirconium make up a third class of elements that segregate to grain boundaries. These elements are from Group II, III and IV and are very odd sized in atomic diameter.

2.3 STRUCTURAL FEATURES

2.3.1 The Austenitic Matrix

Alloys with an austenitic matrix and high cobalt content are favoured by most designers for high temperature and long-time

FIGURE 1

ELEMENTS IMPORTANT IN THE CONSTITUTION
OF COBALT-NICKEL-BASE SUPERALLOYS[15]

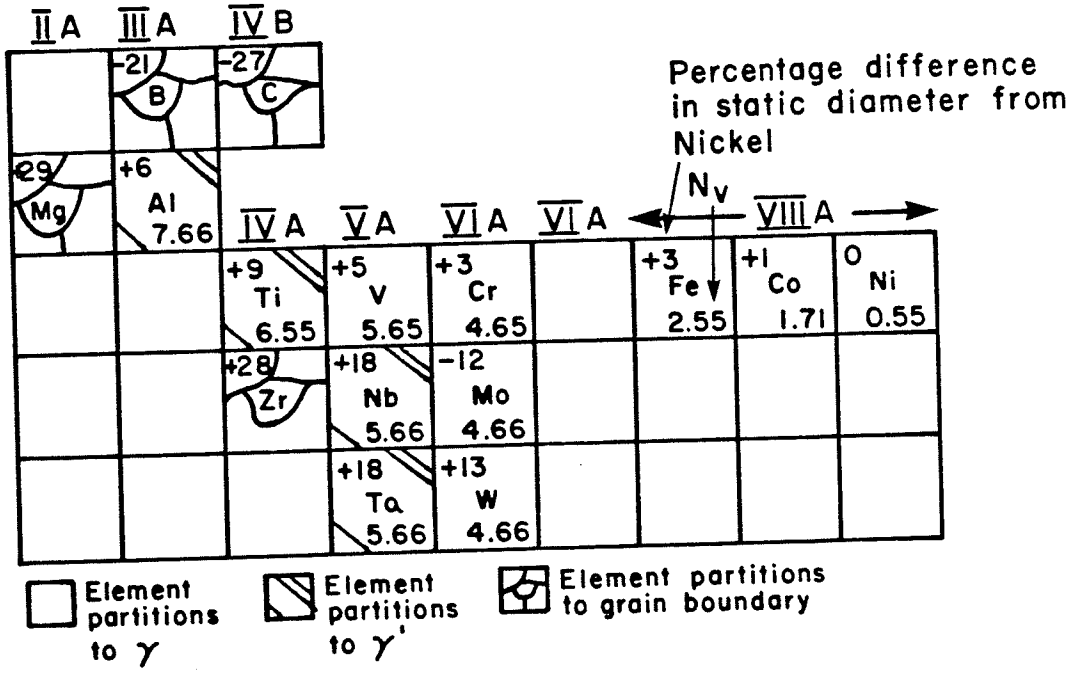

Atomic diameter of carbon, boron, zirconium, magnesium — Goldschmidt for CN12.

Atomic diameter of other elements from lattice parameter effect in nickel binary alloys.

FIGURE 1

exposure in air atmospheres. These alloys can be used up to 0.8Tm (melting point) and for times up to 100,000 hours.

The cobalt-nickel-base alloys offer a combination of the following properties of the cobalt-base and nickel-base alloys:

1. The cobalt-base alloys are more stable at high temperatures.
2. The cobalt-base alloys have slightly higher thermal conductivity compared to nickel-base alloys and have slightly lower thermal expansion properties.
3. Nickel has a high tolerance for alloying without phase instability owing to its nearly filled third electron shell[15].
4. These alloys, with chromium additions, tend to form Cr_2O_3-rich protective scales having low cation vacancy content. This film restricts the outward diffusion of metallic elements as well as the inward diffusion of oxygen, nitrogen, sulfur and other aggressive atmospheric elements[15].
5. These alloys tend to form Al_2O_3-rich scales at high temperatures which have exceptional resistance to oxidation.

2.3.2 Solid-Solution Strengthening of the Matrix

Cobalt, nickel, chromium and titanium often exhibit bivalency while niobium and aluminum are often trivalent. Also, it can be seen that all these elements are reasonably close together (Co,Ni: Group VIII; Cr: Group VI; Nb: Group V; Al: Group III) in the periodic table of elements. Figure 1 shows that cobalt, chromium,

titanium, niobium and aluminum differ from nickel by 1 - 18% in atomic diameter. From the foregoing statements, it is reasonable to expect solid-solution formation on the basis of Hume-Rothery's rules[16]. Furthermore, the size factor being within the favourable limit (15%) for solid-solution formation, could lead to hardening as a result of lattice expansion due to differing diameters. Hardening could also result from the lowering of stacking fault energy by the alloying elements which would make cross slip in the matrix more difficult.

2.3.3 The Gamma Prime (γ') Phase

The cobalt-nickel-base superalloys are, in most cases, strengthened by the precipitation of γ', Ni_3 (Al,Ti, Nb) phase which has an ordered F.C.C. structure. In many cases these precipitates occur as small cubes with sides parallel to $\{100\}$[17-20]. It has been observed that there is a strong tendency for these cubes to be aligned along the <100> directions[21]. According to Ardell and Nicholson[22], a modulated structure develops from an initially random precipitate distribution gradually changing to one where cube precipitates are aligned along <100> directions.

In commercial superalloys, the shape of individual γ' precipitates varies from perfectly spherical to perfectly cubical, although most particles have some intermediate shape. Hagel and Beattie[2] have suggested that spheres are formed when the lattice misfit between γ' and the matrix is less than 0.5 pct. while cubes

are formed for misfits in the range 0.5 - 1.0 pct. When the misfit is greater than 1 pct., γ' precipitation is inhibited and only a discontinuous precipitation occurs. Cubical γ' precipitates have been observed in Nimonic alloy with a misfit of less than 0.1 pct.[23]. This indicates that the Hagel-Beattie suggestion is only partially valid. It has been suggested by different workers[24,25] that particles which are spherical when small often become cubical upon increasing in size. Kelly and Nicholson[26] have suggested that this type of effect may be associated with the loss of coherency of the particle at an intermediate stage in the aging process. Such an idea could be correlated with those of Brooks[27] and Friedel[28] for loss of coherency, predicting that coherency should break down for γ' particle sizes of the order of 30 - 75nm. However, analysis of diffraction effects from thin foil studies[29] on a binary Ni-Al alloy indicates that such "loss of coherency" is not necessarily implied when γ' particles cease to be spherical.

It was stated earlier that the γ' phase frequently contains dissolved elements that lead to the substitution of solute atoms in both the "Ni" and "Al" portions of the ideal Ni_3Al stoichiometric precipitate. The common replacements for Al are Ti or (Ti+Nb). It is known that the Al/Ti ratio plays an important role in governing the kinetics of γ' precipitation. Nordheim and Grant[30], Beattie and Hagel[31] and Hughes[32] among others have discussed the role of the Al/Ti ratio at length. However, an example of the effect of substitution of a third solute element such as niobium is worth considering.

Alternately, the effect of addition of aluminum to a superalloy containing niobium could be examined. Such an investigation could be particularly worthwhile in the light of the suggestion that in many alloys γ' is a metastable phase overaging to orthorhombic Ni_3Nb phase[33] or hexagonal η-Ni_3Ti[98].

2.3.4 The Carbide Phases

The common classes of carbides are MC, $M_{23}C_6$, M_7C_3 and M_6C. The MC carbides are generally identified as the primary carbides. They take a random cubic morphology and have a F.C.C. structure. They occur from simple combination of carbon with reactive and refractory metals (Ta, Nb, Ti, V, etc.) and often precipitate at the grain boundary. The $M_{23}C_6$ carbides show a marked tendency for precipitation at the grain boundary. The M_6C carbides often exhibit, in addition to grain boundary precipitation, a Widmanstätten, intergranular morphology. The M_7C_3 carbides normally take a blocky intergranular form.

2.4 PROCESS OF PARTICLE COARSENING

The complicated process of Ostwald Ripening[35] in which large particles grow at the expense of small ones by a diffusion-controlled mechanism, was independently solved by Lifshitz and Slyozov[36] and Wagner[37]. In its original form, the Lifshitz-Wagner Theory is applicable to spherical particles dispersed in a fluid matrix, but Li and Oriani[38] have shown that many of the factors that

complicate the coarsening process for particles of arbitrary equilibrium shape in solid matrices[39] can, in principle, be accounted for quantitatively.

2.4.1 Growth of Average Particle

For diffusion-controlled transfer of solute in the matrix and the ideal case of spherical particles coarsening in a fluid matrix, Lifshitz and Slyozov[36] and Wagner[37] have derived the following equations for the growth of the average particle as a function of time:

$$\bar{r}^3 - \bar{r}_o^3 = kt \qquad \ldots\ldots (1)$$

where $\bar{r}$ is the average particle radius at time t, $\bar{r}_o$ is the average particle radius at the onset of coarsening. The rate constant k is given by:

$$k = \frac{2\delta D\, C_e V_m^2}{\rho_c^2\, RT} \qquad \ldots\ldots (2)$$

where δ is the interfacial free energy of the particle/matrix interface, D is the coefficient of diffusion of the solute in the matrix, C_e is the concentration of solute in equilibrium with a particle of infinite size, V_m is the molar volume of precipitate, ρ_c is a numerical constant related to the distribution of particle sizes (theoretically 3/2) and R and T have their usual meaning.

Following Ardell[40], for cuboidal particles $\bar{r}$ is replaced by $\bar{a}/2$ where $\bar{a}$ is the average length of a cube edge. Therefore, the

Lifshitz-Wagner expression becomes:

$$\bar{a}^3 - \bar{a}_o^3 = \frac{64\ \mathcal{D} C_e V_m^2 t}{9\ RT} = k't \qquad \ldots\ldots (3)$$

2.4.2 Theoretical Distribution of Particle Sizes

The distribution of particle sizes evolves towards a "quasi-steady-state" distribution[37], $f_{(r,t)}$ which is independent of final distribution $f_{(r,o)}$. The distribution function is:

$$f_{(r,t)} = f_{(t)}\ \rho^2\ h_{(\rho)} \qquad \ldots\ldots (4)$$

where $f_{(t)}$ is a function of time only,

$$\rho = \frac{r}{\bar{r}},$$

and $h_{(\rho)}$ is given by,

$$h_{(\rho)} = \left(\frac{3}{3+\rho}\right)^{7/3} \left(\frac{3/2}{3/2-\rho}\right)^{11/3} \exp\left(\frac{-\rho}{3/2-\rho}\right) \qquad \ldots\ldots (5)$$

where $\rho < \rho_c = 3/2$; $h_{(\rho)} = 0$; $\rho > \rho_c = 3/2$.

The size distribution is such that particle sizes greater than 1.5 $\bar{r}$ should not exist. The function $\rho^2\ h_{(\rho)}$ is time-invariant and has the property that:

$$\int_0^\infty \rho^2 h_{(\rho)}\ d\rho = \rho_c^2 \qquad \ldots\ldots (6)$$

The "cut-off" radius, $\rho_c = 3/2$ enters into the Wagner formulation through the above equation, and is the only parameter associated with the theoretical distribution of particle sizes in the kinetic equations for coarsening.

2.4.3 Coarsening Kinetics of γ'-Forming Alloys

Kriege and Baris[41] determined the composition and volume fraction of γ' precipitate in several commercial alloys. Ardell[40] and others[42,43] demonstrated that in γ'-forming binary and ternary alloys, growth of the γ' precipitate obeys a diffusion-controlled coarsening model where the average particle radius increases linearly with time to the one-third power. Van der Molen et al[44] working on Udimet 700 and more recently, Chaturvedi and Chung[45,46] on Co-Ni-Cr-Ti alloys found that the coarsening kinetics of γ' precipitate followed the time-law predictions of the Lifshitz-Wagner Theory of diffuion-controlled growth at all aging temperatures.

2.5 STRENGTHENING OF TWO-PHASE ALLOYS

Second-phase particles can increase the strength of an alloy by one of two mechanisms[47]. The particles may act as impenetrable obstacles to dislocations and force them to bow out and by-pass them via the Orowan mechanism[48]. Alternately, the particles may be cut or sheared by dislocations at stresses below the Orowan stress. Under these conditions the strengthening effect of the particles is due to the additional work required to make the dislocation cut the particle. In either case, the theoretical treatments of second-phase particle strengthening are based on the following model, which is physically depicted in Figure 2. The glide dislocation bows out between the particles, and the angle ϕ between two arms of the dislocation is determined by the strength of the particle. When this angle reaches a critical value, the

FIGURE 2

A COUPLED PAIR OF DISLOCATIONS INTERSECTING DIFFERENT ORDERED PARTICLES, SHOWING THE EFFECT OF BEND ANGLE ϕ ON OBSTACLE SPACING. SHADED AREA REPRESENTS ANTIPHASE BOUNDARIES[55,68].

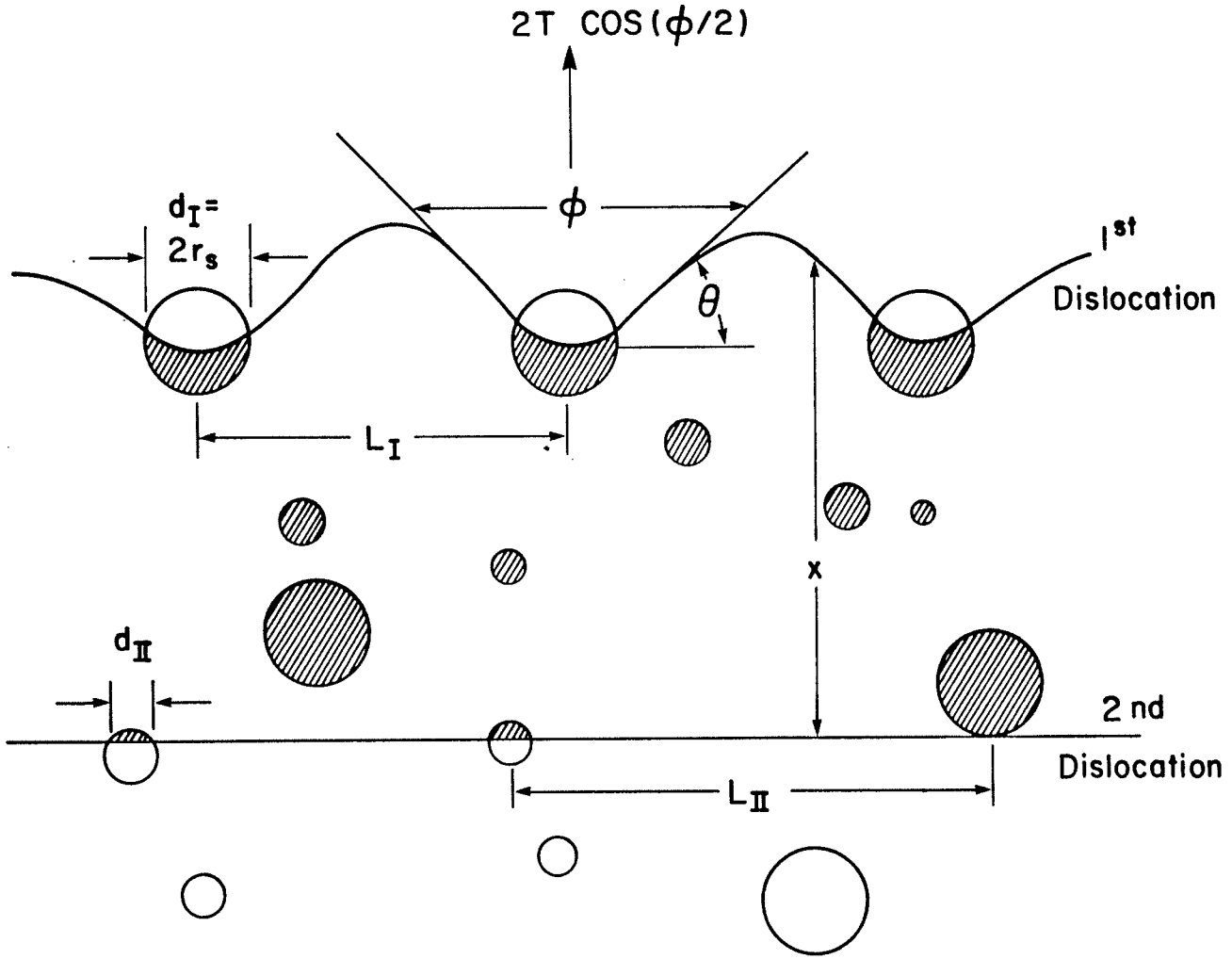
2T COS(ϕ/2)
ϕ
d_I= $2r_s$
θ
1st Dislocation
L_I
x
d_{II}
2 nd Dislocation
L_{II}

FIGURE 2

dislocation breaks away from the paricle. At this critical point, the obstacle strength F is related to the dislocation line tension T by the equation

$$F = 2T \cos(\phi/2) \quad \ldots\ldots (7)$$

When breaking angle $\phi = 0$, the particle behaves as an impenetrable obstacle (Orowan hardening). For $\phi > 0$, the particle can be sheared by the glide dislocation with the required shear force equal to F. The shear stress required to cause the dislocation to break away from the particle will be

$$\tau_f \, b \, L_f = F$$

or,

$$\tau_f = \frac{F}{bL_f}$$

$$= \frac{2T \cos(\phi/2)}{bL_f} \quad \ldots\ldots (8)$$

where L_f is the effective spacing between the particles.

In reality, there will be a distribution of F and L_f values such that the calculation of flow stress involves selecting some average value of F and L_f and thereafter substituting these values into Equation (8).

A number of definitions of 'L_f' are possible - the 'volumetric' spacing, the 'planar' spacing, and the 'mean free path'[47]. For the case of a dislocation moving on a slip plane, the 'planar' spacing, L_f (i.e., the average distance between particles in the slip plane) is the most appropriate. This spacing is related

to N_A, the number of particles intersecting a unit area of slip plane, by the equation

$$L_f = B(N_A)^{-1/2} \qquad \ldots\ldots (9)$$

$$= BL$$

where B is a constant of the order of unity. Therefore, $L = (N_A)^{-1/2}$.

For weak particles which are sheared by glide dislocations, the value of effective particle spacing, L_f, is given by the Friedel relationship

$$L_f = \left(\frac{2T}{\tau_f\, bN_A}\right)^{1/3} = \left(\frac{2TL^2}{\tau_f\, b}\right)^{1/3} \qquad \ldots\ldots (10)$$

where τ_f is the stress required to cause the dislocation to break through the array of particles. Substituting this value of L_f into Equation (8) gives the expression for τ_f.

$$\tau_f = \frac{2T}{b}(N_A)^{1/2}[\cos(\phi/2)]^{3/2} = \frac{2T}{bL}[\cos(\phi/2)]^{3/2} \qquad \ldots\ldots (11)$$

The exact value of particle spacing has been a subject of considerable discussion in the literature[34,49-52]. For a regular square array of impenetrable particles, $L_f = L$. For a random array of particles, sophisticated calculations for the value of L_f by Kocks[50,78] and Foreman and Makin[49,51] give $L_f = 1.19L$ and $1.23L$ respectively.

2.5.1 Deformable Particles

In the case of particles that are cut by glide dislocations ($\phi > 0$) the force F required to cut particles or the value of breaking angle ϕ must be calculated and substituted into Equation (8) or (11). The calculation of this additional shearing force F is mainly based on two strengthening mechanisms:

(a) order strengthening

(b) misfit or coherency strengthening.

(a) Order Strengthening Mechanism

Ham[53] has shown that when a glide dislocation acting under a shear stress τ_I cuts an ordered particle, the force $\tau_I b$ on the dislocation, neglecting the particle-matrix interfacial energy, must balance the antiphase boundary energy (APB energy) created. According to Ham,[53,54]

$$\tau_I b = \frac{2r_s \gamma_{APB}}{L_I}$$

or

$$\tau_I = \frac{2r_s \gamma_{APB}}{L_I b} \qquad \ldots\ldots (12)$$

where γ_{APB} is the APB energy and r_s is the average radius of particle intersected by a slip plane ($r_s = (2/3)^{1/2} r$ where r is the particle radius).

$$\text{Since } N_A = \frac{f_v}{\pi r_s^2} \text{ and } L = \left(\frac{\pi}{f_v}\right)^{1/2} r_s$$

where f_v is the volume fraction of the precipitate particles, the

Friedel spacing (Equation 10) becomes

$$L_I = \left(\frac{2T\pi r_s}{f_v \tau_I b}\right)^{1/3} \quad \ldots\ldots (13)$$

Substituting Equation (13) into Equation (12), the stress necessary to force the dislocation through the particle is given by

$$\tau_I = \frac{\gamma_{APB}^{3/2}}{b}\left(\frac{4f_v r_s}{\pi T}\right)^{1/2} \quad \ldots\ldots (14)$$

The fraction of dislocation line cutting particles is given by

$$\frac{2r_s}{L_I} = \left(\frac{4\gamma_{APB} f_v r_s}{\pi T}\right)^{1/2}, \quad \frac{\pi T f_v}{4\gamma_{APB}} \leq r_s \leq \frac{T}{\gamma_{APB}} \quad \ldots\ldots (15)$$

The upper limit on this fraction for increasingly bent dislocations is set by the condition $r_s = T/\gamma_{APB}$ for which $L_I = L$; i.e., just at the point of Orowan bowing

$$\frac{2r_s}{L_I} = \frac{2r_s}{L} = \left(\frac{4f_v}{\pi}\right)^{1/2} \quad \ldots\ldots (16)$$

where $r_s = T/\gamma_{APB}$

At and above this critical fraction, the stress to shear a particle becomes

$$\tau_I = \frac{\gamma_{APB}}{b}\left(\frac{4f_v}{\pi}\right)^{1/2} \quad \ldots\ldots (17)$$

This stress must be below the Orowan bowing stress in order for particle shear to continue.

The lower limit of $\frac{2r_s}{L_I}$ (Equation 16) is given by the value of L_I for a perfectly straight dislocation and corresponds to the case of very small particles, i.e.,

$$\frac{2r_s}{L_I} = f_v \ , \quad r_s \leq \frac{\pi T f_v}{4\gamma_{APB}} \qquad \ldots\ldots (18)$$

When the first dislocation is just cutting the particles as in Figure 2, the second dislocation is pulled forward by the APB energy remaining in all particles cut by the first dislocation[53-56]. If the two dislocations assume the same shape and the separation x (see Figure 2) between the two dislocations is sufficiently small (but larger than r_s) the second dislocation may lie outside of all the particles. Then, at equilibrium, the total forward stress on the second dislocation balances the repulsive force between the two dislocations. Thus,

$$\tau_{II} b = \frac{Gb^2}{2\pi(1-\nu)x} \qquad \ldots\ldots (19)$$

The term $(1-\nu)$ in the above equation is applicable for edge dislocations, and equals unity for screw dislocations.

In general, however, the second dislocation does not come into contact with APB and is nearly straight. The more APB cut by the second dislocation, the less effective the particles become as obstacles. Then, referring to Figure 2, the force balance is as follows:

On dislocation I, $\tau b + \frac{Gb^2}{2\pi(1-\nu)x} - \frac{\gamma_{APB}\, d_I}{L_I} = 0$ . . . . . (20)

On dislocation II, $\tau b + \frac{\gamma_{APB} d_{II}}{L_{II}} - \frac{Gb^2}{2\pi(1-\nu)x} = 0$ . . . . . (21)

On solving Equations (20) and (21) simultaneously, the following relation for the forward stress on the first dislocation is obtained.

$$2\tau b + \frac{\gamma_{APB} d_{II}}{L_{II}} = \gamma APB \frac{d_I}{L_I} \qquad \ldots\ldots (22)$$

Since the second dislocation is observed to be straight during shear by the first dislocation, Equation (18) may be substituted for $\frac{d_{II}}{L_{II}}$ and Equation 15 for $\frac{d_I}{L_I}$. Then Equation (22) becomes

$$2\tau b + \gamma_{APB} f_v = \left(\frac{4\gamma_{APB} f_v r_s}{\pi T}\right)^{1/2} \gamma_{APB} \qquad \ldots\ldots (23)$$

Rearranging Equation (23),

for $r_s < \frac{T}{\gamma_{APB}}$,

$$\tau = \frac{\gamma_{APB}}{2b}\left[\left(\frac{4\gamma_{APB} f_v r_s}{\pi T}\right)^{1/2} - f_v\right] \qquad \ldots\ldots (24)$$

For $r_s > \frac{T}{\gamma_{APB}}$, Equation (24) is modified by using Equation (16) in Equation (22).

Then, $\tau = \frac{\gamma_{APB}}{2b}\left[\left(\frac{4f_v}{\pi}\right)^{1/2} - f_v\right]$ . . . . . (25)

For $r_s \leq \frac{\pi T f_v}{4\gamma_{APB}}$, using Equation (18) in Equation (22),

$$\tau = 0.$$

This can be seen from an examination of Equation (24).

The flow stress given by Equation (24) would reduce to one half the stress given in Equation (14) for single dislocation. Figure 3 gives a schematic summary of the basic features of this model.

(b) Coherency Strengthening Mechanism

There have been attempts to relate the influence of coherency strains to CRSS. However, these attempts failed to explain the dependence of CRSS on particle size. Subsequently, a model has been developed by Gerold and Haberkorn[57] where the interaction between dislocations and elastic strain fields around coherent precipitates is assumed to play a dominant role. Their[57] model begins with the following expression for the increase in flow stress due to interaction of dislocations with the strain fields.

$$\Delta\tau = \frac{K}{bL''} \qquad \ldots\ldots (26)$$

where K is the maximum repelling force of the strain field of a single particle on a moving dislocation and L" is the average distance between the force centers. The problem is to find the appropriate expressions for K and L". K is found to be equal to or less than T, the line of tension of an edge dislocation. For L", instead of using the Friedel spacing (Equation 9), they[57] have used the following expression in which the obstacle spacing depends on the bend angle, $\theta = 1/2(\pi-\phi)$.

According to them,

$$L'' = \frac{r_{s\pi}^{1/2}}{(\theta f_v)^{1/2}}, \quad \frac{9\pi f_v}{16} < \theta < 3/2 \qquad \ldots\ldots (27)$$

FIGURE 3

SCHEMATIC AGE-HARDENING CURVES ILLUSTRATING RELATION BETWEEN ORDER STRENGTHENING AND OROWAN BOWING AS A FUNCTION OF PARTICLE SIZE(56)

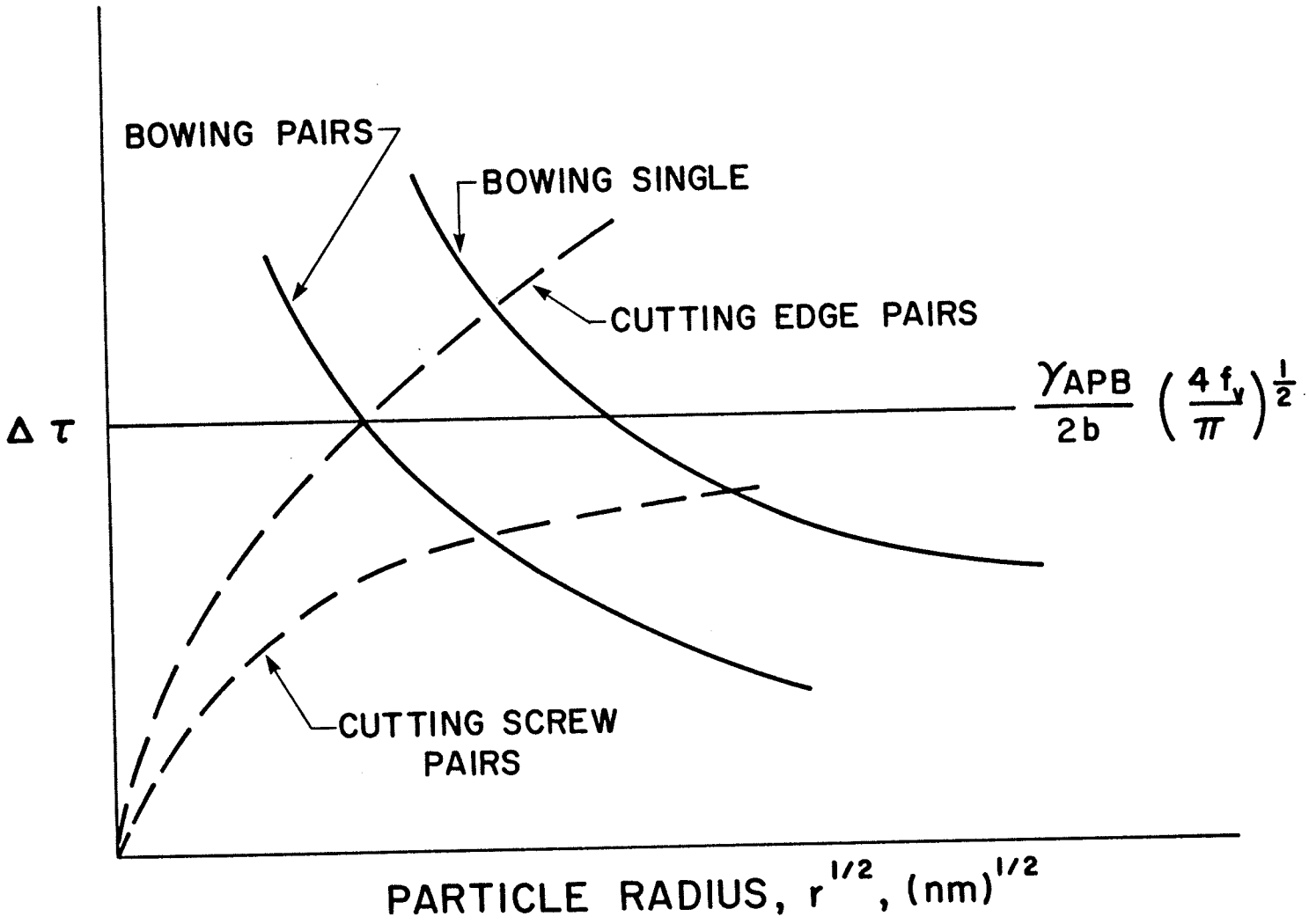
BOWING PAIRS
BOWING SINGLE
CUTTING EDGE PAIRS
$\frac{\gamma_{APB}}{2b}\left(\frac{4f_v}{\pi}\right)^{\frac{1}{2}}$
$\Delta\tau$
CUTTING SCREW PAIRS
PARTICLE RADIUS, $r^{1/2}$, $(nm)^{1/2}$

FIGURE 3

The angle to which a dislocation is bent by the force K before escaping the particle is given by

$$2 \sin \theta \simeq \frac{k}{2T} \qquad \ldots\ldots (28)$$

Combining Equations (26), (27) and (28), the widely used expression for the CRSS of edge dislocations has been obtained by Gerold and Haberkorn[57].

$$\Delta\tau = \beta G \varepsilon^{3/2} \left(\frac{r_s f_v}{b} \right)^{1/2} \qquad \ldots\ldots (29)$$

In the above equation, for edge dislocations

$$\frac{9\pi f}{16} < \frac{3|\varepsilon| r_s}{b} < 1/2$$

and $\beta = 3$

and for screw dislocations,

$$\frac{9\pi f}{16} < \frac{|\varepsilon| r_s}{b} < 1/2$$

and $\beta = 1$.

Based on experimental data for Cu-Co and Al-Zn alloys, it was concluded[57] that edge dislocations control the CRSS. It was also concluded[57] that for small particles ($r_s/b < 20$), the particles cut the precipitates, and for larger particles dislocations will by-pass the particles by the Orowan mechanism.

Gleiter[58] has also discussed the effect of coherency strain fields on CRSS in a two-phase alloy. He has followed the

steps outlined above but with different assumptions as to the flexibility of dislocation lines and the averaging procedure for obstacle distribution. He has obtained the following expression.

$$\Delta\tau = 11.8\ G\epsilon^{3/2}\ f^{5/6}\left(\frac{r_s}{b}\right)^{1/2} \qquad \ldots\ldots (30)$$

The main difference between Equations (29) and (30) is the volume fraction parameter.

(c) Other Mechanisms for Strengthening due to Deformable Particles

i. Surface Hardening

Additional energy is necessary to create a particle/matrix interface when a particle is sheared by dislocation.

According to Kelly and Nicholson[26],

$$\tau = \frac{\sqrt{6}}{\pi}\ \gamma_s\ \frac{f}{R} \qquad \ldots\ldots (31)$$

where γ_s = particle/matrix interfacial energy,

f = volume fraction of precipitate and

R = particle radius.

The Harkness and Hren version[59] gives a different value for τ as follows:

$$\tau = \frac{60.4}{b^3}\left(\frac{T}{b}\right)^{-1/2}\ (\gamma_s)^{3/2}\ R^2 f^2 \qquad \ldots\ldots (32)$$

ii. Stacking-Fault Hardening

Difference between the stacking-fault energies of particle and matrix could cause a hardening particularly if both belong to the same crystal system.

According to Hirsch and Kelly[60], the value of τ due to stacking fault hardening is given by

$$\tau = \frac{4}{\pi}\left(\frac{2}{\pi}\right)^{1/2}\left(\frac{\gamma_2-\gamma_1}{b}\right)\left(\frac{3K(\alpha)\ln\frac{\gamma_2}{\gamma_1}}{E}\right)\frac{\bar{\omega}}{R} \times \left(1 - \frac{3\pi\bar{\omega}}{32R}\right)^{1/2} (f)^{2/3} \quad \ldots\ldots (33)$$

where R = particle radius

γ_2 = stacking-fault energy of the matrix

γ_1 = stacking-fault energy of the precipitate

$\bar{\omega}$ = mean ribbon width

$K(\alpha)$ = partial dislocation separation force times the separation distance

Gerold and Hartman[61] have derived the following expression.

$$\tau = \left(\frac{8}{\pi}\right)^{1/2} G\left(\frac{\gamma_2-\gamma_1}{Gb}\right)^{3/2}\left(\frac{R}{b}\right)^{1/2} f^{1/2}\, I_m \quad \ldots\ldots (34)$$

where I_m = a complex function of R and the stacking-fault energy of the precipitate.

iii. Modulus Hardening

The differences between the elastic moduli of matrix and particle lead to this type of hardening. Knowles and Kelly[62] have derived the following expression.

$$\tau = \frac{\Delta G}{4\pi^2}\left(\frac{3\Delta G}{Gb}\right)^{1/2}[0.8-0.143\ln(R/b)]^{3/2} \times (R)^{1/2}(f)^{1/2} \quad \ldots\ldots (35)$$

where ΔG = difference in shear modulus between matrix and precipitate and G = matrix shear modulus (and R>2b).

According to Weeks et al[63], however, the value of τ is given by,

$$\tau = \frac{\Delta G b}{2\pi L}\left[\frac{\pi^2}{12} + \ln \frac{2R}{r_o}\right] \qquad \ldots\ldots (36)$$

However, the strengthening of the underaged alloy is considered mainly due to coherency and/or order mechanisms.

2.5.2 Superposition of Order and Coherency Mechanisms

Mihalisin and Decker[4] and Fine[64] suggest that the major contributing factor to γ' - forming alloys in the underaged condition is the coherency strains. However, V. A. Phillips[65,66] and Singhal and Martin[67] determined the two effects, namely coherency strengthening and order strengthening to be additive i.e., each mechanism contributing to the CRSS the value it would contribute if it were acting alone. Raynor and Silcock[68] attributed hardening of γ' containing alloys with high Ti/Al ratio mainly to order strengthening.

Chaturvedi and coworkers[69] explained the behaviour of Co-Ni-Cr-Ti alloys strengthened by γ' phase in the particle-shearing stage on the basis of Brown and Ham's model[54,91] of an order strengthening mechanism. Munjal and Ardell[70] observed that the strengthening of the Ni-Al alloys containing small γ' particles and small volume fractions of γ' to be primarily due to order strengthening in the

underaged condition. This was confirmed by Ardell[71] on the basis of temperature independence of precipitation hardening in the underaged Ni-Al alloys. Melander and Persson[72] concluded for Nimonic 80A, that order strengthening contributed about 60% to that portion of the strength attributable to the γ' precipitates in the underaged alloy and about 45% in the peak-aged alloy.

More recently, Chaturvedi and Han[73] determined that the yielding of underaged Inconel 718 occurs by shearing of the coherent ordered BCT - γ'' and ordered F.C.C. γ' precipitates by glide dislocations which move in pairs. They suggest that the yield strength of the material could be adequately accounted for mainly by the coherency hardening mechanism. Therefore, it seems that the applicability of a particular strengthening mechanism varies from one alloy system to another.

2.5.3 Non-deformable Particles

The particle cutting models agree that as the particles grow beyond a critical size, the dislocations may by-pass them by bowing. The Orowan bowing model[48] is generally considered to be most applicable for austenitic superalloys. This model is illustrated in Figure 4. The increment in flow stress $\Delta\tau$ due to bowing is given by consideration of the radius of curvature to which a flexible dislocation can be bent by an applied stress.

$$\Delta\tau\, b = \frac{T}{\rho} \qquad \ldots\ldots (37)$$

The minimum value of ρ is half the interparticle spacing of the particles, L and corresponds to $\theta = \frac{\pi}{2}$ as shown in Figure 2. Therefore, Equation (37) becomes

$$\Delta\tau b = \frac{2T}{L} \qquad \ldots\ldots (38)$$

T is often assumed to be equal to the line energy of the dislocation, roughly $\frac{Gb^2}{2}$.

Equation 38 has been modified by Ashby[74-76] assuming a bulging of dislocations between equally spaced particles. According to him, the bulging dislocation is in a critical configuration, requiring the maximum applied stress when the two arms of the dislocation, one on each side of the particle, first become parallel. The dislocations shown in Figures 5 and 6 are in this configuration. It can then be argued that at each particle a small forward displacement pulls out a dipole of width equal to the particle diameter, $2r_s$. The critical, or Orowan stress is then that stress which is just capable of elongating appropriate dipoles of width $2r_s$ spaced L apart. Thus, according to Ashby[74-76],

$$\tau_{edge} = \frac{1}{2\pi}\frac{Gb}{L}\ln\frac{2r_s}{r_o} \qquad \ldots\ldots (39)$$

and

$$\tau_{screw} = \frac{1}{2\pi(1-\nu)}\frac{Gb}{L}\ln\frac{2r_s}{r_o} \qquad \ldots\ldots (40)$$

where r_o is the inner cut-off radius, b the Burger's vector, G the matrix shear modulus and ν the Poisson's ratio.

FIGURE 4

THE OROWAN MECHANISM(77)

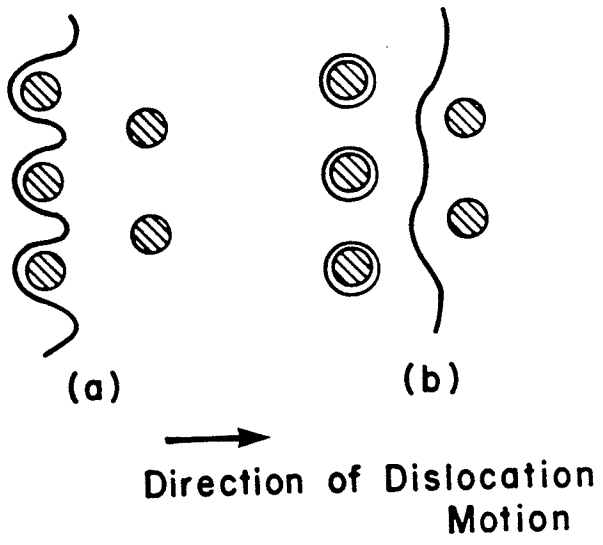

FIGURE 4

FIGURE 5

A DISLOCATION BENDING BETWEEN PARTICLES[74]

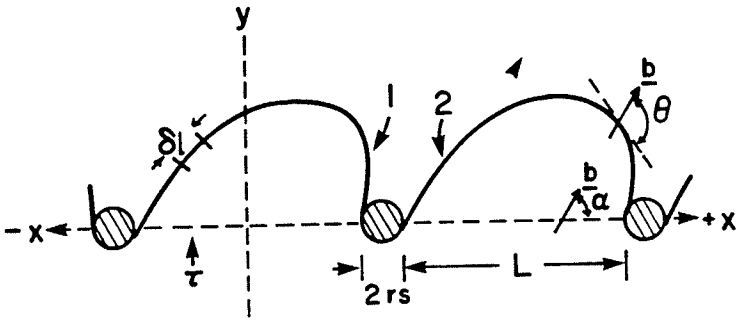

FIGURE 5

FIGURE 6

THE SHAPE OF AN EDGE, A MIXED, AND A SCREW DISLOCATION WHICH BULGE BETWEEN EQUALLY SPACED PARTICLES SUCH THAT THE ARMS ON EACH SIDE OF SINGLE PARTICLE ARE JUST PARALLEL[74]

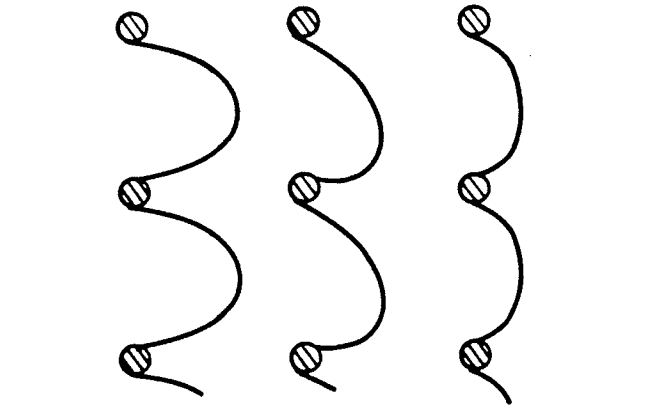

FIGURE 6

In reality, all the particles do not have the same spacing, and a distribution of particle spacings will exist. Kocks[78], and Foreman and Makin[52] have analysed the effect of random spacing. Every spacing between a pair of particles has its own passing stress. At a given applied stress, σ, a dislocation segment which has successfully bowed through one "transparent" spacing may find itself pressed against some others which may not be transparent. Kocks[78] and Foreman and Makin[52] have shown that extensive slip can first occur at the critical value of the applied stress, such that about one third of the spacings between the particles is transparent. If the critical configuration is that at which the angle ϕ between the two arms of dislocation is zero, then a statistical factor about 0.85 relates the macroscopic flow stress of the random array to the average local Orowan stress by the relation

$$\sigma = 0.85\tau \qquad \ldots\ldots (41)$$

$$\sigma_{edge} - \sigma_{matrix} = 0.85 \frac{Gb}{2\pi L} \ln \frac{2r_s}{r_o} \qquad \ldots\ldots (42)$$

$$\sigma_{screw} - \sigma_{matrix} = 0.85 \frac{Gb}{2\pi(1-\upsilon)L} \ln \frac{2r_s}{r_o} \qquad \ldots\ldots (43)$$

The particle size $2r_s$ is usually much smaller than their spacing L. When this is so, L should be replaced by $(L - 2r_s)$.

The Orowan looping process has been discussed by Hirsch and Humphreys[77]. They conclude that both edge and screw dislocations will bypass particles at the same stress. They have used the statistical theory of Kocks[78], and computer calculations of Foreman and Makin[52],

which show that the particle spacing L_o is 0.81 $N_A^{-1/2}$. Assuming the shape of the loop to be an ellipse, Hirsch and Humphreys[77] have determined the CRSS as follows.

$$\tau = \frac{0.81\ Gb}{2\pi L_o (1-\nu)^{1/2}} \ln \frac{2r_s}{r_o} \qquad \ldots\ldots (44)$$

The effect of dislocation self-interaction on the Orowan stress for collinear, impenetrable circular objects has been analyzed by Bacon et al[79]. They have developed an expression for the flow stress of a self-interacting dislocation moving through a random array of impenetrable obstacles.

$$\tau = \left(\frac{\ln 2r_s}{\ln L_o}\right)^{1/2} \frac{Gb}{2\pi L_o} \ln \frac{2r_s}{r_o} \qquad \ldots\ldots (45)$$

where $\frac{Gb}{L_o}$ is the classical Orowan value, $\ln \frac{2r_s}{r_o}$ accounts for the interactions over one bowing loop and $\left(\frac{\ln 2r_s}{\ln L_o}\right)^{1/2}$ describes the effect of mutual loop interactions and the randomness of the obstacle array.

3. EXPERIMENTAL PROCEDURES

3.1 PREPARATION OF ALLOYS

50 gm melts of Alloy A and Alloy B (Table 1) were made in an argon-arc furnace for study of hardness and structural changes. The alloying elements were 99.99% pure except for niobium which was 99.9% pure. The alloys always contained some carbon as an impurity. A positive pressure (250 mm Hg) of argon was maintained in the furnace during the melting process. The ingots were 1 cm in thickness and 8 cm in length.

650 gm melts of Alloy A were made in an induction furnace for study of tensile properties. Here also, a positive pressure of argon was maintained as described above. All the elements except aluminum were melted in a zirconia crucible. Aluminum was held in a hopper inside the furnace and was added only after complete melting of the other elements. The melt was then sand cast into ingots 2.6 cm^2 in area of cross-section and 10 cm in length.

3.2 HEAT TREATMENT OF ALLOYS

The ingots were homogenized at 1473K and cold-rolled/cold-swaged with frequent intermediate anneals at 1473K. The final products of the alloys melted in the argon arc furnace were rods 5 mm in diameter. These rods were used for hardness specimens, extractions replicas and for the electrolytic extraction of precipitates for determination of volume fraction of precipitates and X-ray diffraction.

TABLE 1

COMPOSITIONS OF EXPERIMENTAL ALLOYS
(Weight %)

ALLOY A	40.0 Co	38.0 Ni	17.0 Cr	3.5 Nb	1.5 Al
ALLOY B	40.0 Co	38.0 Ni	17.0 Cr	3.5 Ti	1.5 Al

The alloy melted in the induction furnace (Alloy A) was given similar treatment as described in the previous paragraph to produce strips 1mm thick. Some strips were further rolled with intermediate anneals to produce strips 0.22mm thick.

The final solution treatment temperature was always 1473K. All heat treatment were carried out with specimens sealed in argon-filled vycor capsules followed by a rapid quench in iced brine.

3.3 HARDNESS MEASUREMENTS

Hardness specimens (3mm in thickness and 5mm in diameter) were aged between 873 and 1073K for various lengths of times and the hardness values were determined using a Vickers Hardness Tester. Each value was obtained as an average of twenty measurements.

3.4 VOLUME FRACTION OF GAMMA PRIME PRECIPITATE AND X-RAY DIFFRACTION ANALYSIS

The volume fraction of γ' in the aged samples was measured by an extraction method. Extraction of γ' precipitate was performed by anodic dissolution of the matrix using an electrolyte composed of 1 pct ammonium sulfate and 1 pct. citric acid in water[80]. The electrolysis was carried out at 8 volts. It is known[81] that the volume fraction of γ' can be taken as the weight fraction of γ' and that the extraction method is more reliable than replica electron microscopy, in view of the large scatter in the latter technique.

Precise lattice parameters of filed and annealed specimens as well as extracted precipitates were detemined using Co-K_α radiation and the Nelson-Riley technique.

3.5 ELECTRON MICROSCOPY

3.5.1 Specimen Preparation

Thin foils of electron microscopy were prepared by a modified Bollmann technique using a solution of 10 pct perchloric acid in methanol at 233 to 223K.

Extraction replicas of various aged specimens were also prepared. Polished specimens were etched in a solution of 50 pct lactic acid, 33 pct hydrocloric acid and 10 pct nitric acid to reveal the γ' particles, which were then shadowed with carbon at 2×10^{-5} mm Hg pressure. The carbon films were loosened by electrolysis in a solution of 10 pct sulphuric acid in methanol, and were subsequently collected on copper grids.

3.5.2 Electron Microscopy Procedure

The γ' particle sizes were determined using dark field micrographs obtained with (100) superlattice spots, the foil plane being (100).

In addition to the morphological studies related to γ' particles, the grain boundary precipitates (such as carbides, sigma phase, etc.) were also analysed with respect to size, shape and composition.

Systematic investigation of the γ' particle/dislocation interactions were carried out using thin foils prepared from aged and deformed tensile specimens.

3.6 TENSILE TESTS

3.6.1 Tensile Specimen Preparation

Flat tensile specimens (Alloy A) of two different thicknesses (1mm and 0.22mm) were prepared. They were all of 35mm gauge length and 12mm gauge width (Figure 7).

The grain size of the 1mm thick tensile specimens was 56×10^{-4}cm The grain size of the 0.22mm thick tensile specimens was 21×10^{-4}cm The grain sizes were all measured subsequent to solution treatment at 1473K and checked after aging to various times at 1073K. Extreme care was taken to maintain the same final grain size in the specimens of the same thickness.

The extracted γ' precipitate was analysed by the available atomic absorption technique. Only Ni, Co and Cr could be analysed, and therefore, the balance was deduced to be (Nb and Al) content. It has been observed[80] that the ratio of Ti and Al in γ' is the same as that present in the parent alloy. This observation was extended to the experimental alloy (Alloy A) to calculate the amount of Nb and Al. From this analysis, the composition of the residual matrix (i.e. the composition of matrix from which all of γ' phase was precipitated)

FIGURE 7

TENSILE SPECIMEN

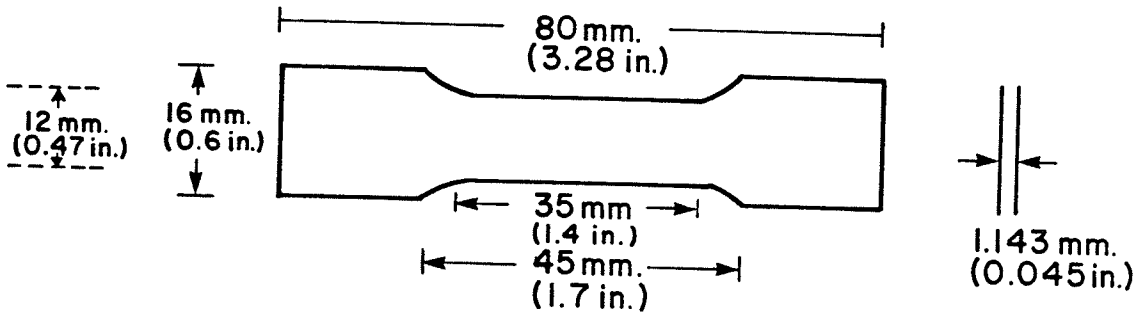
80 mm.
(3.28 in.)
12 mm.
(0.47 in.)
16 mm.
(0.6 in.)
35 mm
(1.4 in.)
45 mm.
(1.7 in.)
1.143 mm.
(0.045 in.)

FIGURE 7

was determined. Tensile specimens with this composition (Co - 42.9 w/o, Ni - 36.30 w/o, Cr - 18.43 w/o, Nb - 1.73 w/o and Al - 0.74 w/o) were prepared and tested in the solution treated condition.

3.6.2 Tensile Test Procedure

The specimens were tested in uniaxial tension at room temperature on an Instron testing machine at a constant strain rate of 3×10^{-3} min^{-1}.

The 0.2 pct proof stress was determined for each 1mm. thick tensile specimen. The 0.22mm thick tensile specimens were deformed to 1 - 3% plastic strain and were used subsequently for electron microscopy.

3.6.3 Special Tensile Tests

Several tensile specimens were solution treated at 1473K and aged at 1073K for 1, 2 and 16 hours. Thereafter, the specimens were tested in uniaxial tension at 77, 177, 293 and 373K on an Instron testing machine at a constant strain rate of 3×10^{-3} min^{-1}. Two strain gauges (one on the front surface and one on the rear surface) were mounted on each specimen to eliminate ambiguity in strain readings due to any elastic deformation of the frame of the machine. Adequate care was taken to ensure stability of the strain gauges at the test temperature. Modulus corrected 0.2% yield strength values normalized with respect to the 77K data were determined.

4. EXPERIMENTAL RESULTS

4.1 HARDNESS MEASUREMENTS

The aging kinetics of the two alloys were followed by hardness measurements and the variation in hardness with aging time at 873, 973 and 1073K are shown in Figures 8 and 9. It is seen that both the alloys exhibit normal aging behaviour i.e., as the temperature of aging is reduced, the time required to attain both the peak hardness value and a particular hardness value is increased.

4.2 VARIATION OF VOLUME FRACTION OF γ' PRECIPITATE WITH TIME

The results of volume fraction analysis of γ' precipitate are shown in Figure 10, which is a plot of volume fraction of γ' against aging time of Alloy A at 1073K. It is seen that the volume fraction increases up to 10 hours of aging and then remains constant up to 1000 hours of aging. This would suggest that the growth of γ' particles might follow "Ostwald Ripening"[35] or the Lifshitz-Wagner theory of diffusion controlled coarsening[36-38]. A detailed analysis of growth of γ' particles is presented in Section 4.5.

4.3 VARIATION OF THE LATTICE PARAMETERS OF γ AND γ' WITH TIME

The variation of the lattice parameter of γ (matrix) and γ' (extracted precipitate) for Alloy A is shown in Figure 11. The lattice parameter of the matrix (i.e., solution-treated and quenched alloy) was 0.3558nm. The lattice parameter of the matrix decreased

FIGURE 8

THE EFFECT OF AGING ON THE HARDNESS VALUES OF SPECIMENS OF ALLOY A AGED AT 873K, 973K, and 1073K

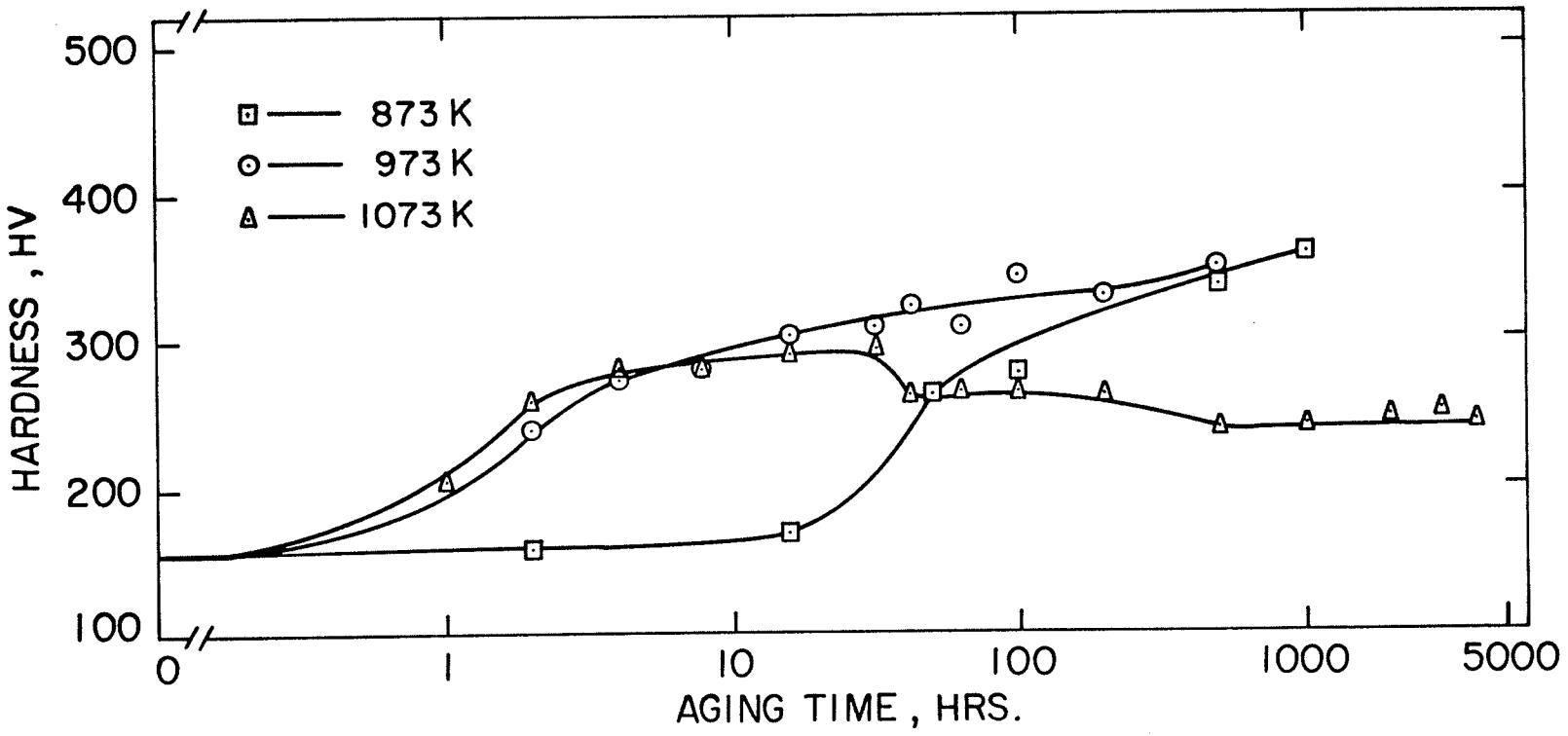
500
400
300
200
100
HARDNESS , HV
873 K
973 K
1073 K
0
1
10
100
1000
5000
AGING TIME , HRS.

FIGURE 8

FIGURE 9

THE EFFECT OF AGING ON THE HARDNESS VALUES OF SPECIMENS OF ALLOY B AGED AT 873K, 973K, and 1073K

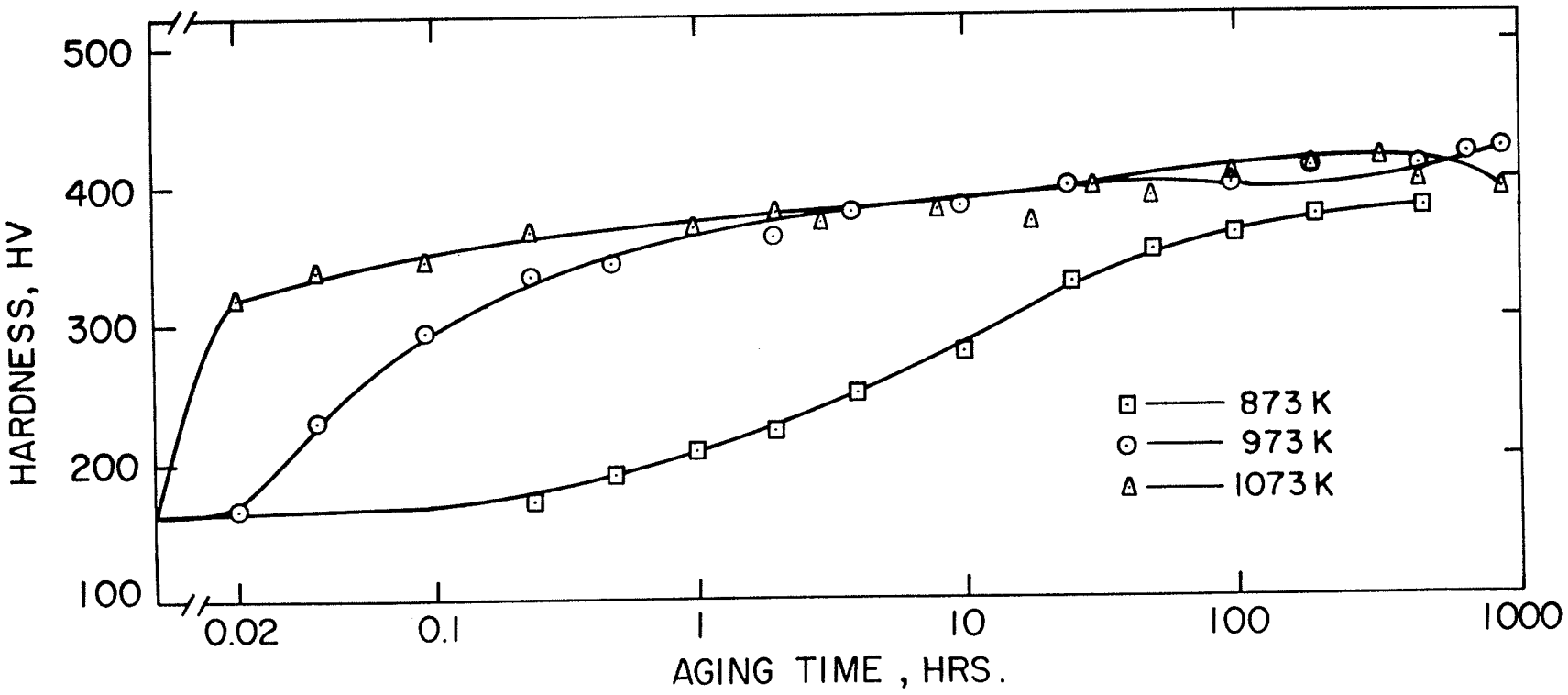
500
400
300
200
100
HARDNESS, HV
0.02
0.1
1
10
100
1000
AGING TIME , HRS.
873 K
973 K
1073 K

FIGURE 9

FIGURE 10

VARIATION OF VOLUME FRACTION OF γ' PRECIPITATE

WITH TIME DURING AGING OF ALLOY A

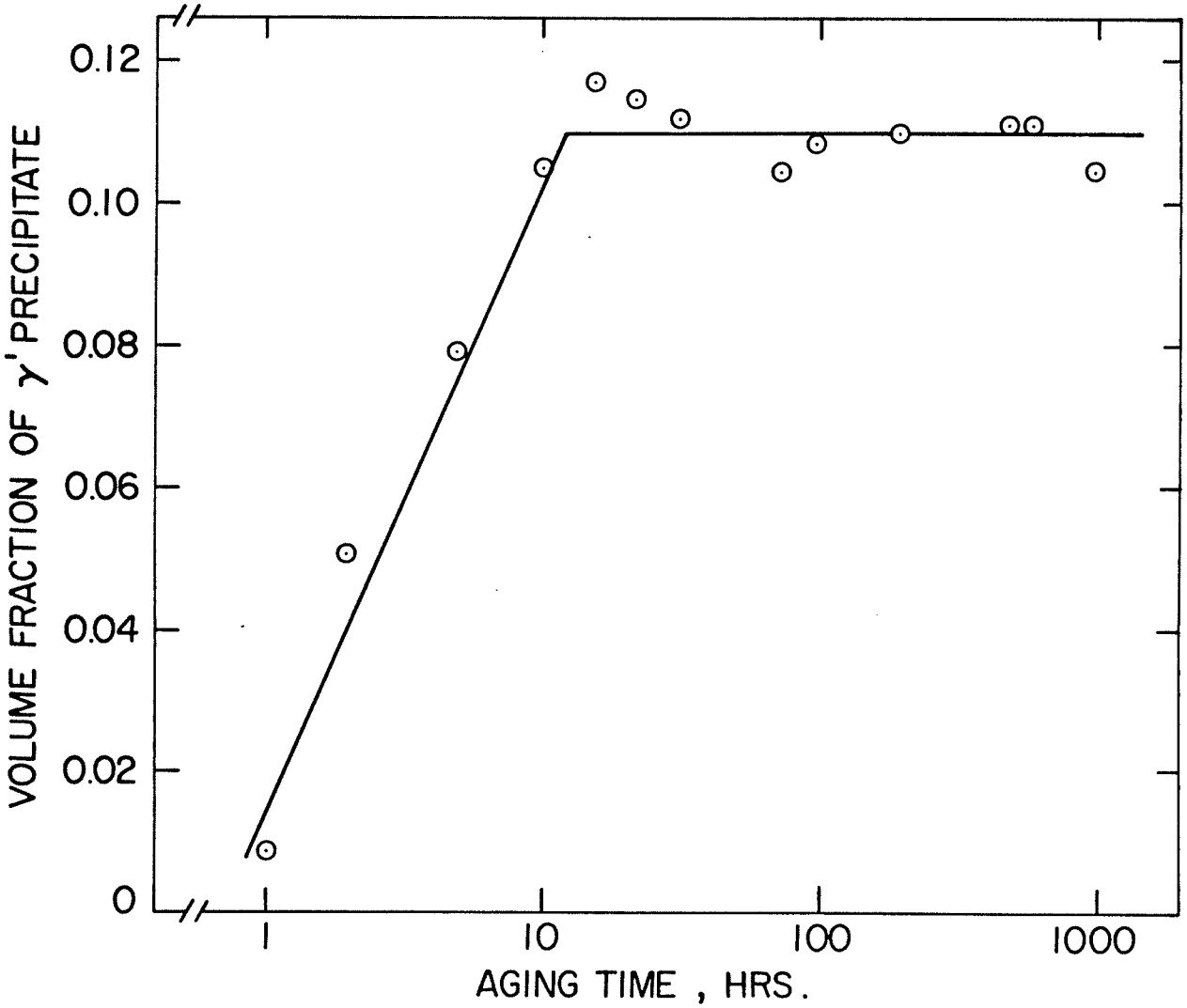
VOLUME FRACTION OF γ' PRECIPITATE
0.12
0.10
0.08
0.06
0.04
0.02
0
1
10
100
1000
AGING TIME , HRS.

FIGURE 10

FIGURE 11

VARIATION OF LATTICE PARAMETERS OF γ AND γ'

WITH TIME DURING THE AGING OF ALLOY A

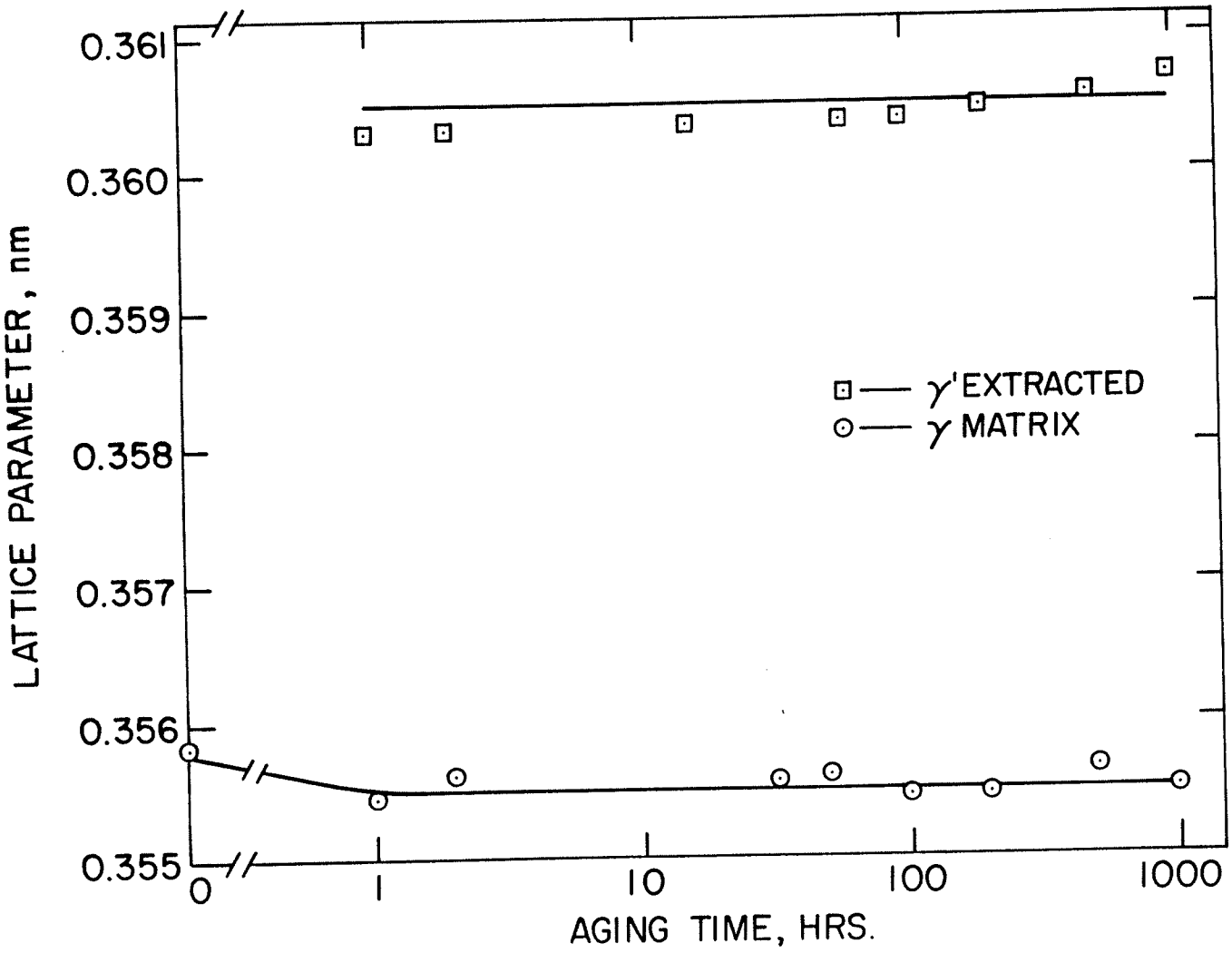
0.361
0.360
0.359
0.358
0.357
0.356
0.355
LATTICE PARAMETER, nm
γ'EXTRACTED
γ MATRIX
0
1
10
100
1000
AGING TIME, HRS.

FIGURE 11

on aging to 1 hour at 1073K and thereafter remained almost constant at 0.3555nm on aging up to 1000 hours. The lattice parameter of the extracted precipitate was constant althrough the aging period at 0.3603nm.

4.4 ELECTRON MICROSCOPY OF PRECIPITATION

The structural changes on aging were determined mainly by electron microscopy. The major precipitation reaction at all the aging temperatures was the formation of γ' phase which has an ordered Cu_3Au type F.C.C. structure. A very limited amount of carbide precipitate within the grains as well as at the grain boundaries, and sigma phase at the grain boundaries were also observed. The precipitation and growth of these phases is described below.

4.4.1 Early Stages of Precipitation

In the early stages of aging, the presence of γ' particles gave rise to a modulated matrix structure (Figure 12) and superlattice spots in the diffraction pattern. The earliest stage when the individual γ' particles could be clearly seen was on aging for two hours at 1073K. A dark field micrograph with the (100) superlattice spot of γ' is shown in Figure 13. The particles are about 4nm in radius and they seem to be of mixed shape, i.e., cubic as well as spherical. In certain areas, they seem to be aligning themselves in the <100> directions.

As aging was continued, the γ' particles developed a well defined cubic shape and aligned themselves along <100> directions.

FIGURE 12

MODULATED MATRIX STRUCTURE IN SPECIMEN OF ALLOY A AGED FOR 1 HOUR AT 1073K

FIGURE 13

DARK-FIELD MICROGRAPH SHOWING γ' PARTICLE IN SPECIMEN OF ALLOY A AGED FOR 2 HOURS AT 1073K

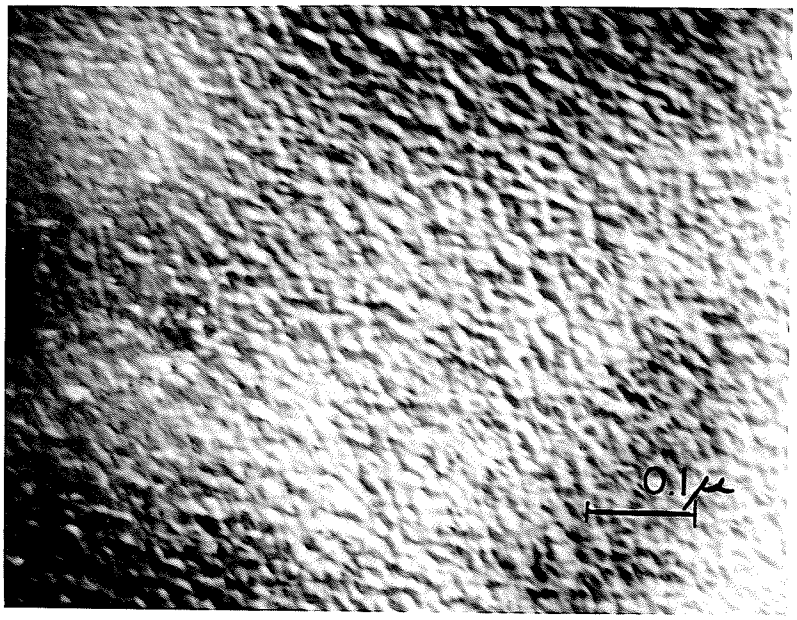

FIGURE 12

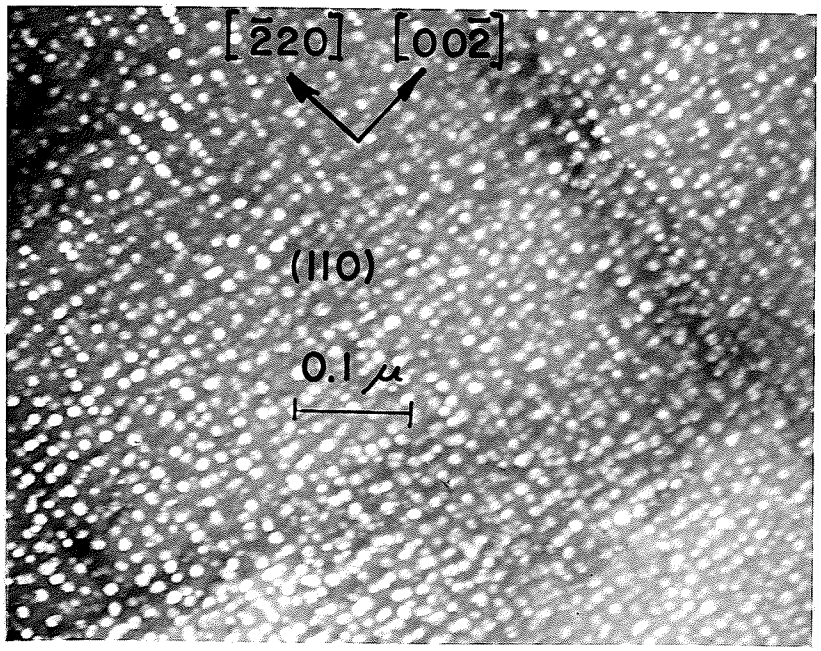

FIGURE 13

An example of this is shown in Figure 14 which is the microstructure of a specimen of Alloy A aged for 64 hours at 1073K.

4.4.2 Overaging

On continued aging, γ' particles start to agglomerate while continuing to be aligned along <100> directions (Figure 15). At the same time, these particles start to lose coherency and start to reveal extinction fringes due to depth periodicity of the transmitted beams at the precipitate/matrix interface. Also, in several of the precipitates, lines of contrast perpendicular to the extinction fringes are visible which are structural dislocations introduced in the interface to reduce the strain energy due to misfit between the precipitate and the matrix. Such a feature can be distinctly seen in foils of Alloy A aged to 3000 hours at 1073K (Figure 16). The transition point of coherent to noncoherent precipitate could not be determined accurately. However, such networks of interfacial dislocations were not seen in specimens aged for less than 1000 hours at 1073K.

Aging was continued up to 4000 hours at 1073K but the structure of γ' particles remained ordered F.C.C. Nonetheless, further coarsening occurred during the aging to 4000 hours, showing merging of two particles (Figure 17), and subsequently four particles into shapeless masses (Figures 18 and 19) with distinct walls of dislocations around them.

FIGURE 14

DARK-FIELD MICROGRAPH SHOWING γ' PARTICLES IN SPECIMEN OF ALLOY A AGED FOR 64 HOURS AT 1073K

FIGURE 15

DARK-FIELD MICROGRAPH SHOWING γ' PARTICLES IN SPECIMEN OF ALLOY A AGED FOR 200 HOURS AT 1073K

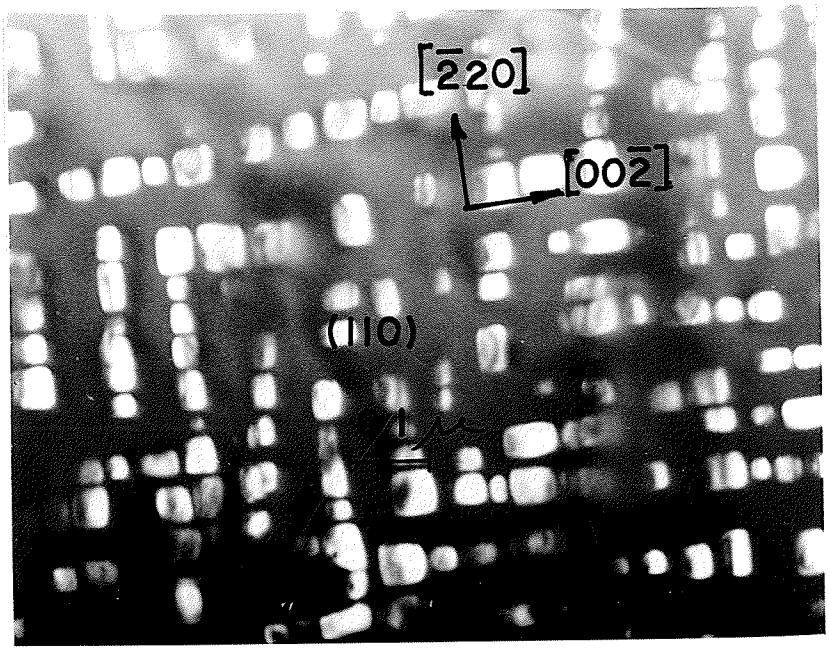

FIGURE 14

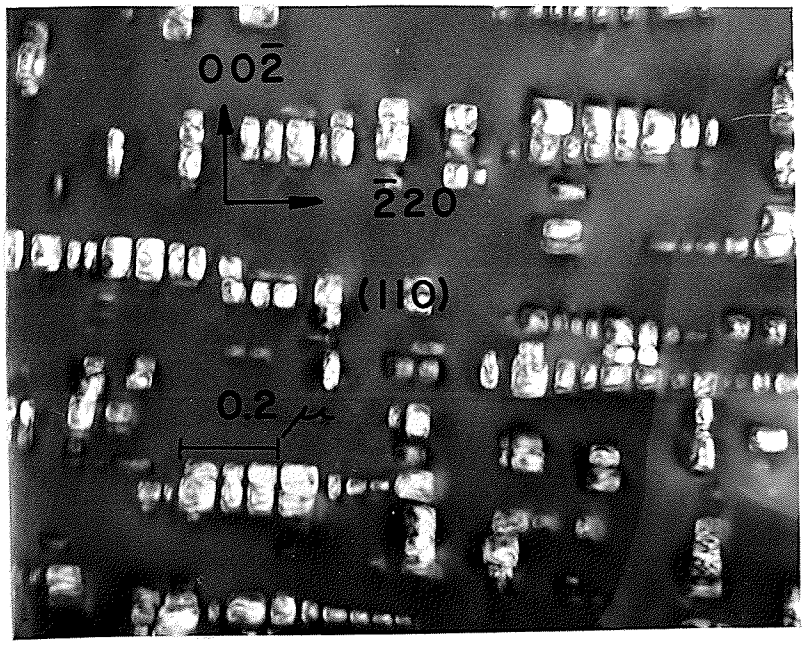

FIGURE 15

FIGURE 16

DISLOCATIONS AT THE PARTICLE/MATRIX
INTERFACE IN SPECIMEN OF ALLOY A
AGED FOR 3000 HOURS AT 1073K

FIGURE 17

AGGLOMERATION OF γ' PARTICLES IN SPECIMEN OF
ALLOY A AGED FOR 4000 HOURS AT 1073K

FIGURE 16

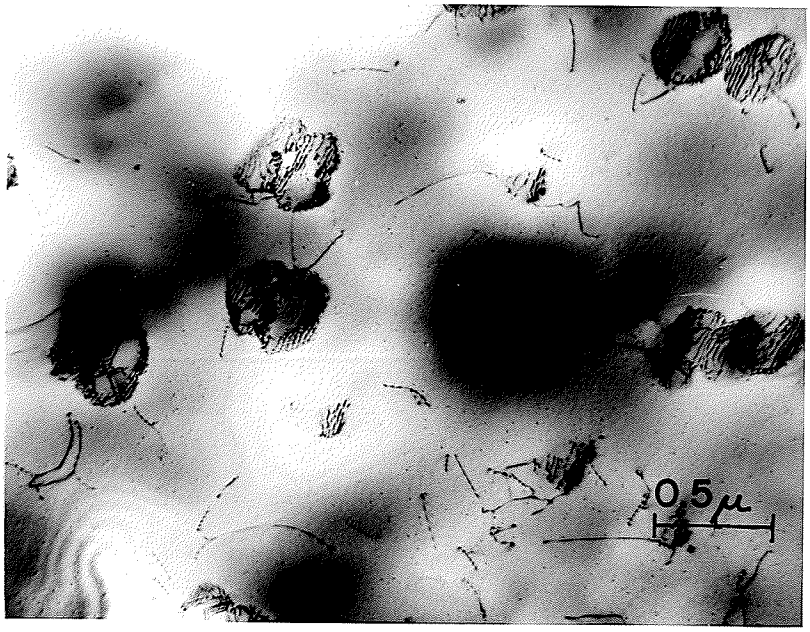

FIGURE 17

FIGURE 18

AGGLOMERATION OF γ' PARTICLES IN SPECIMEN OF ALLOY A AGED FOR 4000 HOURS AT 1073K

FIGURE 19

AGGLOMERATION OF γ' PARTICLES IN SPECIMEN OF ALLOY A AGED FOR 4000 HOURS AT 1073K

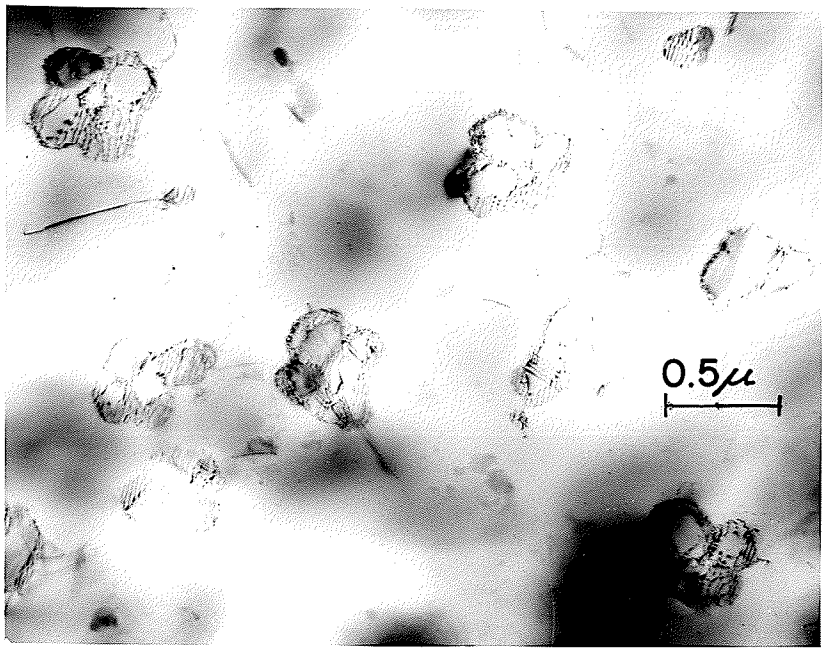

FIGURE 18

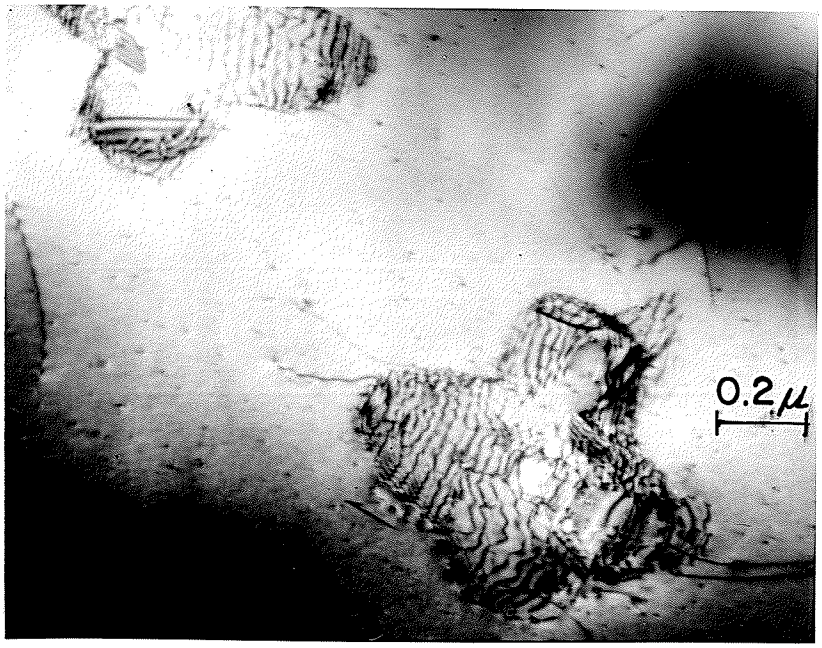

FIGURE 19

4.4.3 Carbide Precipitation

The limited amount of carbon which was present as an impurity gave rise to NbC or TiC precipitation depending on whether it was Alloy A or Alloy B. The presence of these Carbide phases was confirmed by X-ray powder diffraction analysis, and they appeared mainly at the grain boundaries as shown in Figure 20. The presence of the grain boundary precipitate was always accompanied by a precipitate-denuded zone around the grain boundary (Figure 20). Qualitatively, the width of the denuded zone was directly proportional to the size of the NbC particles at the grain boundaries i.e., the width of the denuded zone associated with larger carbide particles was always greater than that associated with smaller NbC particles.

The size of the grain boundary carbide was observed to increase with continued aging as did the width of the associated denuded zone around the grain boundary. Typical values of the width of γ' precipitate denuded zone determined in thin foils of Alloy A with (100) orientation are given in Table 2.

4.4.4 Stacking Fault Precipitation of Carbide and Associated Ni_3Nb Precipitation

In addition to grain boundary precipitation, NbC was also observed to occur, occasionally, in association with stacking faults. An example of this is shown in Figure 21. The dark-field structure was obtained with a (002) reflection in a near two beam condition. The nature of the stacking fault was determined by analysing the

TABLE 2

TYPICAL VALUES OF WIDTH OF γ' PRECIPITATE DENUDED ZONE ON EITHER SIDE OF GRAIN BOUNDARY IN THIN FOILS OF ALLOY A

Aging Treatment Subsequent to Solution Treatment	Approximate Width, μm
973K/200 hours	0.04
973K/500 hours	0.06
1073K/11 hours	0.13
1073K/100 hours	0.15
1073K/200 hours	0.16
1073K/500 hours	0.33
1073K/1000 hours	0.40
1073K/3000 hours	0.60

FIGURE 20

PRECIPITATE-DENUDED ZONE IN SPECIMEN
OF ALLOY A AGED FOR 1 HOUR AT 1073K

FIGURE 21

STACKING FAULT PRECIPITATION OF NbC IN
SPECIMEN OF ALLOY A AGED FOR 10 HOURS AT 1073K

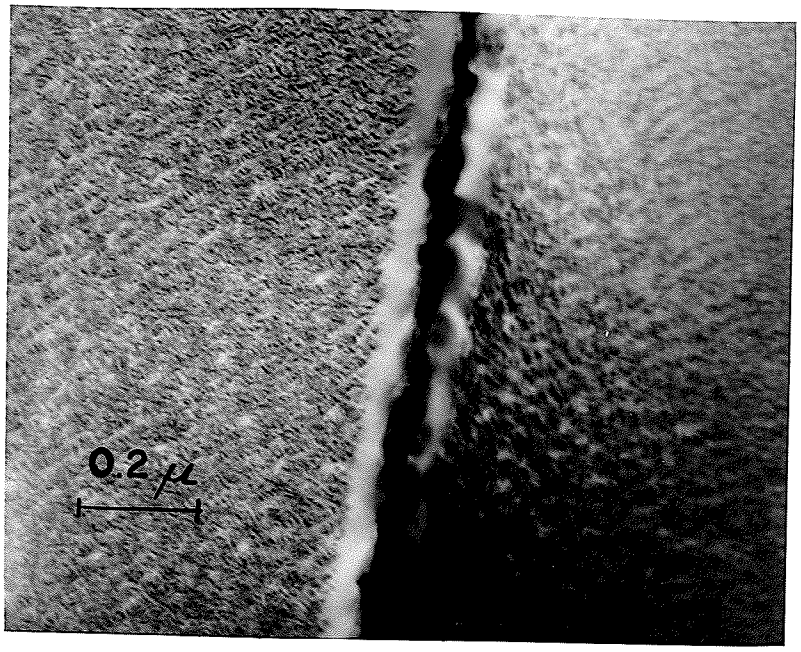

FIGURE 20

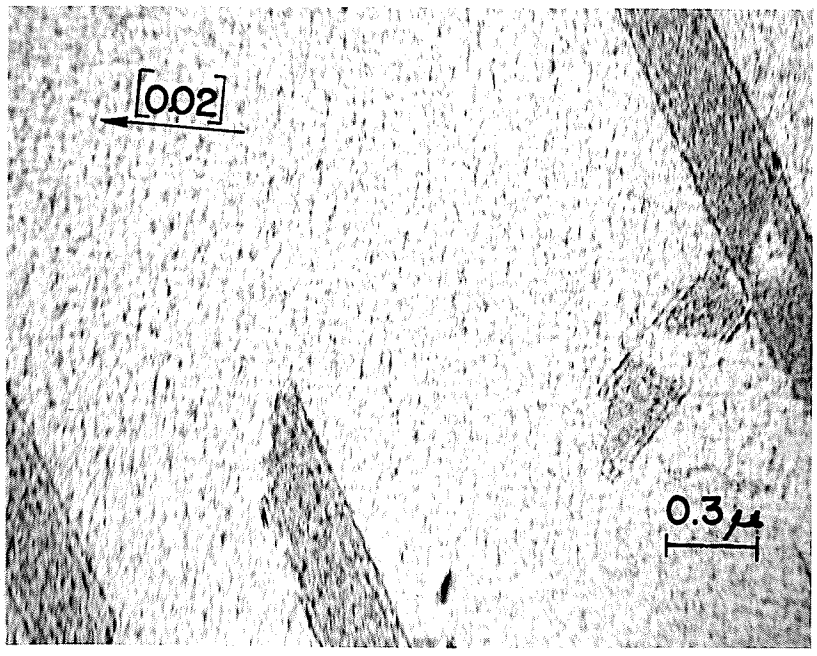

FIGURE 21

dark field image and by Gevers rule[82]. They were determined to be extrinsic in nature, lie on {111} matrix planes and were similar to those observed in other superalloys[83] and austenitic stainless steels[84,85].

On continued aging, stacking fault precipitation of NbC was not observed but laths of orthorhombic β-Ni_3Nb precipitate were observed. Figure 22 is a bright field photograph and Figure 23 is its dark field image taken with (012) reflection of β-Ni_3Nb phase. It is possible that this β-Ni_3Nb phase is produced by the transformation of NbC as observed by Chung and Chaturvedi[86].

4.4.5 Sigma Phase Precipitation

Occasionally, tetragonal sigma phase was also present at the grain boundaries in specimens of Alloy A aged for over 1000 hours at 1073K. An example of this phase in a specimen aged for 2000 hours is shown in Figure 24. The lattice parameters, by electron diffraction were calculated to be a_o = 0.8895nm and c_o = 0.4656nm. These were confirmed by X-ray powder diffraction data and are in close agreement with those of Cr-Co sigma phase[87].

4.4.6 Discontinuous Precipitation

Discontinuous precipitation of γ' phase was observed as a localized phenomenon in thin foils of both Alloy A and B aged to various times at 1073K. Figure 25 shows the bright-field structure of such a feature in Alloy A aged for 3 hours at 1073K. The thin

FIGURE 22

BRIGHT-FIELD MICROGRAPH OF ORTHORHOMBIC β-Ni_3Nb IN A SPECIMEN OF ALLOY A AGED FOR 64 HOURS AT 1073K

FIGURE 23

DARK-FIELD MICROGRAPH OF ORTHORHOMBIC β-Ni_3Nb IN FIGURE 22

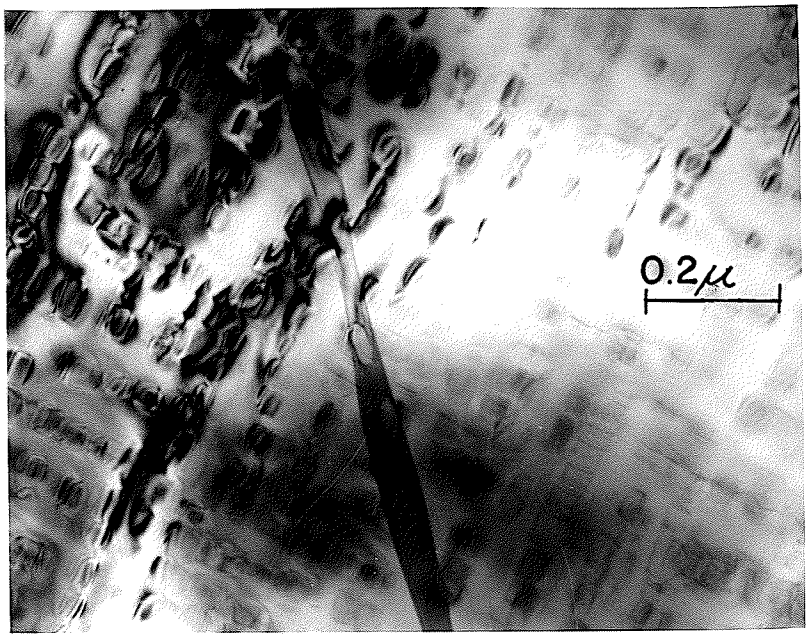

FIGURE 22

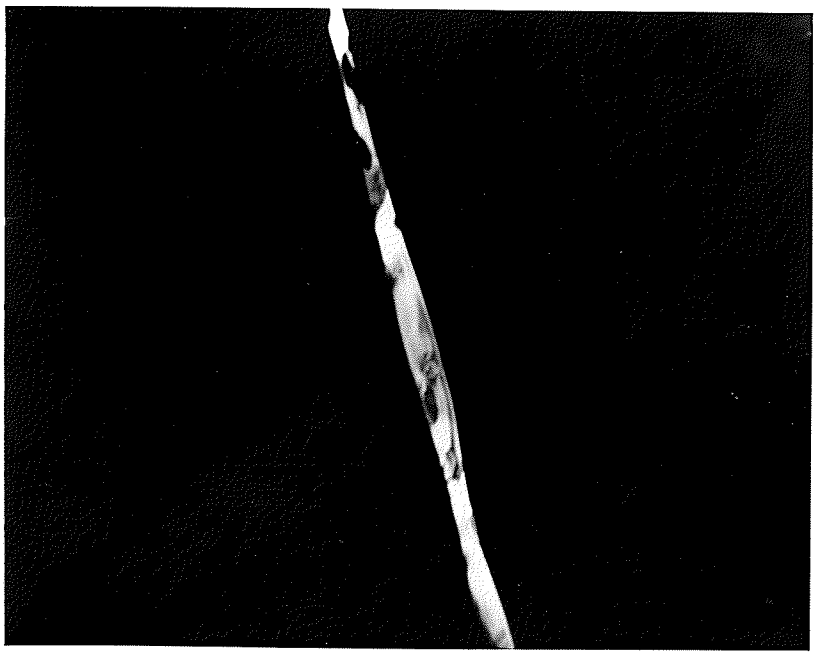

FIGURE 23

FIGURE 24

DARK-FIELD MICROGRAPH OF Cr-Co SIGMA PHASE IN SPECIMEN OF ALLOY A AGED FOR 2000 HOURS AT 1073K

FIGURE 25

BRIGHT-FIELD MICROGRAPH OF DISCONTINUOUS PRECIPITATION OF γ' IN SPECIMEN OF ALLOY A AGED FOR 3 HOURS AT 1073K

FIGURE 24

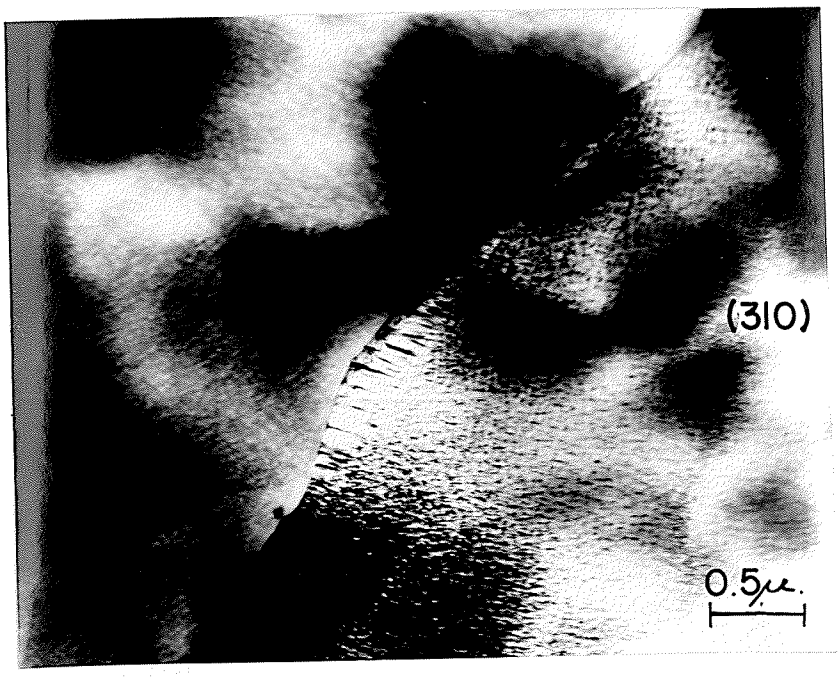

FIGURE 25

foil normal of the specimen is near [310]. Figure 26 and 27 show the dark-field structures taken with (001) superlattice reflection of γ' precipitate at two different magnifications.

Figure 28 is a bright-field electron micrograph of a thin foil of Alloy B aged for 210 hours at 1073K. The micrograph also shows a discontinuous precipitation. The precipitate particle was identified to be γ'.

These micrographs demonstrate the following:

(a) The γ' precipitates form in these localized regions by discontinous precipitation;

(b) Such localized grain boundary regions are generally devoid of carbide precipitates, or have carbide precipitates of relatively small size;

(c) The γ' precipitates formed grew into each other; and

(d) The above phenomenon appears at grain boundary with sharp corner, and appears to be accompanied by "straightening" of the curves in the grain boundary on either side of the sharp corner, as in Figures 25 and 26 (straight portion of grain boundary indicated by an arrow in Figure 26).

4.5 COARSENING OF γ' PRECIPITATE

The growth characteristics of γ' particles were studied with particular interest in the application of the Lifshitz-Wagner

FIGURE 26

DARK-FIELD MICROGRAPH OF SUPERLATTICE (100) SPOT
SHOWING DISCONTINUOUS PRECIPITATION OF γ' AS IN FIGURE 25

FIGURE 27

DARK-FIELD MICROGRAPH AS IN FIGURE 26
BUT AT A HIGHER MAGNIFICATION

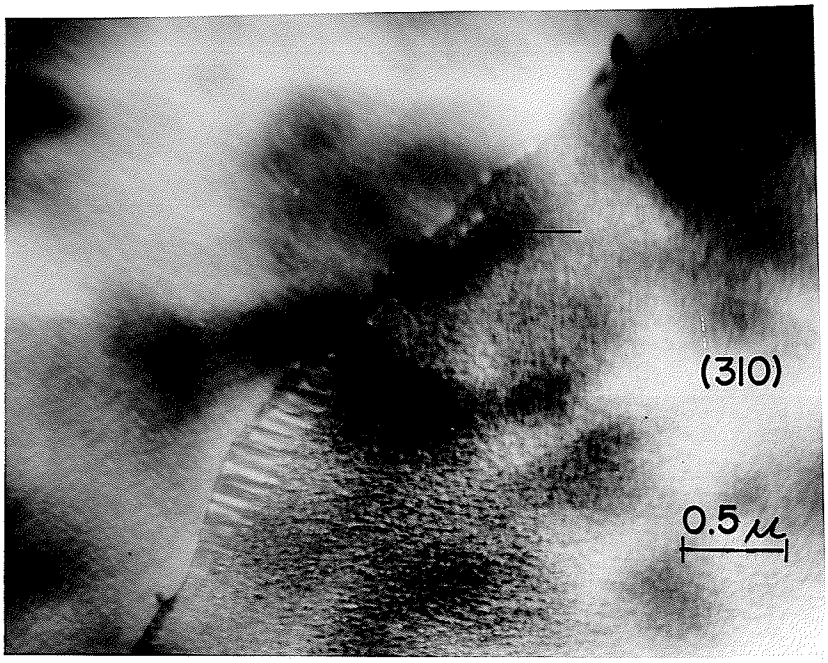

FIGURE 26

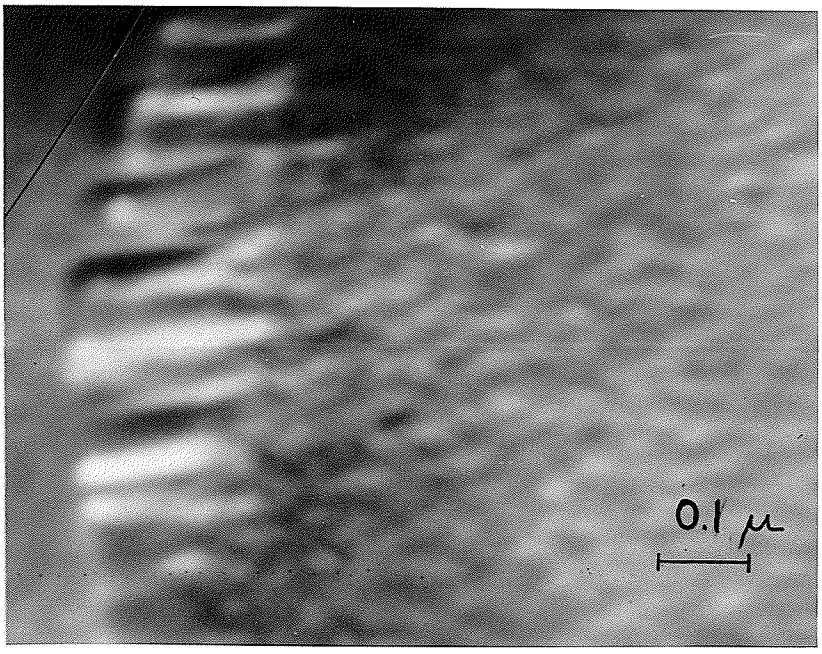

FIGURE 27

FIGURE 28

BRIGHT-FIELD MICROGRAPH OF DISCONTINUOUS PRECIPITATION OF γ'

IN A SPECIMEN OF ALLOY B AGED FOR 210 HOURS AT 1073K

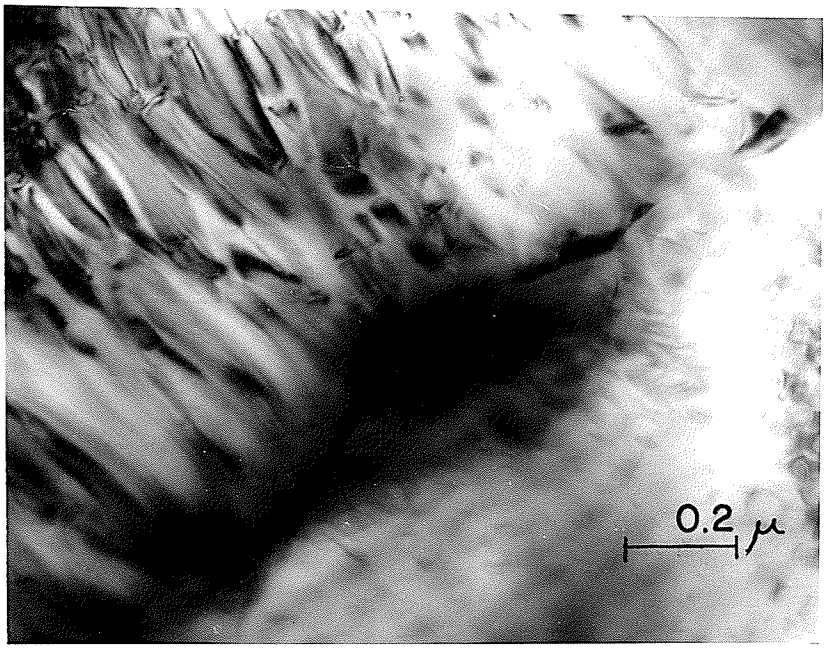

FIGURE 28

theory of diffusion controlled coarsening. As discussed in Section 2.4.1, according to this theory, the size of cubic precipitate particle follows the relationship[40,88,89]

$$\bar{a}^3 - \bar{a}_o^3 = \frac{64\delta D C_e V_m^2 t}{9RT} \qquad \ldots\ldots (3)$$

where,

$\bar{a}$ = average cube edge length of the particle after time t,

$\bar{a}_o$ = average cube edge length at the start of coarsening process,

δ = interfacial free energy of the matrix/particle interface,

V_m = molar volume fraction of the precipitate,

C_e = concentration of solute in equilibrium with a particle of infinite radius,

R = gas constant, and

T = absolute temperature.

The above expression can be rewritten as: $a^3 - a_o^3 = k't$

To evaluate the growth kinetics of γ' in Alloy A its particle size was measured in specimens aged for various times at 1073K. These measurements were made in thin foils mainly in $\{100\}$ orientation and occasionaly in $\{110\}$ orientation where cube edge only along <100> direction was measured. The edge length of cubes, a was plotted against the cube root of aging time t. This plot is a straight line (Figure 29), and suggest that the growth of γ' particles follows the Lifshitz-Wagner theory of diffusion controlled growth. It should be noted that the value of a at t = 0 is not zero, which suggests that the nucleation of γ' had occured before the measurements were made, as observed in other alloys also[86,90].

FIGURE 29

VARIATION OF MEAN γ' PARTICLE SIZE WITH AGING TIME FOR SPECIMENS OF ALLOY A AT 1073K

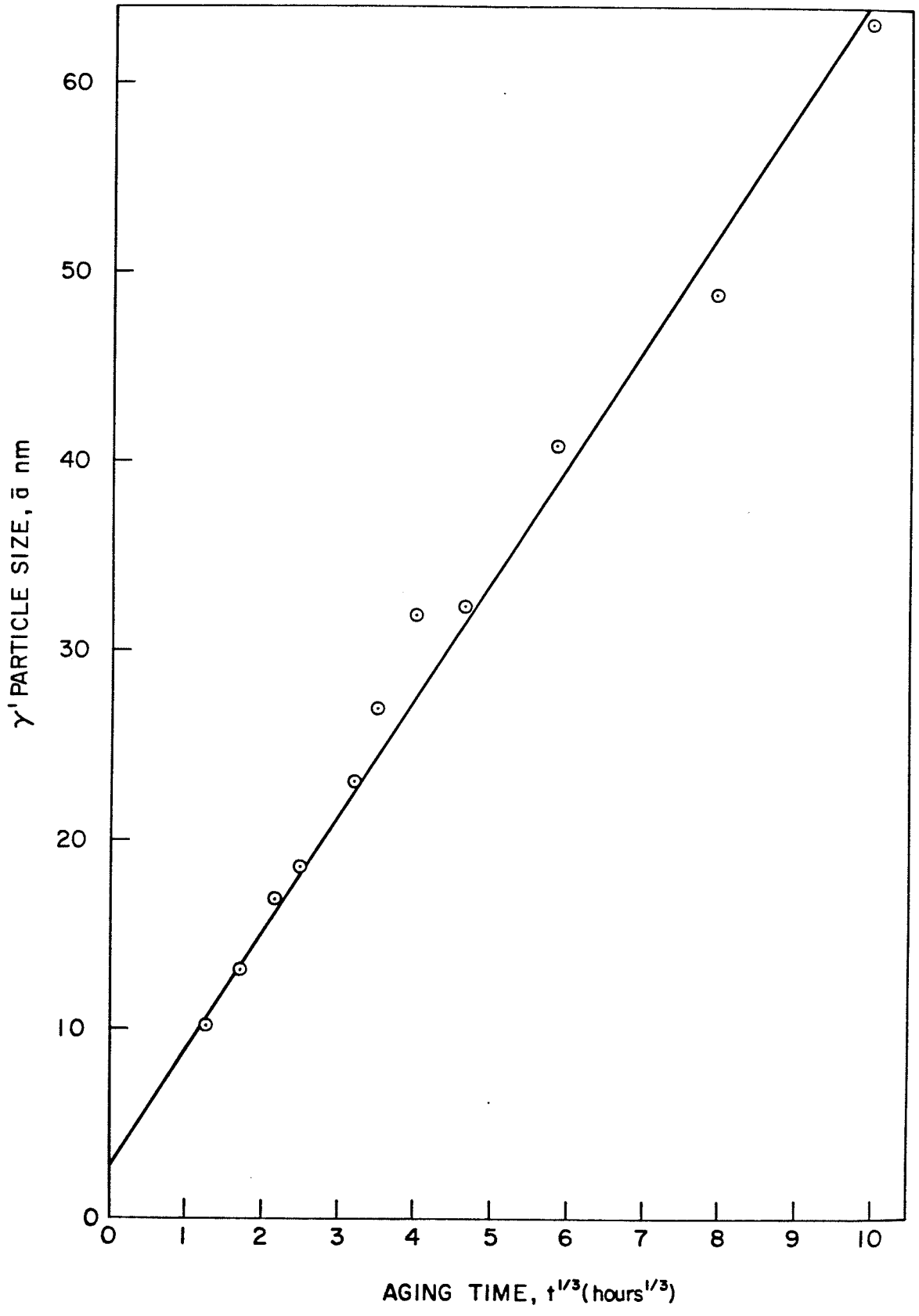
γ' PARTICLE SIZE, ā nm
0
10
20
30
40
50
60
0
1
2
3
4
5
6
7
8
9
10
AGING TIME, t^1/3 (hours^1/3)

FIGURE 29

4.6 DEFORMATION TESTS

The deformation mechanisms in Alloy A were studied by (1) room temperature tensile testing of specimens aged at 1073K, (2) examination of the deformed structure of specimens aged at 1073K, and (3) tensile testing of underaged and peak-aged specimens in 77-373K temperature range.

4.6.1 Room Temperature Tensile Tests

The 0.2% yield strength values of specimens aged for various lengths of time at 1073K were determined, and the aging curve obtained is shown in Figure 30. This exhibits a classical aging behaviour which is in agreement with the hardness-aging time curve shown in Figure 8. It is seen that the peak strength is attained at approximately 32 hours of aging at that temperature. Incremental yield strength values due to γ' precipitation were determined by subtracting the 0.2% yield strength σ_o, of the matrix from the yield strength values σ_y obtained for aged specimens.

The value of σ_o was determined as follows. The composition of γ' precipitate was determined using the Atomic Absorption Spectrometer. From the data obtained and assuming[80] niobium and aluminum to be partitioned in the same ratio as in the original alloy, the composition of the residual matrix was determined to be:

	Cobalt	Nickel	Chromium	Niobium	Aluminum
w/o	38.87	16.01	16.85	-------Balance------	

FIGURE 30

THE EFFECT OF AGING ON THE YIELD STRENGTH OF SPECIMENS OF ALLOY A AGED AT 1073K

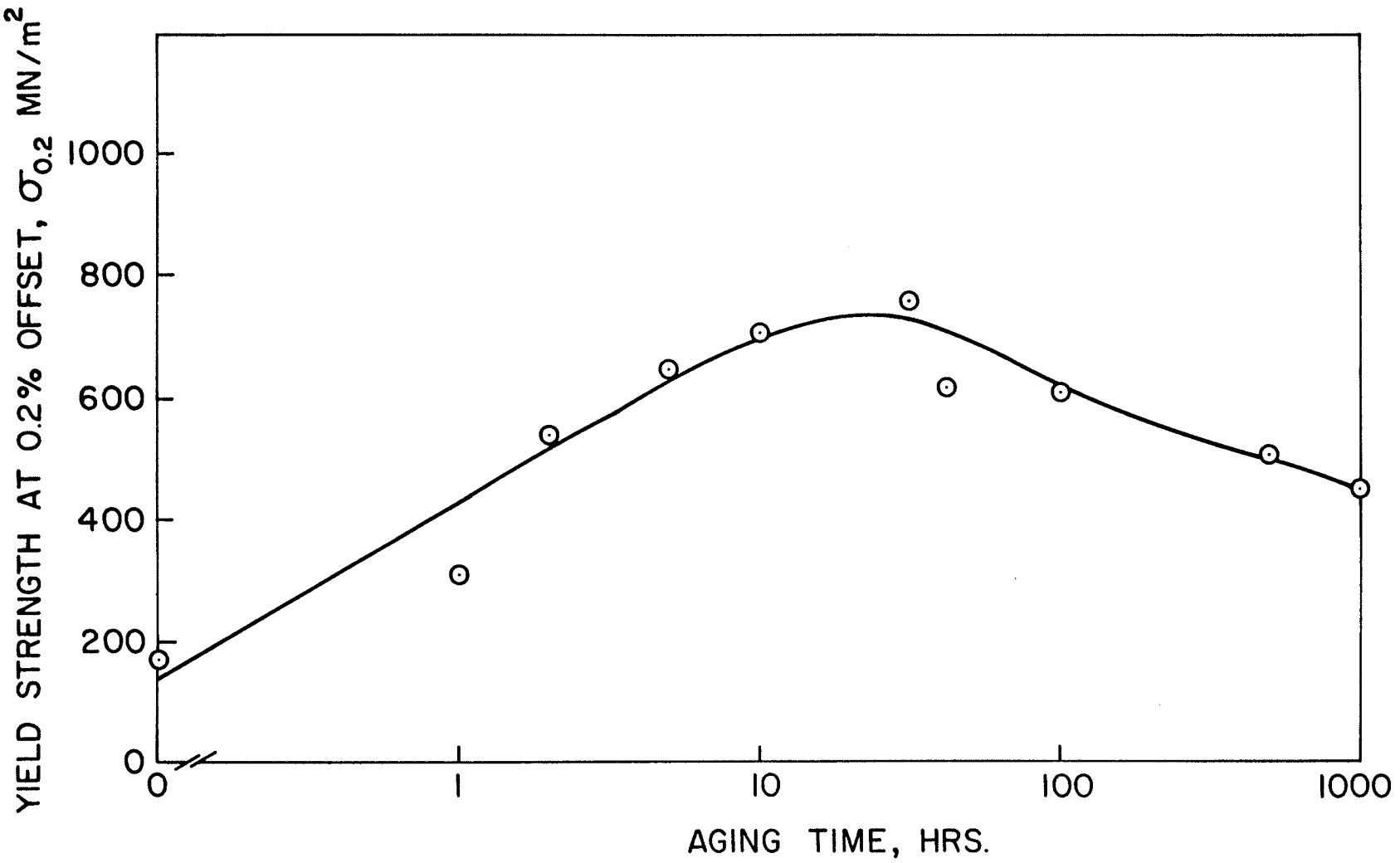
YIELD STRENGTH AT 0.2% OFFSET, $\sigma_{0.2}$ MN/m^2
1000
800
600
400
200
0
0
1
10
100
1000
AGING TIME, HRS.

FIGURE 30

A melt of this composition was prepared and solution treated to obtain the 0.2% yield strength of the matrix (σ_o). It was assumed that solid solution strengthening of the residual matrix resulting from niobium and aluminum is not very significant. The increase in the critical resolved shear stress (CRSS), was then obtained by dividing ($\sigma_y - \sigma_o$) by the Taylor factor of 3.0. This value of Taylor factor for F.C.C. materials is in close agreement with a value of 3.1 used by Chaturvedi and Han[73] during their study of Inconel 718, a value of 3.03 used by Melander and Persson[72] in their study of Nimonic 80A alloy and a value of 3.06 suggested by Thompson[93]. Figure 31 shows the particle size dependence of CRSS in Alloy A. It seems that as the particle size increases, the CRSS first increases and then decreases. The peak in the CRSS is seen to occur at a γ' particle radius of 10nm. In the early stages of aging i.e., up to peak-aged condition or 32 hours at 1073K, the APB model of Brown and Ham[91] (Equation 24) and the coherency model of Gerold and Haberkorn[57] (Equation 29) were used to determine the strengthening mechanism in the alloy.

$$\Delta\tau_{order} = \frac{\gamma_{APB}}{2b}\left[\left(\frac{.4\gamma_{APB} r_s f}{\pi T}\right)^{1/2} - f_v\right] \quad \ldots\ldots (24)$$

where $T = \frac{3}{8} Gb^2$

and

$$\Delta\tau = \beta\, G(\epsilon)^{3/2}\left(\frac{r_s f_v}{b}\right)^{1/2} \quad \ldots\ldots (29)$$

If either/or both of the above equations are satisfied, a plot of $\Delta\tau$ vs. $(r_s)^{1/2}$ should yield a straight line. Figure 32

FIGURE 31

THE γ' PARTICLE SIZE DEPENDENCE OF

CRSS IN ALLOY A AGED AT 1073K

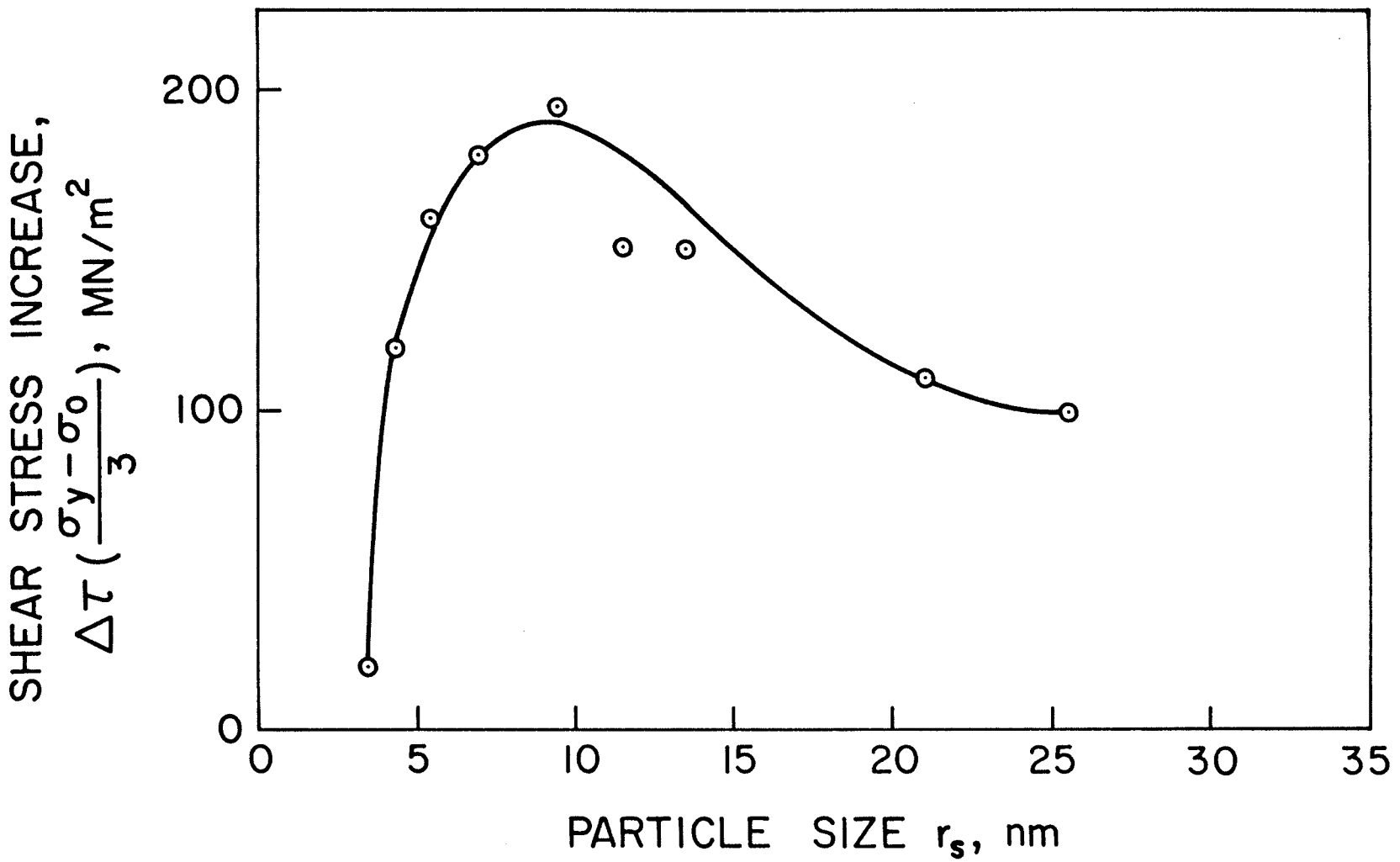
SHEAR STRESS INCREASE,
$\Delta\tau\left(\frac{\sigma_y - \sigma_0}{3}\right)$, MN/m^2
200
100
0
0
5
10
15
20
25
30
35
PARTICLE SIZE r_s, nm

FIGURE 31

FIGURE 32

The Square Root of Particle Size/CRSS Increase Relationship for Alloy A aged at 1073K

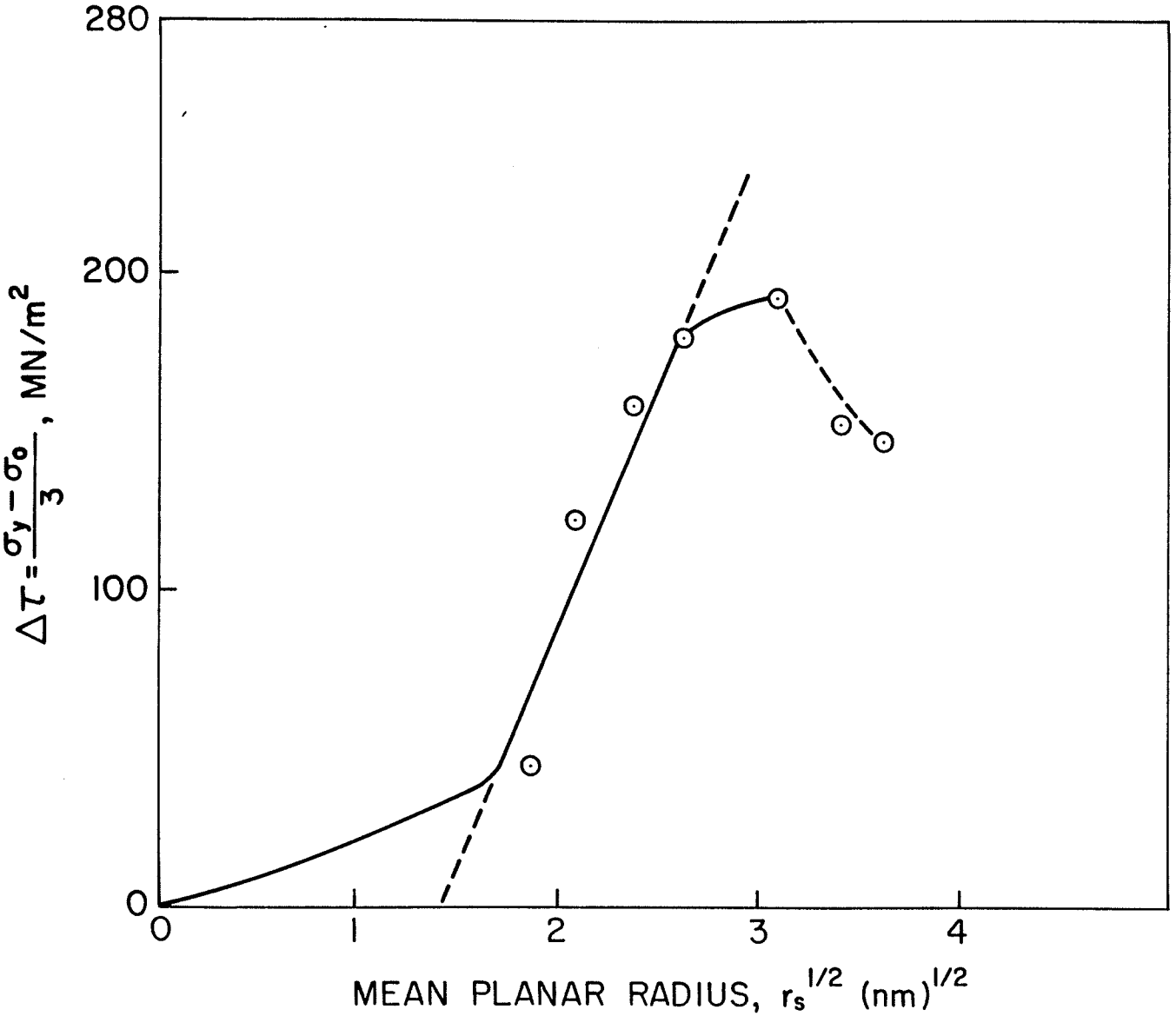
280
200
100
0
0
1
2
3
4
$\Delta\tau = \frac{\sigma_y - \sigma_0}{3}$, MN/m^2
MEAN PLANAR RADIUS, $r_s^{1/2}$ (nm)$^{1/2}$

FIGURE 32

shows such a straight line for particle whose radii are in the range of 3.5 -7nm. Thereafter, $\Delta\tau$ starts to decrease with increasing particle size.

4.6.2 Temperature Dependence of Yield Stress

The influence of temperature on the yield strength of specimens of Alloy A aged at 1073K was also studied to determine the strengthening mechanisms operating in the underaged alloy. The specimens of Alloy A aged for 1, 2 and 16 hours at 1073K were subjected to tensile tests at 77, 160, 293 and 373K. By using strain gauges, the modulus of elasticity was also determined, from which the shear modulus was calculated. The shear modulus corrected yield strength values normalized with respect to the 77K data are in Table 3.

4.7 ANTIPHASE BOUNDARY ENERGY

In order to calculate the theoretical CRSS by order hardening model the antiphase boundary energy was determined.

Raynor and Silcock[68] have determined the antiphase boundary energy by two different methods, viz., (a) Minimum Orowan-loop Size Method, and (b) Dislocation-pair Spacing Method. They found that the latter method gave values of A.P.B. energy 20% lower than the former method. Singhal[94] has modified the Raynor and Silcock expression[68] for determining the A.P.B. energy by the Minimum Orowan-loop Size Method. He took into account the presence of coherency strains around

TABLE 3

EFFECT OF TEMPERATURE ON THE YIELD STRENGTH OF AGED SPECIMENS

Treatment	------- $\left[\left(\sigma_T/G_T\right) / \left(\sigma_{77}/G_{77}\right)\right]$ -------			
	77K	160K	293K	373K
1 hr at 1073K	1.00	0.99	0.77	0.85
2 hrs at 1073K	1.00	0.99	0.911	0.87
3 hrs at 1073K	1.00	0.89	0.89	0.77

the γ' particles. Thus, the A.P.B. energy γ_{APB} is given by the equation

$$\gamma_{APB} = \frac{Gb^2}{8\pi r_o} \frac{2-\nu}{1-\nu} \ln \frac{8r'_o}{b} + \tau_{applied} b - 2Gb \frac{a_p - a_m}{a_m} \quad \ldots\ldots (46)$$

where

G = shear modulus

b = Burgers vector

r'_o = minimum loop radius

ν = Poisson's ratio

$\tau_{applied}$ = applied shear stress

a_p = lattice parameter of γ' precipitate particle

and

a_m = lattice parameter of the matrix.

In order to determine the A.P.B. energy of Alloy A, the above expression was used. The minimum loop was determined by measuring approximately 50 loops in a specimen aged to 2 hours at 1073K and deformed. The average minimum loop radius measured was 5.2nm and the average particle radius was 4.3nm. With $G = 60\ GN/m^2$, $\tau_{applied} = 233\ MN/m^2$ and $a_p = 0.3603nm$ and $a_m = 0.3556nm$, γ_{APB} was calculated to be $182\ mJ/m^2$.

The above value for APB energy was verified by an independent method.

Flinn[55] has theoretically derived an expression for the energy of an antiphase boundary in $L1_2$ type ordered structure.

According to him, the APB energy/unit area associated with an a/2 <100> type A.P.B. is given by the equation

$$\gamma_{APB} = \frac{2V_{L1_2}}{a_p^2} \frac{h}{(N_{h.k.l.})^{1/2}} \qquad \ldots\ldots (47)$$

where

$$V_{L1_2} = \frac{k\, T_c^{(112)}}{2F_A F_B Z_{AB}}$$

$N = h^2+k^2+1^2$

k = the Boltzmann constant

$= 1.380 \times 10^{-16}$ ergs/deg.

T_c = the critical ordering temperature, °C

F_A, F_B = atomic fractions of A and B atoms

and

Z_{AB} = number of the first nearest neighbour atoms.

Marcinkowski[95] has proposed a more accurate expression for V_{L1_2} based on quasi chemical treatments, as follows:

$$V_{L1_2} = \frac{k\, T_c}{0.82} \qquad \ldots\ldots (47A)$$

High-temperature X-ray studies by Guard and Westbrook[96] have indicated that the compound Ni_3Al remains ordered at least up to 1273K. Based on their finding and the successful use of their data by others[97], T_c is assumed to be 1273K (1000°C). Thus, we get $\gamma_{APB} = 184$ mJ/m^2. This is in excellent agreement with the value determined for APB energy by the minimum Orowan loop Size Method.

4.8 DEFORMATION STRUCTURES

To study the dislocation - precipitate interaction, the deformation structures of variously aged specimens were examined. Solution treated and aged tensile specimens of Alloy A were deformed to 1-4% plastic strain at room temperature. Thin foils prepared from the gauge length part of these specimens were then examined.

In specimens of Alloy A aged for 15 minutes at 1073K, dislocations often appeared to be paired as shown in Figure 33. There was little evidence of cross-slip. At this stage, the γ' particles were not visible, and the matrix surface showed a modulated structure. Clear evidence of particle cutting and very limited bowing was observed in specimen aged for 2 hours as shown in Figures 34 and 35. In the specimen aged for 3 hours, the precipitate particles continued to be cut by pairs of dislocations. An example of this is shown in Figure 36. When an ordered particle is sheared by a glide dislocation an antiphase boundary is created within a particle. This causes a second dislocation to be pulled forward removing the disorder within the particle. Therefore, whenever ordered particles are sheared, dislocations are seen to occur in pairs. The presence of dislocation pairs in the aged and deformed specimens suggests that the deformation of underaged specimens of Alloy A occurs by the shearing of ordered precipitate particles by glide dislocations.

In the near peak-aged specimens in addition to pair-wise motion a certain amount of bowing of leading dislocation was also

FIGURE 33

DOUBLE-DISLOCATION PILE-UP IN ALLOY A AGED FOR 15 MINUTES AT 1073K AND DEFORMED AT ROOM TEMPERATURE

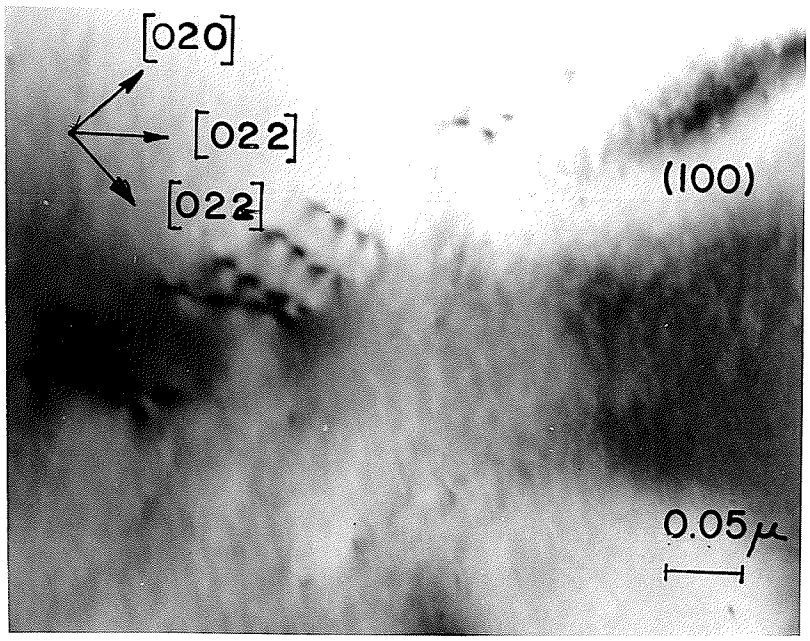

FIGURE 33

FIGURE 34

PARTICLE CUTTING IN ALLOY A
AGED FOR 2 HOURS AT 1073K
AND DEFORMED AT ROOM TEMPERATURE

FIGURE 35

PARTICLE CUTTING AND LIMITED BOWING IN ALLOY A
AGED FOR 2 HOURS AT 1073K AND DEFORMED AT ROOM TEMPERATURE

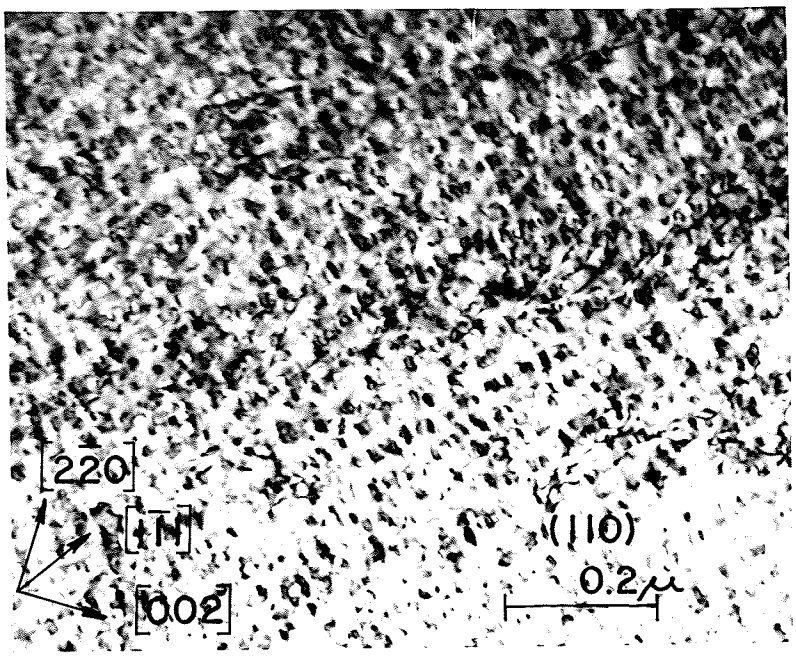

FIGURE 34

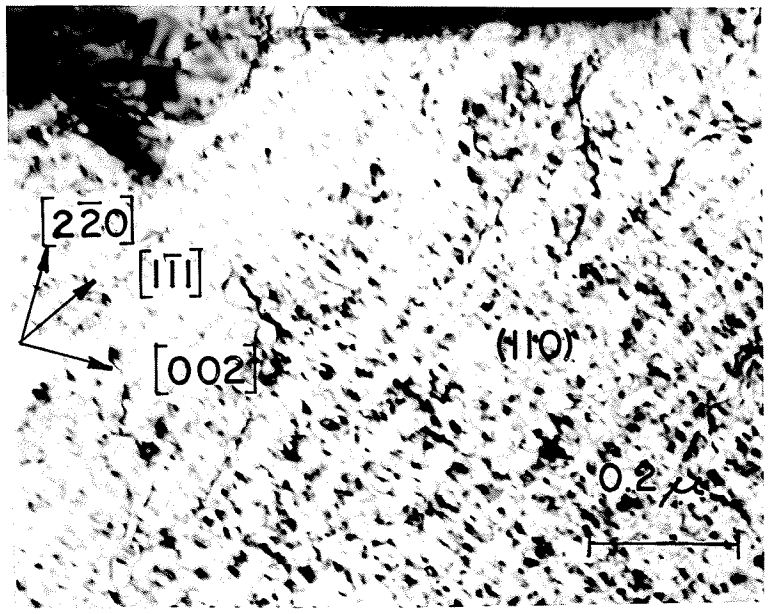

FIGURE 35

observed. This is shown in Figure 37 which is the structure of a specimen aged for 5 hours at 1073K. However, the presence of dislocation-pairs suggests that particle shearing continued to occur.

On aging the specimen to the peak strength a well defined transition in the dislocation-precipitate interaction had occured. i.e., the dislocations were observed to be bowing out in between the particles leaving Orowan loops around them. An example is shown in Figure 38, which is a structure of a specimen aged for 32 hours at 1073K and subsequently deformed. Figures 39 and 40 show the above features under high magnification. Arrays of dislocation loops left behind in slip bands can be seen in Figures 41 and 42.

In the overaged specimens of Alloy A, arrays of individual dislocations were seen to move between columns of agglomerated γ' precipitates until stopped by them. Complex entanglements were seen to occur between the γ/γ' interfacial dislocations and the dislocations generated during deformation. Figure 43 shows these features.

The foregoing results suggest that shearing by pairs of dislocations was the mode of precipitate/dislocation interaction in the early stages of aging. At peak-aged condition, a transition from particle-cutting to particle-looping could be seen. In the overaged condition, the arrays of dislocations were seen to move and looping of dislocations around particles continued to be a major feature.

FIGURE 36

DISLOCATION-PAIRS TOUCHING THE SAME PARTICLES
IN ALLOY A AGED FOR 3 HOURS AT 1073K
AND DEFORMED AT ROOM TEMPERATURE

FIGURE 37

BOWING AND LOOPING OF DISLOCATIONS IN
ALLOY A AGED FOR 5 HOURS AT 1073K
AND DEFORMED AT ROOM TEMPERATURE

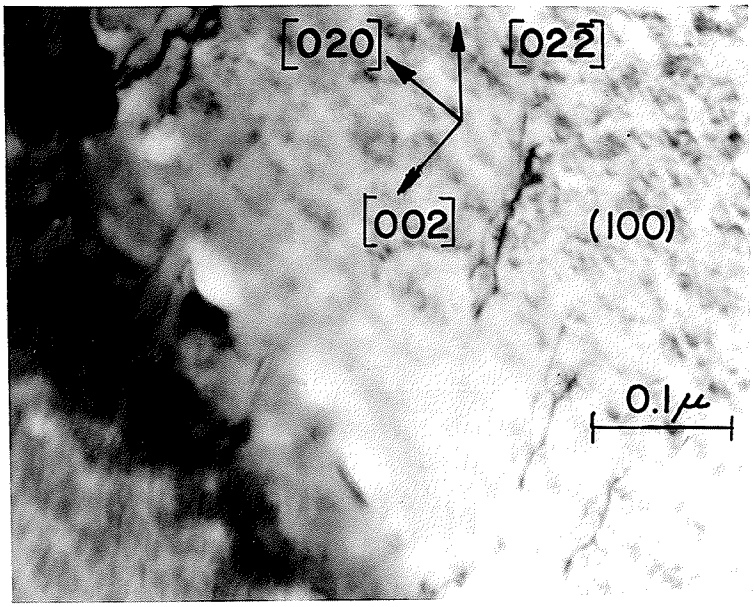

FIGURE 36

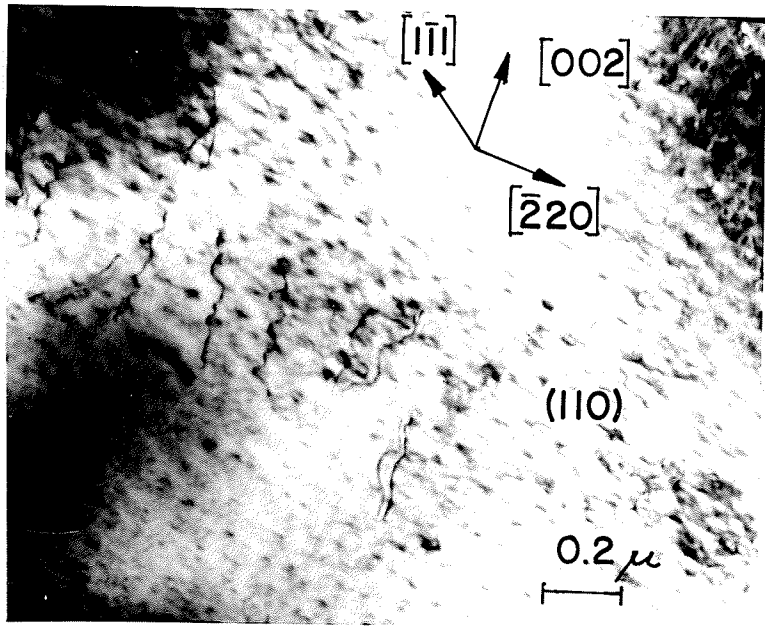

FIGURE 37

FIGURE 38

OROWAN LOOPS IN ALLOY A AGED FOR 32 HOURS AT 1073K AND DEFORMED AT ROOM TEMPERATURE

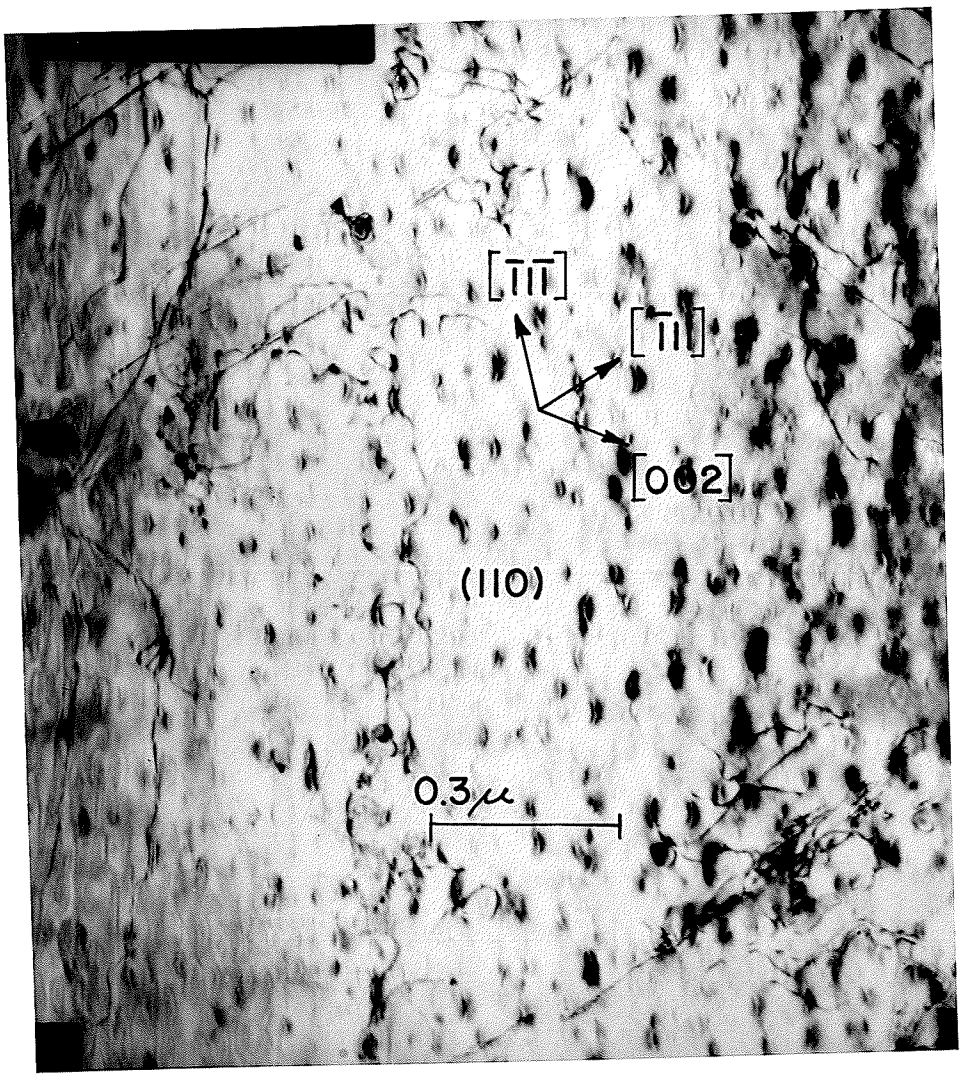

FIGURE 38

FIGURE 39

DISLOCATION LOOPS IN ALLOY A AGED FOR 32 HOURS
AT 1073K AND DEFORMED AT ROOM TEMPERATURE

FIGURE 40

DISLOCATION LOOPS IN ALLOY A
AGED FOR 32 HOURS AT 1073K
AND DEFORMED AT ROOM TEMPERATURE

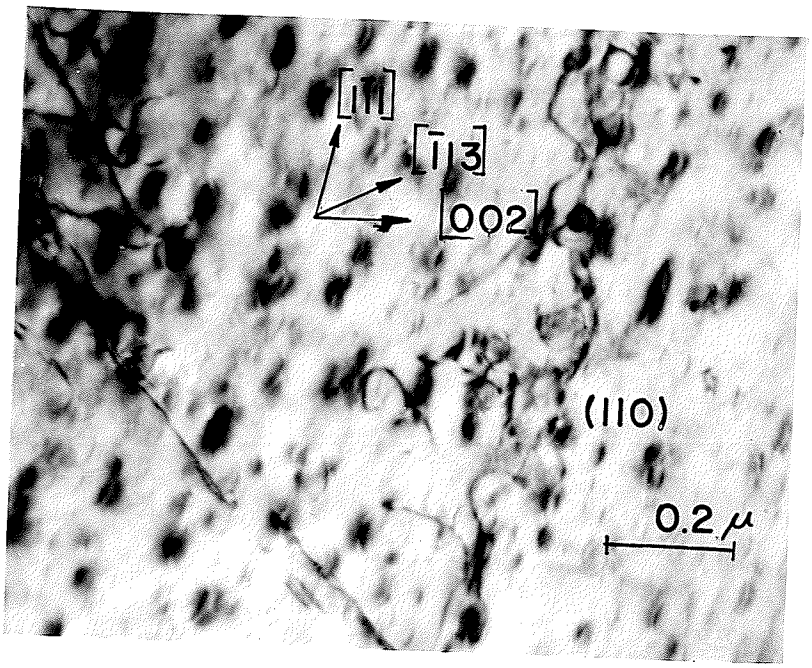

FIGURE 39

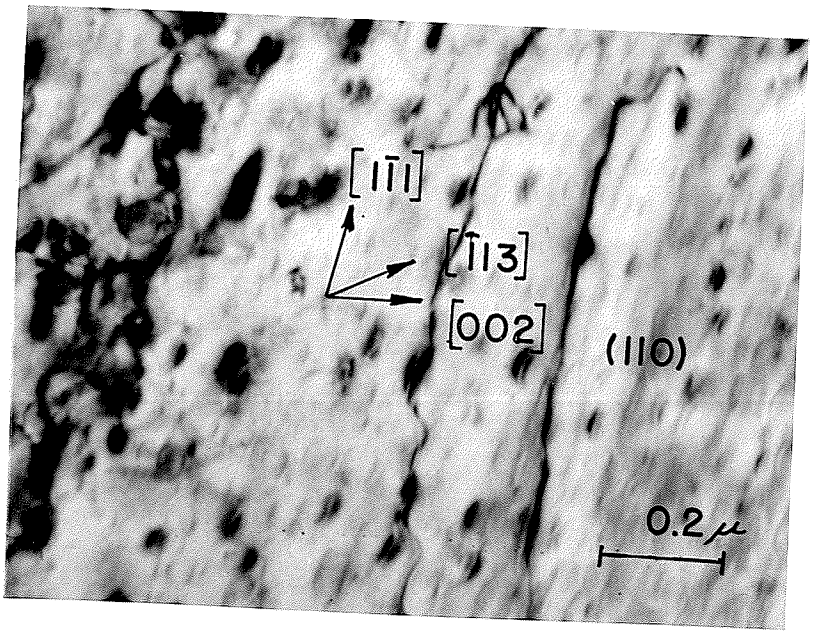

FIGURE 40

FIGURE 41

DISLOCATION LOOPS IN SLIP BAND IN ALLOY A

AGED FOR 32 HOURS AT 1073K

AND DEFORMED AT ROOM TEMPERATURE

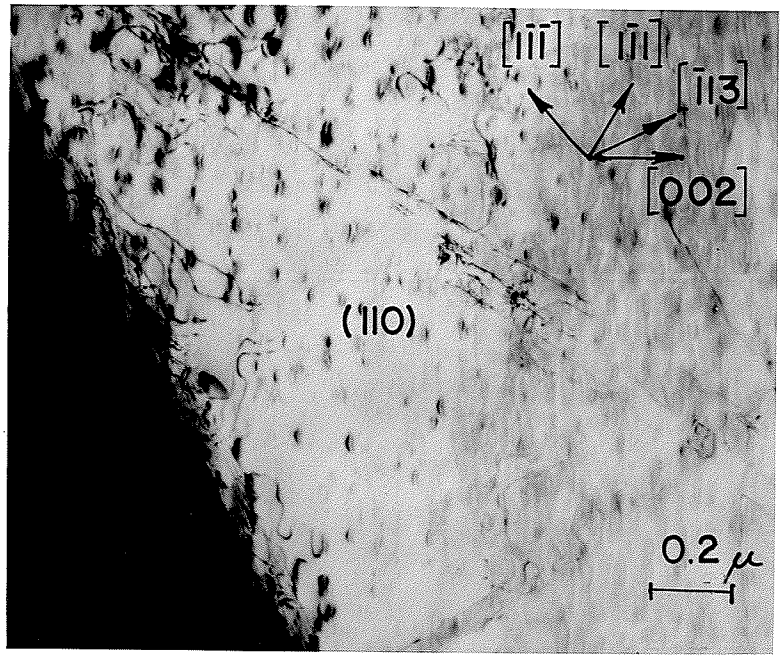

FIGURE 41

FIGURE 42

DISLOCATION LOOPS IN SLIP BAND IN ALLOY A

AGED FOR 32 HOURS AT 1073K

AND DEFORMED AT ROOM TEMPERATURE

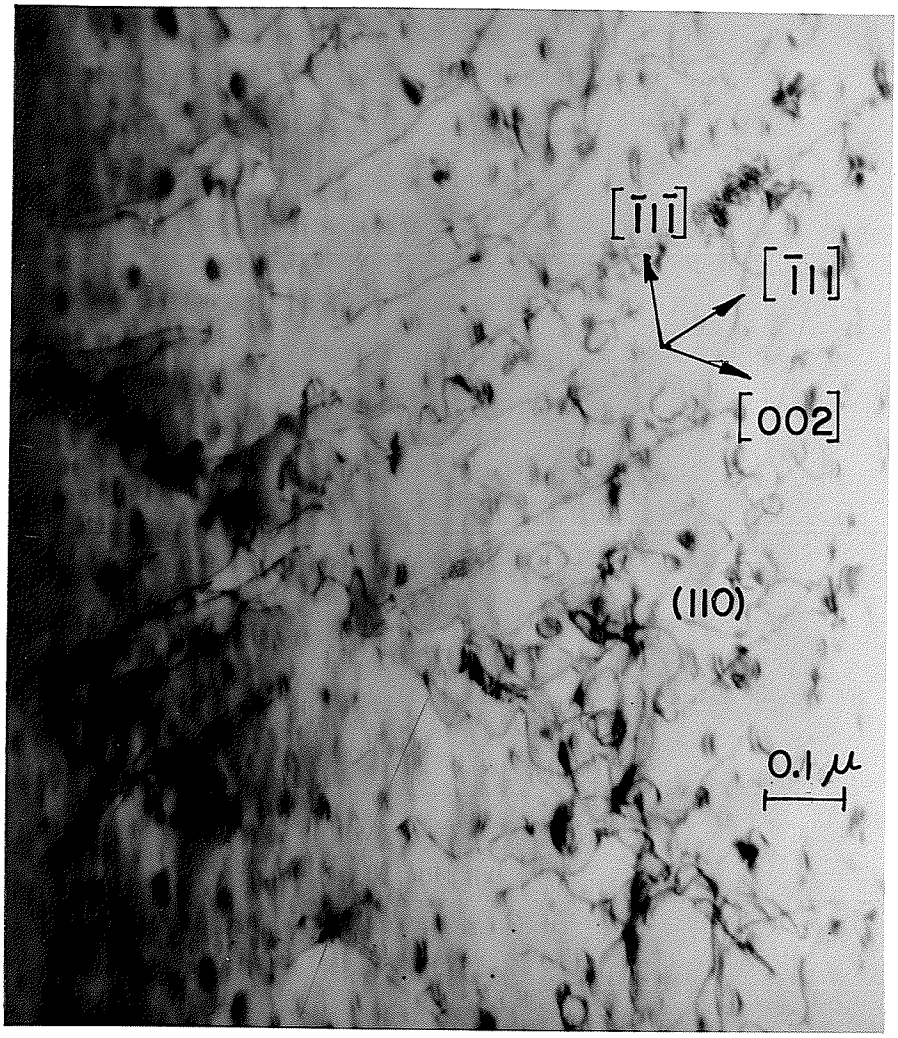

FIGURE 42

FIGURE 43

DISLOCATIONS IN BROAD SLIP BANDS

PILING AGAINST γ' RAFTS IN ALLOY A AGED FOR 500 HOURS

AT 1073K AND DEFORMED AT ROOM TEMPERATURE

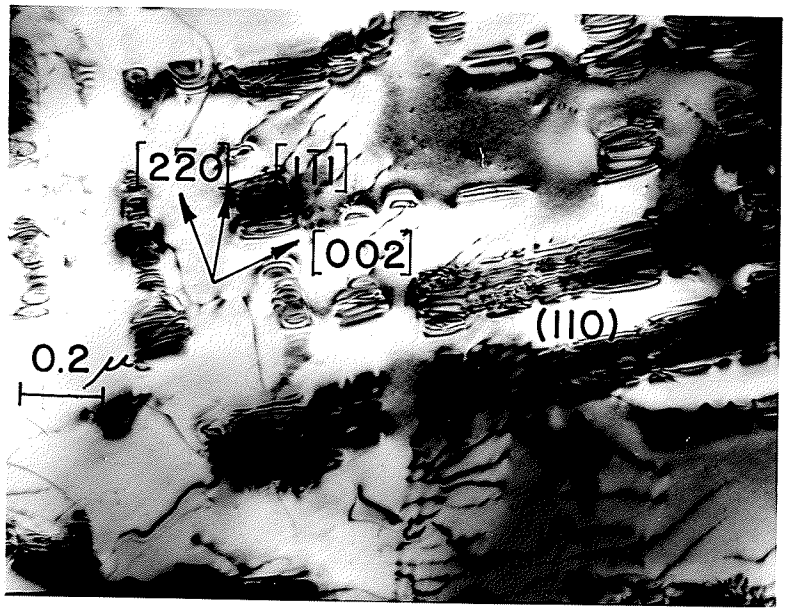

FIGURE 43

5. DISCUSSION

The results of the present investigation have shown that on aging in the 873-1073K range the main precipitating phase in both the alloys was γ'. However, some carbide and sigma phases were also observed. In this chapter, the precipitation process is discussed in the light of the Engel-Brewer theory of intermetallic phase formation. This is followed by a discussion of the strengthening mechanisms that might be operative in the underaged as well as overaged alloys.

5.1 APPLICATION OF ENGEL-BREWER THEORY TO PRECIPITATING PHASES

The major precipitation reaction in both the alloys was the formation of γ' which has a $L1_2$ type or ordered F.C.C. structure. In the previous study of an aluminium free alloy with a similar composition, the chief precipitating phase was found to be orthorhombic Ni_3Nb[98]. Therefore, it is concluded that the addition of 1.5% aluminum promotes the formation of γ' precipitate in Alloy A.

According to the Engel-Brewer correlations based on valence electrons[99] the number of s and p electrons determine the crystal structure of an element, solid solution or compound. Quist et al[100] have extended the Engel-Brewer analysis to the formation of γ'. According to them the $L1_2$ type of structure is favoured by an (s+p) electron concentration between 2.75 and 3.0. Aluminum with an e/a value of 3.0 (F.C.C.) would not only favour the formation of γ'

precipitate but would also discourage the formation of DO_{22} type Ni_3Nb phase (B.C.T.) which is a favoured structure when e/a values are in the range 2.50 to 2.62. An attempt was made to evaluate the applicability of these suggestions to Alloy A. Only Ni, Co and Cr contents of the precipitate could be analysed by the available atomic absorption technique. Therefore, the balance was deduced to be (Nb+Al) content. It has been observed[80] that the ratio of Ti and Al in γ' is the same as that present in the parent alloy. This observation was extended to the present alloy[101] in order to calculate the amount of Nb and Al present in the γ' precipitate. The composition of γ' was estimated to be Ni - 52.97 A/o, Co - 13.68 A/o, Cr - 3.83 A/o, Nb - 12.23 A/o and Al - 18.03 A/o. The e/a ratio for this compound is calculated to be 2.68. Similarly, the e/a ratio of β - Ni_3Nb orthorhombic precipitate observed in an Al-free Co-Ni-Cr alloy[98], was calculated to be 2.32.

Precipitation of γ' in Alloy A is in fairly good agreement with the observations of Quist et al[100]. Also, the e/a ratio of several orthorhombic phases quoted in the literature[92] are between 2.1 and 2.5. Therefore, the occurrence of β - Ni_3Nb is in agreement with this and the observations of the previous study[98]. It may be concluded that the addition of Al whose e/a ratio is 3.0, increases the e/a ratio of the precipitate from 2.32 to 2.68 thus causing the precipitation of γ'. However, the present results are in disagreement with the suggestion of Quist et al[100] and that of Hagel and Beattie[2,102] that for the precipitation of γ', the lattice mismatch should be under 1.0%, since in the present alloy it is about 1.3%.

It has been proposed that in the case of sigma phases, aluminum donates its own valence electrons (3 per atom)[103]. Using the e/a values listed in the literature[103], the e/a value for the binary sigma phases Nb_2Al and Ta_2Al is calculated to be 2.5. Brewer[104] has suggested an (s+p) electron concentration in the range 1.2 - 2.9 for the occurrence of sigma phase. It is known that aluminum stabilizes sigma phase in the ternary V-Nb-Al, V-Ta-Al and Ti-Ta-Al systems[105]. However, aluminum has a destabilizing effect on $(V\text{-}Fe)_\sigma$ and $(Cr\text{-}Co)_\sigma$ presumably because as an electron donor it tends in these cases to increase the electron concentration above the optimum value[105]. Therefore, it is concluded that the formation of $(Cr\text{-}Co)_\sigma$ phase is this alloy is a localized phenomenon and not a general effect.

5.2 APPLICATION OF PHACOMP ANALYSIS TO SIGMA PHASE PRECIPITATION

Phase Computation Analysis (PHACOMP) based on electron density calculations[106-108] was also made with a view to predicting the formation of sigma phase. This is the standard method for predicting the potential for the formation of sigma phase in superalloys and, in essence, depends upon calculating the average periodic column position of the matrix composition. The residual matrix composition was determined for both Alloys A and B following the method of Woodyatt et al[107]. The electron valency numbers were calculated as $\bar{N}_v = 2.164$ for Alloy A and $\bar{N}_v = 2.405$ for Alloy B. Murphy et al[108] suggest that below a general value of $\bar{N}_v = 2.52$, sigma phase is not expected to form. It has been observed[111] that PHACOMP does not take into account the temperature dependence of sigma phase formation. However, occasional precipitation of sigma phase suggests a possibility

that localized chemical heterogeneity in the vicinity of grain boundaries could have caused the value of $\bar{N}_v$ to rise above 2.52, thus confirming the earlier observations (Section 5.1) based on the Engel-Brewer Analysis.

5.3 PRECIPITATION OF γ'PHASE

5.3.1 Shape of the γ'Particles

The γ' precipitate particles in the two alloys nucleate homogenously throughout the matrix and are coherent with the parent lattice. The particles initially observed to be spherical or cubic (Figure 13) developed into clearly discernible cubes (Figure 14) as Alloy A was aged from 2 hours to 64 hours at 1073K. The shape of a particle is known to depend on its size[109] and particles which are spheres become cubes when they are large. The subsequent tendency to coalesce to cubic or rectangular shape (Figure 15) and continued alignment of such particles is in agreement with earlier observations[22,110]. On aging Alloy A for 1000 hours and over at 1073K, part of the coherency strains are seen to be relieved as suggested by the presence of interfacial dislocations (Figures 16-19), and the resulting interface may be semi-coherent. The precipitate/matrix interface changes are attributed to particle size effect and/or γ/γ' misfit[12]. The γ/γ' mismatch (Figure 11) has not changed significantly as Alloy A is aged at 1073K. It is therefore suggested that the precipitate/matrix interface changes observed are due to the particle size effect alone.

5.3.2 Lattice Parameters of Matrix and γ'Precipitate

On aging the specimens of Alloy A, an initial decrease in the lattice parameter of the matrix was observed (Figure 11). The extracted γ' precipitate has a lattice parameter larger than that of matrix. The precipitate particles will therefore be restrained from expanding by the compressive elastic forces in the matrix. Attention has been drawn by Baker et al[112] to hydrostatic stresses arising during the growth of a coherent precipitate. The γ' precipitate can cause a depletion of aluminum and niobium in the matrix and thus lead to a decrease in the lattice parameter of the matrix, since the lattice parameters of Al and Nb are greater than those of Co, Ni and Cr atoms. (Atomic radii: Al = 0.143nm, Nb = 0.146nm, Co = 0.125nm, Cr = 0.127nm and Ni = 0.124nm).

5.4 GRAIN BOUNDARY PRECIPITATION OF NIOBIUM CARBIDE

Grain boundary precipitation of NbC was always accompanied by a precipitate free or denuded zone around it. The presence of such a zone around a grain boundary has been explained in different ways as follows:

1. The boundary acts as a sink for vacancies so that there are very few vacancies in the region near the boundary. Thus, there is a lack of nuclei in this region.[113]
2. The growth of $Cr_{23}C_6$ on the boundaries causes a depletion of chromium locally, and in that region γ' is more soluble because the lower chromium content increases the solubility of γ'.[114]

3. Grain boundary precipitation of MC type carbides reduces the solute content of M in its vicinity, and creates a precipitate free zone.[86]

The average size of γ' particles in along the edge of the denuded zone was the same as that in grain interior. Previous workers[115,116] observed that the average particle size was larger along the edge of the zones formed due to vacancy depletion. In the case of Alloys A and B, no tendency was seen for the development of a larger average size of precipitate particle along the edge of the zone. Also, the width of the denuded zone and the grain boundary carbide particle size increased with aging temperature and time. Therefore, it is concluded that the denuded zones around the grain boundaries are not due to vacancy depletion.

In this alloy the second mechanism does not operate as the carbide was NbC, not $M_{23}C_6$. Also, the width of the precipitate free zone around grain boundaries was, qualitatively, found to be dependent upon the NbC precipitate size. Therefore, it would seem that the precipitate free areas around the grain boundaries are due to a lack of Nb atoms.

5.5 STACKING FAULT PRECIPITATION OF NIOBIUM CARBIDE

The extrinsic stacking faults observed in the early stages of precipitation[101,117] (for example, 10 hours at 1073K as in Figure 21) were associated with NbC precipitation. It has been found that an extrinsic stacking fault can form by the dissociation of a matrix dislocation in the following manner if it does not lie on its own

slip plane.

$$1/2\ [110] \rightarrow 1/3\ [111] + 1/6\ [11\bar{2}]$$

A normal dislocation cannot split in this way. The following model for the nucleation and growth of stacking fault precipitation of NbC in austenitic steel, proposed by Silcock and Tunstall[118] and confirmed by Chaturvedi[117] should be applicable to Alloy A. It is known[118] that an expansion of 23% is associated with the formation of the F.C.C. NbC particle from the F.C.C. matrix. As a result, the precipitation of NbC on dislocations emits dislocation loops which move by climb. Part of such loops may lie on planes which are not their slip planes and can dissociate into a Frank and Shockley partial bounding an extrinsic stacking fault. The Frank partial provides nucleating sites for NbC precipitates. As these particles grow, strain in the matrix due to size differences between the NbC and matrix unit cells is accomodated by the vacancies produced by the climb of the Frank partial to a new position. In its new position the Frank partial provides new nucleating sites for the NbC precipitates and the process continues until the supply of Nb and/or Carbon atoms is exhausted. The presence of planar array of fine NbC particles (Figure 21) are in agreement with such a mechanism.

Undissolved NbC particles have been observed frequently at grain boundaries in quenched specimens of Alloy A (Figure 20). While these could increase the nucleation sites by increasing the dislocation density with the concomitant increase in stacking fault formation, the excess vacancies retained during quenching could retard the growth of these faults.

The same specimen of Alloy A, on aging for an additional 32 hours at (i.e., for a total of 64 hours at 1073K) shows β-Ni_3Nb plates as in Figures 22 and 23. The dissolution of NbC in favour of the formation of β-Ni_3Nb is in agreement with similar observations in other alloys[86,119,120].

5.6 DISCONTINUOUS PRECIPITATION

Occasional discontinuous precipitation (Figures 26-28) was seen in grain boundaries with no carbide particles or with small carbide particles. Phillips[121] in his study of a Cu - 3.1 w/o Co alloy found that the discontinuous precipitation appeared to proceed by a mechanism of grain boundary migration, and that the driving force for this migration was derived from residual supersaturation in the grain being consumed and from the free energy released by re-solution of precipitate. The dissolution of grain boundary precipitate has also been observed by Singhal and Martin.[116]

The absence of any grain boundary precipitate in discontinuously precipitated region coupled with the observations of Phillips[121] and Singhal and Martin[116] suggests that discontinuous precipitation of γ' observed during present investigation is also associated with the dissolution of grain boundary precipitate.

The chromium content of both the alloys, A and B is 17 w/o. The observed discontinuous precipitation of γ ' in these two alloys is in disagreement with the observations of Hagel and Beattie[122].

During their investigation of five superalloys, they found that the discontinuous precipitation of γ' was a feature in alloys without chromium, and was absent in alloys containing chromium in the range 16.74 - 20.84 w/o. However, the facts that the γ' particles overlapped in the discontinuously precipitated region, and the measured lattice mismatch of Alloy A is 1.3% corroborate with the suggestion[122] that lattice mismatch values of over 1% are essential to promote cellular precipitates, which grow to impinge into each other.

Williams and Edington[123] in their study of Al-Li alloys concluded that the reaction is initiated by grain boundary straightening or localized coarsening of particles touching the grain boundary. The "straightening" of the grain boundary on either side of corners (as in Figures 25 and 26), and the growing of γ' particles into each other in these regions (as in Figure 28) are in agreement with their[123] conclusions.

5.7 STRENGTHENING MECHANISMS

A study of the deformation structures revealed that in the early stages of aging, when the particle diameter is 7-20nm, particle shearing by pairs of dislocations is a predominant mode of deformation. However, deformation by Orowan looping is seen to be prevalent at particle diameter values of 20nm and more. Although, occasional looping was seen at a particle diameter of 8nm (specimens aged for 2 hours at 1073K). Such loops may be due to presence of larger γ' particles in this area. The presence of particles as large as 2.5 r_s

has been observed. However, both shearing of particles and formation of loops around particles were seen in the transition range of particle diameter, 9-20nm.

5.7.1 Strengthening in the Early Stages of Aging

When the particles are sheared by mobile dislocations, the strengthening of the alloy can be due to (a) coherency strain hardening, (b) order hardening, (c) surface hardening, (d) stacking-fault hardening, and (e) modulus hardening.

Surface hardening can almost be considered as part of order hardening[68], and both surface hardening and modulus hardening have been found[70] to be negligible relative to measured values of CRSS, $\Delta\tau$. Stacking fault hardening is not expected to contribute to strengthening of this alloy. The strengthening of the underaged alloy should be mainly due to order and/or coherency strengthening mechanisms.

The relative contributions of the two mechanisms, namely order strengthening and coherency strengthening has been a matter of considerable debate, and various investigators have assumed or concluded:

1. that the contributions of order strengthening and coherency strengthening should be additive[65,67] (misfit: 0.0042 and 0.0057) and each mechanism contributes to the yield stress as if it were acting alone;

2. that the major contribution to strengthening is due to coherency strains[124] (mismatch: 0.0068-0.0078);
3. that strengthening is entirely due to order hardening[68,70] (misfit: 0.0019 and 0.0036);
4. that the order strengthening contributed to about 60% of CRSS in the underaged state and about 45% of CRSS in the peak-aged state[72] (misfit: 0.0035); and
5. that the precipitation hardening of underaged Nickel-base alloys can be accounted for perfectly adequately by the theory of order hardening, without any need to invoke other strengthening mechanisms[71] (misfit: 0.00225).

Therefore, the strengthening of the underaged specimens will be discussed in terms of the coherency and order hardening mechanisms.

5.7.2 Order Strengthening

The contribution of CRSS, $\Delta\tau$ due to order strengthening by spherical precipitates[91] is given by:

$$\Delta\tau = \left(\frac{\gamma_{APB}}{2b}\right)\left[\left(\frac{4\gamma_{APB} r_s f}{\pi T}\right)^{1/2} - f_v\right] \qquad \ldots\ldots (24)$$

where $T = 3/8Gb^2$

The regression line obtained by plotting the theoretical CRSS values calculated using the above expression against the experimental CRSS values is shown in Figure 44. The slope of this line is 0.889 ± 0.069, and demonstrates fairly close agreement between the theoretical and experimental CRSS values (Table 4).

FIGURE 44

RELATIONSHIP BETWEEN THEORETICAL AND EXPERIMENTAL CRSS INCREMENTS IN THE UNDERAGED CONDITION OF ALLOY A

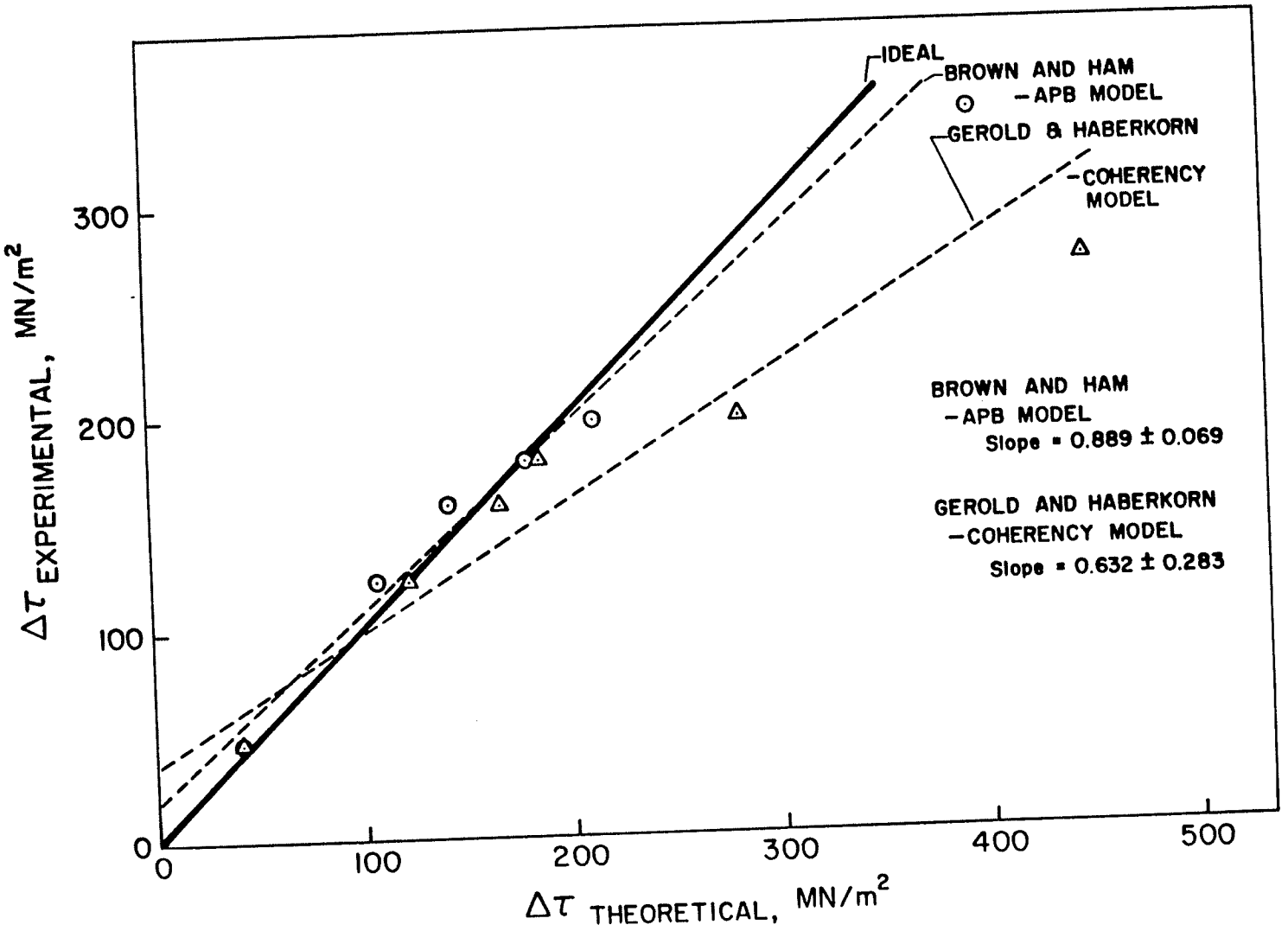
IDEAL
BROWN AND HAM
-APB MODEL
GEROLD & HABERKORN
-COHERENCY MODEL
BROWN AND HAM
-APB MODEL
Slope = 0.889 ± 0.069
GEROLD AND HABERKORN
-COHERENCY MODEL
Slope = 0.632 ± 0.283
Δτ EXPERIMENTAL, MN/m²
Δτ THEORETICAL, MN/m²
0
100
200
300
400
500

Figure 44

TABLE 4

Relationship between Experimental and Theoretical CRSS - Underaged Condition

Aging Time at 1073K	r_s nm	Observed (Exptl.) MN/m^2	Coherency Model Gerold & Haberkorn MN/m^2	APB / Order Model Brown & Ham MN/m^2
1 hour	3.5	45.3	42.1	42.07
2 hours	4.3	122.2	121.8	106.1
5 hours	5.6	159.0	167.3	142.4
10 hours	6.8	178.8	210.9	179.8
32 hours	9.6	195.5	282.3	211.7

5.7.3 Coherency Strengthening

The incremental CRSS due to coherency hardening was determined using the relation developed by Gerold and Haberkorn[57].

$$\Delta\tau = \beta\ G\ \epsilon^{3/2}\left(\frac{r_s f_v}{b}\right)^{1/2} \qquad \ldots\ldots (29)$$

where β = constant (usually, 3 for edge dislocations and 1 for screw dislocations).

However, the average value used for β has varied widely (for example, Gleiter[58]: 11.8, Munjal and Ardell[70]: 6.14). Accordingly, the calculated $\Delta\tau$ can vary widely. In a recent study on Cu - 1.2 at. % Ti single crystals, Greggi and Soffa[125] found that a value of 1.3 for β gave a reasonable fit to their data. The calculated $\Delta\tau$ values were plotted against the experimental values and the regression line obtained (Figure 44) has a slope of 0.632 ± 0.283. This suggests that the results agree significantly better with those predicted by the order hardening mechanism (Table 4).

No attempt was made to use the expression for coherency hardening as modified by Gleiter[58] (Equation 30) as it is obvious that this will result in $\Delta\tau$ values several times larger than that predicted by Equation (29).

5.7.4 Contributions of Order and Coherency Mechanisms to Strengthening of Underaged Alloy

The expression for incremental CRSS, $\Delta\tau$ due to coherency hardening (Equation 24) suggests that the linear portion of the

$\Delta\tau$ vs. $r_s^{1/2}$ plot (Figure 32) should pass through the origin when extrapolated. However, it is seen that the extrapolated portion gives a negative y-intercept. According to the expression for order strengthening (Equation 24), the extrapolated intercept of the linear portion is - ($\gamma f/2b$). This can be used to calculate the value of APB energy. Such a calculation gives a value of 181.45 mJ/m^2 for APB energy which is in excellent agreement with the values obtained from the flow stress (γ_{APB} = 182 mJ/m^2) and by following the theoretical method of Flinn[55] (γ_{APB} = 184 mJ/m^2). This also suggests that the strengthening of this alloy in the underaged condition is by the order hardening mechanism.

The temperature dependence of CRSS was also used to determine the roles of order and coherency mechanisms in strengthening of this alloy in the underaged condition. The increment in the CRSS due to coherency strengthening, obeys an equation of the type,

$$\Delta\tau \quad \alpha \quad G\epsilon^{3/2} \, r_s^{1/2} \text{ (see Equation 29).}$$

Here, ϵ is the constrained lattice misfit, and is strongly temperature dependent. For example[70], in the Ni-Al system which is precipitation hardened by Ni_3Al-γ' precipitate, the value of ϵ has been observed to increase from 0.255% at 77K to 0.355% at room temperature. In the peak-hardened Cu-Co system[126] where the strengthening is entirely due to coherency hardening mechanism, as the testing temperature is increased from 77K to 303K the value of flow stress is also seen to increase in proportion to the increase in the value of ϵ. Therefore, in the present alloy, if the two mechanisms are complementary in

some proportion, the shear modulus corrected yield strength would be expected to increase systematically and measurably with temperature. However, the data in Table 3 demonstrates that there is no such increase in yield strength in Alloy A with increasing temperature in the range 77-273K. Therefore, coherency strengthening does not seem to be operative in the underaged condition of Alloy A. It is concluded that the strength of Alloy A in the underaged condition is almost entirely due to order hardening.

5.7.5 Strengthening in Overaged Alloy

In the overaged condition, Orowan looping was the predominant deformation mechanism. In this range, the expressions due to Hirsch and Humphreys[77], (Equation 44), Bacon et al[79] (Equation 45) and Ashby[74-76] (Equations 42 and 43) were used to analyse the precipitation strengthening mechanisms.

$$\Delta\tau = \frac{0.81Gb}{2\pi L_o(1-\nu)^{1/2}} \ln \frac{2r_s}{r_o} \quad \ldots\ldots (44)$$

$$\Delta\tau = \left(\frac{\ln 2r_s}{\ln L_o}\right)^{1/2} \frac{Gb}{2\pi L_o} \ln \frac{2r_s}{r_o} \quad \ldots\ldots (45)$$

$$\Delta\tau_{edge} = 0.85 \frac{Gb}{2\pi L_o} \ln \frac{2r_s}{r_o} \quad \ldots\ldots (42)$$

$$\Delta\tau_{screw} = 0.85 \frac{Gb}{2\pi L_o(1-\nu)} \ln \frac{2r_s}{r_o} \quad \ldots\ldots (43)$$

According to these equations, a plot of $\Delta\tau$ vs. $\frac{1}{L_o} \ln \frac{2r_s}{r_o}$ should yield a straight line. Figure 45 shows such a plot for particle diameters in the range of over 14nm.

The observed incremental CRSS and the theoretical CRSS determined using the expressions (Equations 42-45) of Ashby[74-76], Hirsch and Humphreys[77] and Bacon et al.[79] are shown in Table 5. It can be seen that the experimental values of CRSS are almost average values of the CRSS determined from the Ashby expressions[74-76] for screw and edge dislocations. However, the theoretical CRSS determined using the equation proposed by Bacon et al[80] result in an excellent correlation with the experimental CRSS (Figure 46) the slope of the line being 0.952 ± 0.086. It is also observed that the plot between the theoretical values and experimental values due to the Hirsch and Humphreys expression[77] results in a line of slope 0.901 ± 0.077. The term $(0.81/L_o)$ in the Hirsch and Humphreys expression[77] takes into account the mean planar spacing between a random array of point obstacles based on the statistical theory of Kocks[78] and computer calculations by Forman and Makin[52]. The term $(1-\nu)$ is the correction for screw dislocation. In the expression of Bacon et al[79], the term $\frac{\ln 2r_s}{\ln L_o}$ takes into account the randomness of the obstacle array. Thus, it is not surprising that both the above expressions result in almost identical theoretical CRSS values.

FIGURE 45

RELATIONSHIP BETWEEN THE CRSS INCREASE

AND PARTICLE SPACING FOR ALLOY A AGED AT 1073K

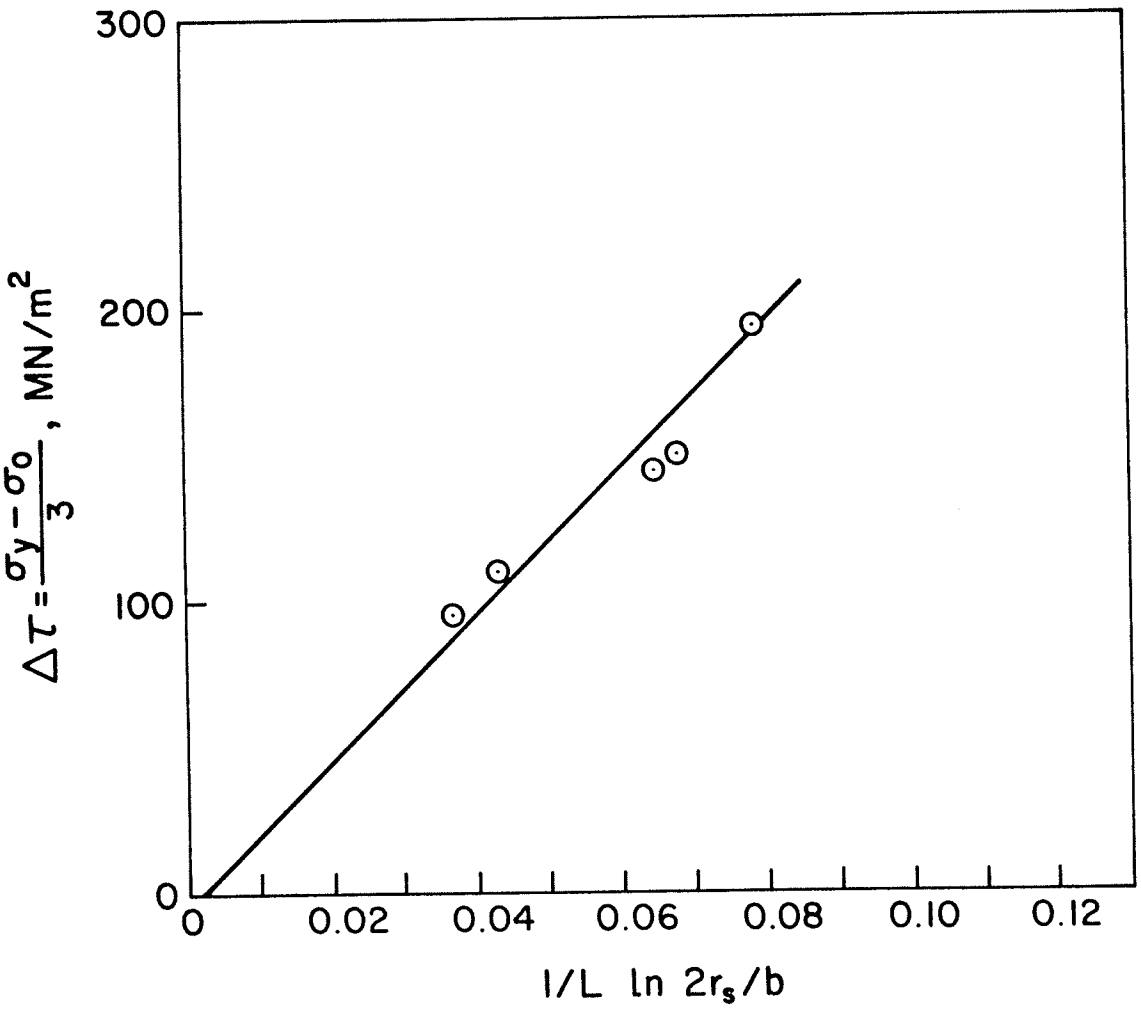
300
200
100
0
0
0.02
0.04
0.06
0.08
0.10
0.12
$\Delta\tau = \frac{\sigma_y - \sigma_o}{3}$, MN/m^2
1/L ln $2r_s/b$

FIGURE 45

FIGURE 46

RELATIONSHIP BETWEEN THEORETICAL AND EXPERIMENTAL CRSS INCREMENTS IN THE OVERAGED CONDITION OF ALLOY A

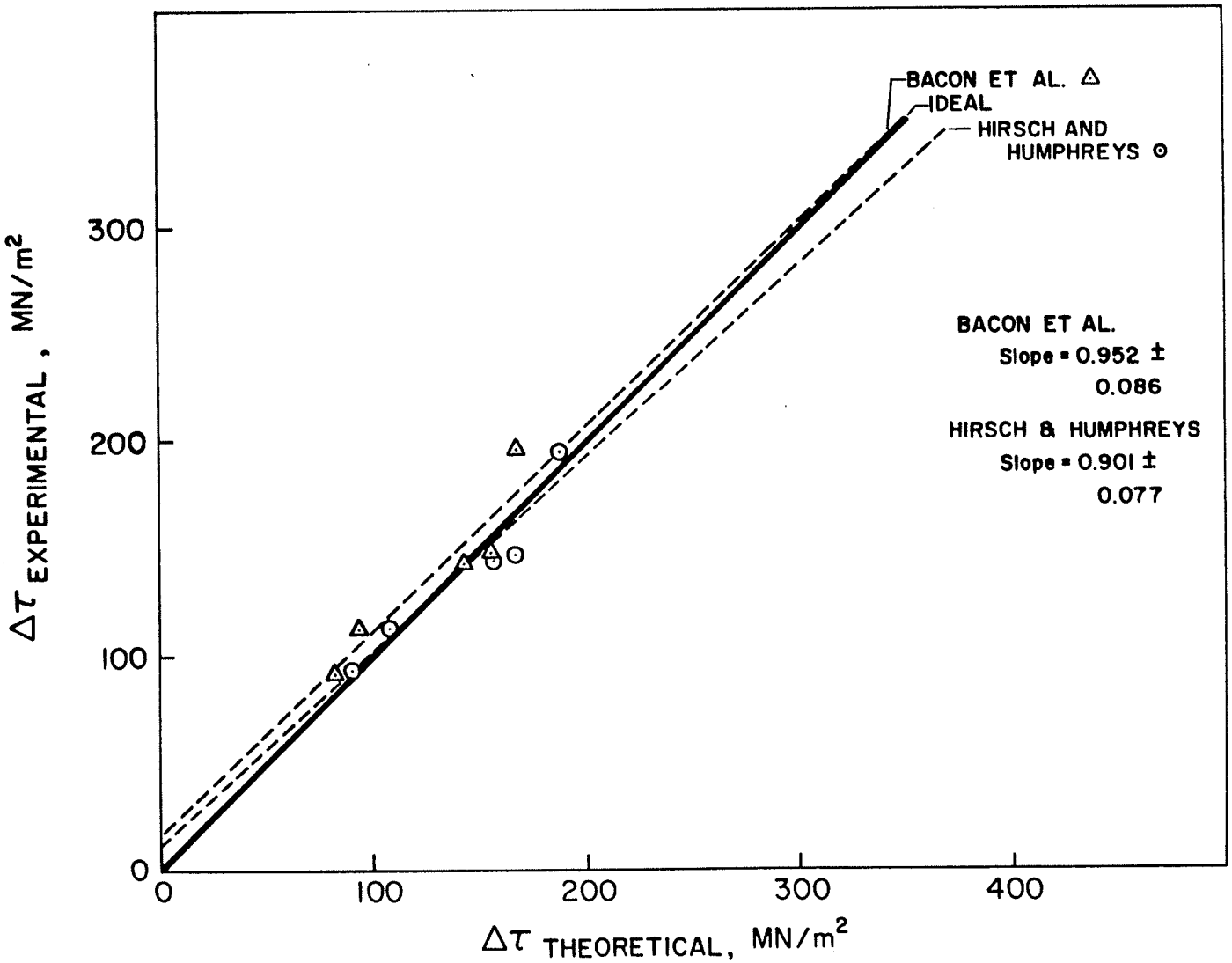
BACON ET AL. △
IDEAL
HIRSCH AND HUMPHREYS ⊙
BACON ET AL.
Slope = 0.952 ± 0.086
HIRSCH & HUMPHREYS
Slope = 0.901 ± 0.077
Δτ EXPERIMENTAL , MN/m²
Δτ THEORETICAL, MN/m²
0
100
200
300
400

FIGURE 46

TABLE 5

Relationship between Experimental and Theoretical CRSS - Overaged Condition

Aging Time at 1073K	r_s	Observed (Exptl.)	Ashby		Hirsch & Humphreys	Bacon et al
			Edge	Screw		
	nm	MN/m^2	MN/m^2	MN/m^2	MN/m^2	MN/m^2
32 hours	9.6	195.5	161.3	240.7	189.8	173.3
64 hours	11.7	149.3	143.6	214.2	168.7	155.1
100 hours	13.4	147.9	132.3	197.4	155.7	143.5
500 hours	21.3	112.2	92.6	138.2	108.9	93.8
1000 hours	26.0	94.4	76.4	114.0	89.8	83.4

6. CONCLUSIONS

6.1 The addition of aluminum promotes the formation of $L1_2$ ordered γ' phase which nucleates homogenously and is coherent with the matrix. The lattice mismatch between γ and γ' in the Co-Ni-Cr-Nb-Al alloy was 1.3 pct.

6.2 In the Co-Ni-Cr-Nb-Al alloy, the changes to γ' shape and γ/γ' interface are due to particle size effect alone, and not due to γ/γ' lattice mismatch effect.

6.3 The growth of γ' occurs according to the Lifshitz-Wagner theory of diffusion controlled coarsening. On overaging, the γ' particles maintain their cubic shape and ordered F.C.C. structure but lose coherency. Further aging to prolonged periods resulted in coalescence of several particles into masses of undefinable shape.

6.4 The formation of γ' follows the Engel-Brewer theory of the structure of compounds based on electronic considerations.

6.5 Carbon, present as an impurity element, forms NbC. When it is present at the grain boundary, it gives rise to a precipitate free zone around the grain boundary. Within the grain, NbC precipitates in association with stacking faults.

6.6 Discontinuous precipitation of γ' seems to occur by localized dissolution of grain boundary NbC/TiC precipitate at sharp grain boundary and is initiated by the process of grain boundary straightening.

6.7 Occasionally acicular sigma phase was also observed at the grain boundaries. This is contrary to predictions of the Engel-Brewer theory and the PHACOMP Analysis, and is considered to be due to localized inhomogeneity in composition.

6.8 In the small particle size range of 7-20nm diameter, deformation of the Co-Ni-Cr-Nb-Al alloy occurs by the shearing of γ' particles by pairs of moving dislocations. Large particles over 20nm in diameter are by-passed by Orowan looping. During the approximate range of 9-20nm diameter, a transition stage encompassing progressive increase of looping activity is seen.

6.9 The strengthening of the Co-Ni-Cr-Nb-Al alloy in the underaged condition is almost entirely explained by the order strengthening mechanism as developed by Brown and Ham. The shear modulus corrected yield strength of underaged alloys did not increase with temperature in the range 77K to 373K thus obviating the possibility of contribution due to coherency strengthening.

6.10 In the overaged alloy, deformation occurs by Orowan looping process, and the experimental results are in excellent agreement with the mechanisms proposed by Hirsch and Humphreys and Bacon et al.

7. SUGGESTIONS FOR FUTURE WORK

7.1 In view of the varying suggestions made (Section 5.7.1) on the relative contributions of coherency and APB energy hardening of different alloys, a comprehensive investigation of the temperature dependence of yield stress for all these alloys in the range 77K to 373K is recommended. This will enable substantive comments on the validity of the conclusions of all these investigations.

7.2 A series of Co-Ni-Cr base alloys with gradually varying (Ti+Nb)/Al ratios and hence gradually varying γ/γ' mismatch should be prepared. A study of the strengthening mechanisms in the underaged condition of this alloy will provide a better understanding of the influence of mismatch on their strengthening by the γ' precipitate particle.

7.3 The driving force for grain boundary straightening and its relation to discontinuous precipitation in Co-Ni-base alloys should also be determined (for example, by the method in Reference 127).

7.4 Possible mechanisms for strengthening of γ'-forming alloys aged for prolonged periods and resulting in coalescence of precipitates, and complex interactions between mobile dislocations and γ/γ' interfacial dislocations should be studied.

8. **REFERENCES**

1. C. T. Sims, The Superalloys, C. T. Sims and W. C. Hagel, eds., John Wiley and Sons Inc., New York, 1972, p. 145.

2. W. C. Hagel and H. J. Beattie, Jr., "Precipitation Processes in Steels", Iron and Steel Institute, 1961, p. 98.

3. H. J. Beattie, Jr. and W. C. Hagel, "Precipitation Processes in Steels", Iron and Steel Institute, 1961, p. 108.

4. J. R. Mihalisin and R. F. Decker, Trans. TMS-AIME, 1960, vol. 218, p. 507.

5. D. H. Ben Israel and M. E. Fine, Acta Met., 1963, vol. 11, p. 1051.

6. N. E. Roger and N. J. Grant, Trans. TMS-AIME, 1960, vol. 218, p. 180.

7. H. J. Beattie, Jr. and W. C. Hagel, Trans. TMS-AIME, 1957, vol. 209, p. 911.

8. K. J. Irvine, J.I.S.I., 1961, vol. 199, p. 153.

9. R. Blower and G. Mayer "Metallurgical Developments in High-alloy Steels", Iron and Steel Institute, 1964, p. 185.

10. M. J. Blackburn, Ph.D. Thesis, Cambridge University, 1962.

11. E. J. Dulis, "Metallurgical Developments in High-alloy Steels", Iron and Steel Institute, 1964, p. 162.

12. G. P. Sabol and R. Stickler, Phys. Stat. Sol., 1969, vol. 35, p. 11.

13. P. S. Kotval, Metallography, 1969, vol. 1, p. 251.

14. R. F. Decker and C. T. Sims, The Superalloys, C. T. Sims and W. C. Hagel, eds., John Wiley and Sons Inc., New York, 1972, p. 33.

15. R. F. Decker, "Strengthening Mechanisms in Nickel-base Superalloys", Climax Molybdenum Company Symposium, Zurich, (May 5-6, 1969).

16. R. E. Reed-Hill, Physical Metallurgy Principles, D. Van Nostrand Company Inc., New York, 1964, p. 225.

17. J. Manenc, Rev. Met., 1957, vol. 54, p. 867.

18. C. Buckle, B. Genty and J. Manenc, Rev. Met. 1959, vol. 56, p. 247.

19. J. Manenc, Acta Cryst., 1957, vol. 10, p. 259.

20. J. Manenc, Acta Met., 1959, vol. 7, p. 124.

21. V. A. Phillips, Acta Met., 1966, vol. 14, p. 1533.

22. A. J. Ardell and R. B. Nicholson, Acta Met., 1966, vol. 14, p. 1295.

23. J. Helsop, Cobalt, 1964, vol. 24, p. 128.

24. F. B. Pickering, "Precipitation Processes in Steels", Iron and Steel Institute, 1961, p. 132.

25. P. S. Kotval, unpublished work, as in Ref. 13 above.

26. A. T. Kelly and R. B. Nicholson, Prog. Mat. Sc., 1963, vol. 10, p. 151.

27. H. Brooks, Metal Interfaces, American Soc. for Metals, Cleveland, 1952.

28. J. Friedel, Dislocations, Pergamon Press, Oxford, 1964, p. 371.

29. A. J. Ardell, Phil Mag., 1967, vol. 16, p. 147.

30. R. Nordheim and N. J. Grant, Trans. TMS-AIME, 1954, vol. 200, p. 211.

31. H. J. Beattie Jr. and W. C. Hagel, Trans. TMS-AIME, 1957, vol. 209, p. 911.

32. H. Hughes, J. Iron and Steel Institute (London) 1965, vol. 203, p. 1019.

33. H. J. Wagner and A. M. Hall, Defense Materials Research Center, Columbus, Ohio, Report 217 (1965).

34. E. E. Underwood, Quantitative Stereology, Addison-Wesley, Reading, Mass., 1970.

35. W. Ostwald, A. Phy. Chem., 1900, vol. 34, p. 495.

36. I. M. Lifshitz and V. V. Slyozov, J. Phys Chem. Solids, 1961, vol. 19, p. 35.

37. C. Wagner, Z. Elektrochem. 1961, vol. 65, p. 581.

38. C. Y. Li and R. A. Oriani, Proceedings of Bolton Landing Conference on Oxide-Dispersion Strengthening, G. S. Ansell, ed., Gordon and Breach, New York, 1968.

39. R. A. Oriani, Acta. Met.,1964, vol. 12, p. 1399.

40. A. J. Ardell; Proc. Intern, Symp. on Mechanism of Phase Transformation in Crystalline Solids, pp. 111-16, Inst. of Metals and Monograph and Rept. Series, 1966, vol. 33.

41. O. H. Kriege and J. M. Baris, Trans ASM, 1969, vol. 62, p. 195.

42. E. Hornbogen and M. Roth, Z. Metallk., 1967, vol. 58, p. 842.

43. B. A. Parker and D. R. F. West, Australian Inst. of Metals, 1969, vol. 14, p. 102.

44. E. H. Van der Molen, J. M. Oblak and D. H. Kriege, Met. Trans. 1971, vol. 2, p. 1627.

45. M. Chaturvedi and D. W. Chung, J. Inst. Metals 1973, vol. 101, p. 253.

46. D. W. Chung and M. Chaturvedi, Metallography, 1975, vol. 8, p. 329.

47. P. M. Kelly, International Metallurgical Reviews, 1973, vol. 18, p. 31.

48. E. Orowan, "Symposium on Internal Stresses in metals and Alloys", p. 451, 1948: London (Inst. Metals).

49. A. J. E. Foreman, as in L. M. Brown and R. K. Ham: "Strengthening Mechanisms in Crystals", A. Kelly and R. B. Nicholson, eds., John Wiley and Sons, New York, 1971, p. 9.

50. U. F. Kocks, Canadian Journal of Physics, 1967, vol. 45, p. 739.

51. A. J. E. Foreman and M. J. Makin, Canadian Journal of Physics, 1967, vol. 45, p. 511.

52. A. J. E. Foreman and M. J. Makin, Phil. Mag., 1966, vol. 14, p. 911.

53. R. K. Ham, Trans. J. I. M., 1968, vol. 9, Suppl. 52.

54. L. M. Brown and R. K. Ham, Reference No. 49 above.

55. P. A. Flinn, Trans. TMS-AIME, 1960, vol. 218, p. 145.

56. N. S. Stoloff, The Superalloys, C. T. Sims and W. C. Hagel, eds., John Wiley and Sons Inc., New York, 1972, p. 79.

57. V. Gerold and H. Haberkorn, Phys. Stat. Sol. 1966, vol. 16, p. 675.

58. H. Gleiter, Acta Met., 1968, vol. 16, p. 829.

59. S. D. Harkness and J. J. Hren, Met. Trans., 1970, vol. 1, p. 43.

60. P. B. Hirsch and A. T. Kelly, Phil. Mag., 1965, vol. 12, p. 881.

61. V. Gerold and K. Hartman, ibid., p. 509.

62. G. Knowles and P. M. Kelly as in Ref. 47 above.

63. R. W. Weeks, S. R. Pate, M. F. Ashby and P. Barrand, Acta Met., 1969, vol. 17, p. 1403.

64. M. E. Fine, NPL Symp. Rel. Str. Mech. Prop. Met. (HMSO) 1963.

65. V. A. Phillips, Phil. Mag., 1967, vol. 16, p. 103.

66. V. A. Phillips, Scripta Met., 1968, vol. 2, p. 147.

67. L. K. Singhal and J. W. Martin, Acta Met., 1968, vol. 16, p. 947.

68. D. Raynor and J. M. Silcock, Metal Sci. J., 1970, vol. 4, p. 121.

69. M. C. Chaturvedi, D. J. Lloyd and D. W. Chung, Met. Sci., 1976, vol. 10, p. 373.

70. V. Munjal and A. J. Ardell, Acta Met., 1975, vol. 23, p. 513.

71. A. J. Ardell, Met. Sci., 1980, vol. 15, p. 221.

72. A. Melander and P. A. Persson, Met. Sci., 1978, vol. 13, p. 391.

73. M. C. Chaturvedi and Han Ya-Feng, To be published, Met. Sci., 1982, vol. 16.

74. M. F. Ashby, Physics of Strength and Plasticity, A. S. Argon, ed., The M.I.T. Press, Cambridge, Mass., 1969, p. 113.

75. M. F. Ashby, Acta Met., 1966, vol. 14, p. 679.

76. M. F. Ashby, Proceedings of the Second Bolton Landing Conference on Oxide Dispersion Strengthening, G. S. Ansell, edl, Gordon and Breach, New York, 1968.

77. P. B. Hirsch and F. J. Humphreys, Physics of Strength and Plasticity, A. S. Argon, ed., The M.I.T. Press, Cambridge, Mass., 1969, p. 189.

78. U. F. Kocks, Phil. Mag., 1966, vol. 13, p. 541.

79. D. J. Bacon, U. F. Kocks and R. O. Scattergood, Phil. Mag., 1974, vol. 16, p. 675.

80. O. H. Kriege and J. M. Baris, Trans. ASM, 1969, vol. 62, p. 195.

81. E. K. Van der Molen, J. M. Oblak and O. H. Kriege, Met. Trans., 1971, vol. 2, p. 1627.

82. R. Gevers, A. Art and S. Amelinckx, Phys. Stat. Sol., 1963, vol. 3, p. 1563.

83. P. S. Kotval, Trans. TMS-AIME, 1968, vol. 242, p. 1651.

84. J. S. T. Van Aswegen, R. W. K. Honeycombe and D. H. Warrington, Acta Met., 1964, vol. 12, p. 1.

85. M. C. Chaturvedi, R. W. K. Honeycombe and D. H. Warrington, J. Iron Steel Inst., 1968, vol. 206, p. 1236.

86. D. W. Chung and M. Chaturvedi, Metal Sc. J., 1974, vol. 8, p. 215.

87. ASTM Powder Diffraction File No. 9-56.

88. A. J. Ardell and R. B. Nicholson, Acta Met., 1966, Vol. 14, p. 1295.

89. A. J. Ardell and R. B. Nicholson, J. Phys. Chem. Solids, 1966, vol. 27, p. 1793.

90. A. J. Ardell and R. B. Nicholson, Acta Met., 1966, vol. 14, p. 1295.

91. L. M. Brown and R. K. Ham, Strengthening Methods in Crystals, A. Kelly and R. B. Nicholson, eds., John Wiley and Sons, New York, 1971, p. 67.

92. W. B. Pearson: A Handbook of Lattice Spacings and Structures of Metals and Alloys, Pergamon Press, New York.

93. A. W. Thompson, Met. Trans., 1973, vol. 5, p. 39.

94. L. K. Singhal, Scripta Met., 1971, vol. 5, p. 959.

95. M. J. Marcinkowski, Electron microscopy and Strength of Crystals, G. Thomas and J. Washburn, eds., Interscience, 1963, p. 333.

96. R. W. Guard and J. H. Westbrook, Trans. TMS-AIME, 1959, vol. 215, p. 871.

97. S. M. Copley and B. H. Kear, Trans. TMS-AIME, 1967, vol. 239, p. 984.

98. D. W. Chung and M. Chaturvedi, Metal Sc. J., 1972, vol. 6, p. 134.

99. L. Brewer, as in W. Hume-Rothery, The Engel-Bewer Theories of Metals and Alloys, Progress in Materials Science, B. Chalmers and W. Hume-Rothery, eds., Pergamon Press, 1967, vol. 13, No. 5, p. 247.

100. W. E. Quist, R. Taggart and D. H. Polonis, Met. Trans., 1971, vol. 2, p. 825.

101. C. Ravindran and M. C. Chaturvedi, Met. Trans, 1975, vol. 6A, p. 213.

102. W. C. Hagel and H. J. Beattie Jr., Trans. TMS-AIME, 1959, vol. 215, p. 967.

103. D. I. Bardos and P. A. Beck, Trans. TMS-AIME, 1966, vol. 236, p. 64.

104. Reference No. 99 above, p. 231.

105. A. Raman, Z. Metallk., 1966, vol. 57, p. 301 as in A. K. Sinha, Topologically close-packed Alloys, Progress in Materials Science, B. Chalmers and W. Hume-Rothery, eds., Pergamon Press, 1972, vol. 15, No. 2, p. 174.

106. M. J. Murphy, C. T. Sims and A. M. Beltran, J. of Metals, 1968, vol. 20, p. 46.

107. L. R. Woodyatt, C. T. Sims and J. J. Beattie Jr., Trans. TMS-AIME, 1966, vol. 236, p. 519.

108. H. J. Murphy, C. T. Sims and G. R. Heckman, Trans. TMS-AIME, vol. 239, p. 1961.

109. F. B. Pickering, Precipitation Processes in Steels, Iron and Steel Institute, 1959, p. 132.

110. A. J. Ardell and R. B. Nicholson, J. Phys. Chem. Solids, 1966, vol. 27, p. 1793.

111. R. O. Williams, Met. Trans., 1982, vol. 8A, p. 959.

112. R. G. Baker, D. G. Brandon and J. Nutting, Phil. Mag., 1959, vol. 4, p. 1339.

113. B. R. Clark and F. B. Pickering, J.I.S.I., 1967, vol. 205, p. 70.

114. C. A. Fell et al in "Structural Processes in Creep", ISI Spec. Rep. No. 70, 1961, p. 144.

115. J. D. Embury and R. B. Nicholson, Acta Met., 1965, vol. 13, p. 403.

116. L. K. Singhal and J. W. Martin, J.I.S.I., 1967, vol. 205, p. 947.

117. M. C. Chaturvedi, Metallography, 1980, vol. 13, p. 167.

118. J. M. Silcock and W. J. Tunstall, Phil Mag., vol. 10, p. 361.

119. I. Kirman, J. Iron Steel Inst. 1969, vol. 207, p. 1612.

120. I. Kirman and D. H. Warrington, Met. Trans., 1970, vol. 1, p. 2667.

121. V. A. Phillips, Trans. TMS-AIME, 1964, vol. 230, p. 967.

122. W. C. Hagel and H. J. Beattie Jr., Precipitation Processes in Steels, Special Report #64, ISI, 1959.

123. D. B. Williams and J. W. Edington, Acta Met., 1976, vol. 24, p. 323.

124. R. F. Decker and J. R. Mihalisin, Trans. ASM, 1969, vol. 62, p. 481.

125. J. Greggi and W. A. Soffa, Proceedings of the Fifth International Conference on Strength of Metals and Alloys, Aachen, West Germany, 1979, vol. 1, p. 651.

126. V. A. Phillips, Phil. Mag., 1965, vol. 11, p. 775.

127. R. Fournelle and J. B. Clark, Met. Trans., 1967, vol. 3, p. 2757.